Department of Precision and Microsystems Engineering

Compensating parasitic motions and cross-couplings in compliant mechanisms

N.K. Meinders

Report no : 2021.078
Coach : A. Yaşır
Professor : J.L. Herder
Specialisation : Mechatronic System Design
Type of report : Master Thesis
Date : 14 October 2021

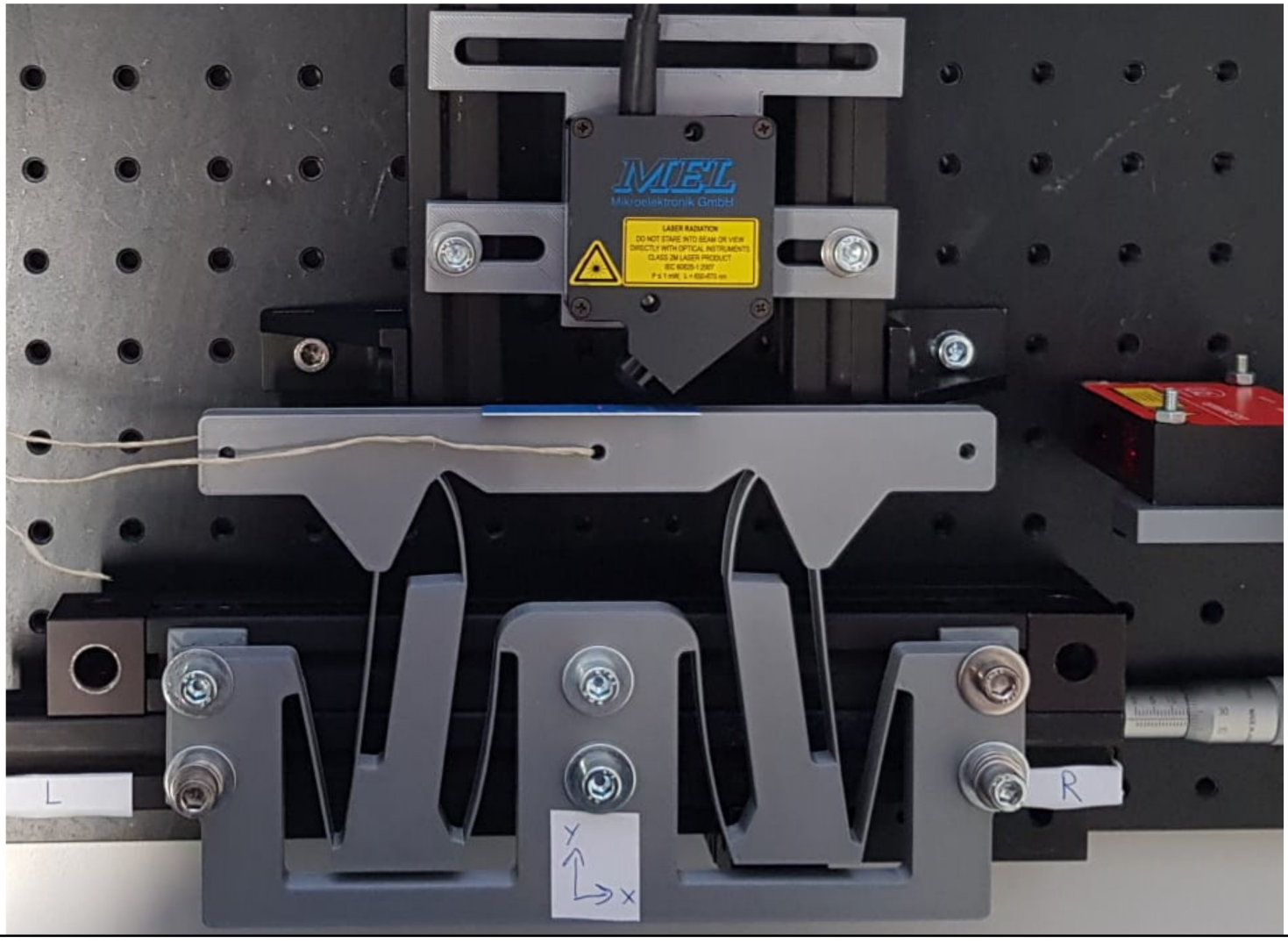

TU Delft Delft University of Technology

Challenge the future

Compensating parasitic motions and cross-couplings in compliant mechanisms

The development of a new compensation strategy to diminish unwanted motions

by

N.K. Meinders

to obtain the degree of Master of Science
at the Delft University of Technology,
to be defended publicly on October 14, 2021 at 11:00 AM.

Student number:	4474279	
Project duration:	November 24, 2020 – October 14, 2021	
Thesis committee:	Ir. A. Yaşır,	TU Delft, daily supervisor
	Prof. dr. ir. J.L. Herder,	TU Delft, supervisor
	Dr. ir. V. van der Wijk,	TU Delft
	Dr. ir. M. Langelaar,	TU Delft

An electronic version of this thesis is available at http://repository.tudelft.nl/.

TU Delft

Summary

There is a constant drive to make the next generation machines in the semiconductor industry more precise and faster. For this machines with a high repeatability, good dynamics and long lifetime are needed. Compliant mechanisms are suitable candidates to be used in this kind of machines because they can be manufactured monolithically, don't wear out over time and do not suffer from backlash which makes them ideal for precision mechanisms. However, in these machines parasitic motions and cross-axis couplings are present. These unwanted motions reduce the precision and increases the control complexity respectively.

Strategies presented in literature to compensate for unwanted motions are summarized in the first part of this report. These strategies are evaluated and by combining two promising strategies a new compensation strategy is proposed. The second part of this report focusses on this new strategy. Using this new strategy a constant stiffness linear joint, a near zero parasitic motion translational guide with well constraint uncontrollable masses and a decoupled 2-DoF mechanism are synthesized. All these case studies needed to have a large range of motion because many effective strategies for small range of motion mechanisms are available in literature.

Twelve different strategies were found in literature and compared with each other. Only three strategies were identified to have the ability in theory to fully compensate for translational and rotational parasitic motion and cross-couplings in a continuous manner. The first strategy is to compensate the overall parasitic motion of a mechanism by placing a compensation module in series with opposite but equal parasitic motion. The second strategy is to compensate the overall parasitic motions in a mechanism by using parasitic motion in the joints of the mechanisms. The third strategy is to optimize the joints to have minimal parasitic motion. If these joints are used in a configuration which is output decoupled and free of parasitic motions a mechanism without unwanted motions is developed.

From these three strategies the use of the first one results in mechanisms with decreased stiffness, uncontrollable masses, increased moving mass and increased size. The second strategy is currently barely used and if applied correctly doesn't effect the systems performance in theory significantly. The last strategy is currently used to design perfect joints (no unwanted motions). A combination of the latter two strategies from the literature study were combined resulting in a new compensation strategy for the parasitic motions and cross-couplings.

This new strategy works as follows. In a mechanism design domains can be assigned in which joints needs to be synthesized. In these design domains two flexures are connected to a base and a moving body. By optimizing the location of the connection points to the rigid bodies and the shape of the flexures new compliant structures to perform the compensation can be found. By using the correct constraints and objective the overall unwanted motions of a mechanism can be minimized. This method does not only allow for minimized unwanted motions, but is also able to control the stiffness and dynamics. This method was implemented in MATLAB and used SPACAR as nonlinear FEA program. The shape of the flexures were described by quadratic Bezier curves. In SPACAR compliant mechanisms can be modelled using beam elements which are cheap to evaluate and makes it a suitable tool to perform the optimization.

In the first case study a linear joint with near constant stiffness was designed. This joint has a maximum parasitic motion of $3.5\mu m$, a stiffness drop of maximum 4.66% and a motion range of $\pm 5mm$. The second case study was a linear guide without uncontrollable masses at low frequencies. In theory the maximum parasitic motion was $232nm$ over a motion range of $\pm 10mm$. The uncontrollable mass frequency is at $113.5Hz$ a factor 12.8 higher as the first eigenfrequency at $8.87Hz$. A 2-DoF mechanism was optimized with a maximum cross-coupling of 0.03% and a parasitic rotation of $34\mu rad$ within the workspace of $100mm^2$.

The linear motion mechanism was 3D printed out of PLA and the parasitic motions were measured experimentally. The measurements showed a maximum parasitic motion of $16\mu m$. The difference between the theoretical and measured parasitic motion can be explained by the stresses in the flexures. Due to the stresses in these flexures the assumed rigid bodies slightly deform causing additional parasitic motion. Nonlinear finite element analysis in COMSOL showed that when the rigid bodies were

modelled rigidly the parasitic motion was almost identical to the one of the optimization model. But, when the compliance in the rigid bodies is taken into account a parasitic motion of $10\mu m$ was found. Flexures of $0.8mm$ were used for this prototype. The severity of this problem can be significantly reduced by using thinner flexures.

Based on this research it is concluded that this new compensation strategy is a suitable method to diminish unwanted motions in compliant mechanisms over a large range of motion. It allows designers to synthesize new types of compensation mechanisms to reduce the parasitic motions and cross-couplings. Additionally, the stiffness and dynamics of the mechanisms can be effectively tuned by implementing extra constraints during the optimization phase. For future research it is recommanded to take the deformations of the rigid bodies into account during the optimization. Then those deformations can also be compensated. To use this method effectively smart input configurations should be used. This improves the optimization results and time. For large models it is recommanded to do the optimization with straight flexures first because less beam elements are needed to describe them accurately. In this way promising topologies can be synthesized relatively quickly. The optimized design can later be further refined by adding curvature to the flexure.

Preface

This document is my final report as a Mechanical Engineering student of the TU Delft. In this thesis I present my research on compliant mechanisms which I did during my graduation project at the department of Precision and Microsystems Engineering. It was an interesting journey in which I learned a lot about parasitic motions and cross-couplings in compliant mechanisms. This thesis is interesting for anyone who is interested in designing compliant mechanisms without unwanted motions.

I would like to thank Abdullah and Just for being my supervisors. Our weekly meetings at Fridays were very helpful and we had some nice, inspiring and interesting discussions about the project. You provided me with lots of useful insights and tips for my project. Thank you for guiding me through the project.

I would like to thank Aris as well for being part of our weekly meetings at Fridays. You always had nice questions and suggestions for my project. Additionally, I enjoyed listening to the presentations of your research and that we could help each other with our projects.

During my experiments I received helpful support from the PME lab support team. Jos from De Meetshop provided me with some laser distance sensors and software to measure and record the tiny parasitic translations in the linear guide I developed. Thank you for the support during my experiments.

I would like to thank Matthijs and Volkert for taking the time to be part of my graduation committee. I hope you find my graduation topic interesting and enjoy reading the report.

I am grateful for the support I got during this project from my family and friends. Especially during the though times during the corona pandemic I appreciated your support and being there for me.

Finally, I would like to thank the Technical University of Delft for all the possibilities I got during my wonderful time as a student.

N.K. Meinders
Delft, October 2021

Contents

1 Introduction

In the semiconductor industry there is a constant drive to make more and tinier products. This requires machines with a higher throughput and an increased precision. Compliant mechanisms, structures achieving their mobility by bending of flexures, are commonly used in this industry because they have a better repeatability and precision compared to their rigid body counterparts. Since, there is no sliding contact in these mechanisms they don't require lubrication and are not wearing out. Often they are manufactured as a single piece (monolithic) which reduces the assembly time and errors. Compliant mechanisms are also used in other industries such as aerospace and health-care. In these industries a need for accurate and repeatable motions is present. For example, to position lenses in a machine, scan substrates or to perform accurate motions with specific tools. For some of these applications the mechanisms move at high frequencies requiring mechanisms with high eigenfrequencies. These motions are often achieved by designing mechanisms build up out of building blocks. For example, linear or rotational joints. By connecting these building blocks together higher mobility parallel or serial mechanisms are constructed. However, in these mechanisms unwanted motions are present. Parasitic motions reduce the mechanisms precision because they can't be compensated. Cross-couplings (movement of an axis resulting in an unwanted movement of another axis) can be compensated but this results in an increased control complexity.

This report consists of two part. The first part (literature study) aims to answer the following question: What are the strategies to minimize parasitic motions and cross-axis couplings in parallel compliant mechanisms? This is done by performing a literature study listing the available strategies and evaluating them. The literature study limits itself to positioning mechanisms. In the second part (graduation project) a new compensation strategy to compensate the unwanted motions is developed and analysed. By combining the most promising compensation strategies from literature a new strategy is created and is analysed using three case studies. The focus of the new strategy in this report is on linear motion mechanisms with large range of motion. With this new strategy a constant stiffness linear motion joint, a linear guide with well constrained middle bodies and a decoupled 2-DoF mechanism are synthesized.

This report has the following structure. In chapter 2 relevant background information and the search & classification method for the literature study is presented. Additionally, the terms cross-coupling, parasitic motion and parallel mechanisms will be explained in more detail. The next chapter presents the strategies found in literature. In chapter 4 the strategies are evaluated and a new strategy is proposed. The new strategy is presented and discussed in chapter 5 with three case studies in a paper format. One of the results of the case studies is experimentally validated in chapter 6. The conclusions and recommendations are presented in chapter 7. Several appendices are added presenting different optimization approaches and the iterative process of the graduation project. Additional information regarding the testing phase can also be found in the appendix.

2

Background

In this chapter the relevant background information is presented to understand the problem definition. After the introduced background information, the problem definition is given. This is followed by presenting the search method and the classification method. Finally, the criteria to compare the strategies are presented.

2.1. Background information

In the following subsections background information will be given on parallel mechanisms, parasitic motions and cross-couplings which are key to understand the problem definition.

2.1.1. Parallel and serial mechanisms

A mechanism can be constructed in a parallel, serial or a combination of both (hybrid) configuration. In serial mechanisms the end effector is able to move because multiple positioning stages are mounted on top of each other [21]. So, the previous stage(s) support the next stage(s) or end-effector. For example, in a XY-manipulator the end-effector is mounted on the Y-axis. This Y-axis is mounted on top of the X-axis. According to Gogu [7] a parallel manipulator is constructed by having multiple actuated kinematic chains which come together at the end-effector to constrain and actuate the mechanism. These types of mechanisms can be found both in rigid body mechanisms as well as in compliant mechanisms.

Both types of mechanism have their own strengths and weaknesses. According to Choi and Kim [2] a compliant parallel mechanism can overcome the following shortcomings of a serial mechanism: the dynamic characteristics is different for each axis and the positional errors of each stage adds up to the positional error of the end-effector. Additionally, serial mechanism have high moving masses, high inertia and low natural frequencies [35]. On the other hand the control and the mechanical structure are simple because all stages can be controlled and designed independently [35]. Parallel mechanisms have a lower inertia, higher stiffness and can be more compact than serial mechanisms, but suffer from a smaller workspace, non-linear dynamics and difficult kinematics [52]. Also, they have a higher load-carrying capacity [35].

2.1.2. Parasitic motions

In both rigid body mechanisms and compliant mechanisms parasitic motions can occur. Lin et al. [36] defined a parasitic motion as a depended motion which occurs when an independent input motion is given. This parasitic motion could be an unwanted motion or something one can benefit from. For example, one benefits from the parasitic motion in a screw. When the rotational input motion (independent motion) is given the screw will also translate (dependent motion) [36]. Another example of parasitic motion in mechanisms is the four-bar mechanism. When the independent horizontal translation to the top link is given the link will also drop slightly. This can be an unwanted motion when this type of mechanism is used to position something. This example is shown in Figure 2.1. In this example Δe_y is the parasitic motion.

Parasitic motions can be a rotational or translational motion [36]. A mechanism can have multiple parasitic motions at once. In fact the previously mentioned four-bar mechanism has also a tiny rota-

tional parasitic motion. The amount of parasitic motions a mechanism has can be expressed with the dimension of a parasitic motion [36]. The equation for this dimension can be found in Equation 2.1. In this equation ζ_P is the dimension of the parasitic motion, M_P potential mobility and M mobility of the mechanism. For the compliant four-bar mechanism (in 2D) the potential mobility is three (all possible motions) and the mobility is one (number of independent input motions). Thus, the dimension of the parasitic motion is two.

$$\zeta_P = M_P - M \tag{2.1}$$

2.1.3. Decoupling in parallel mechanisms

Coupling between different axis in parallel mechanisms can occur. There are different types of decoupling. In this subsection the input (actuator isolation) and output coupling (cross-axis coupling) are elaborated.

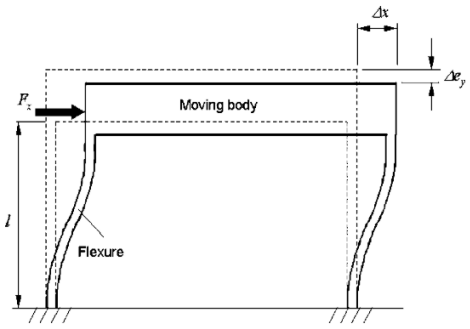

Figure 2.1: Compliant four bar mechanism with parasitic motion (Δe_y). Figure retrieved from [2].

Output decoupling

When a parallel mechanism is fully output decoupled (also known as cross-axis decoupling) the output motion is only affected by the input force along the same axis as described by Hao and Li [12]. In Figure 2.2 different parallel mechanisms designs for a 3-DoF $XY\theta$ stage are shown. Two of them (a & b) are decoupled and one is coupled (c). To control the rotation around the Z-axis and the translation along the X-axis in design (c) actuators A2 and A3 needs to be used and are thus coupled. For design (a) it can easily be observed that all actuators drive a single degree of freedom and are thus decoupled. Design (b) is also output decoupled because each actuator let the stage rotate around a unique axis (T_1,T_2 and T_3). Combining rotations around these three unique axis allows the stage to translate in the XY-plane and rotate around the Z-axis.

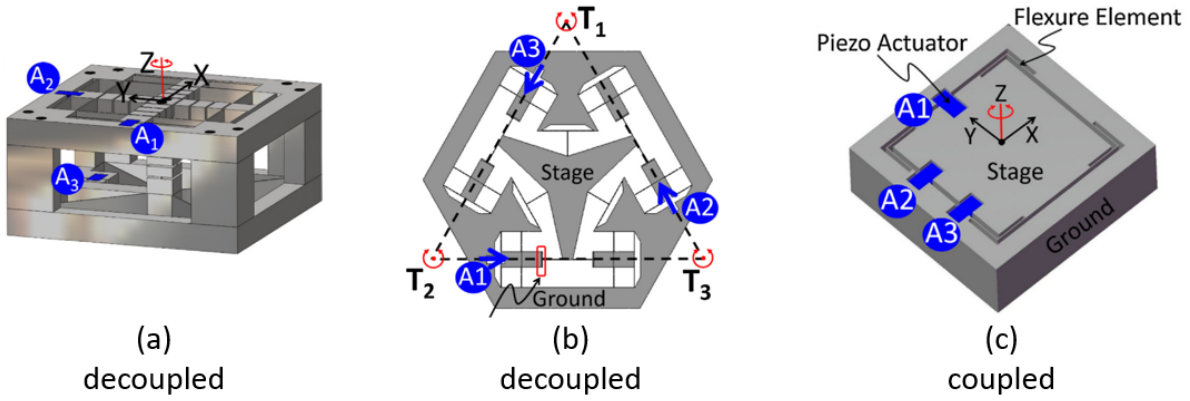

Figure 2.2: Visualization of output (de)coupling in three different $XY\theta$ stage designs. Figures retrieved from [19].

In Figure 2.3 the cross-coupling is visualized for a 2-DoF system. The vectors T_1 and T_2 visualize motions. If these two vectors are orthogonal (90 degrees angle) the motions would be decoupled. They are not orthogonal and therefore if you move in the T_1 direction you also move a bit in the T_2 direction. This coupling makes the control of a mechanism more difficult. For example, in a 2-DoF positioning stage there is a coupling between the X and Y axis. If the input is to move over the X-axis only and there will also be a movement over the Y-axis this causes a positioning error. This could be solved by control [58], but that makes the control more difficult. Therefore, it is best to try to design output decoupled mechanisms.

Lee [26] presented a way to quantify the cross-axis coupling. If the kinematics of a system are known one can construct the Jacobian matrix from it by taking the partial derivatives of the kinematic equations. From this Jacobian matrix the column vectors can be determined. Quoting Lee [26]: ”the cross-coupling between joint motions can be interpreted as a degree of linear dependency between

column vectors of the Jacobian matrix." Lee also presented an equation to quantify the cross-axis coupling. This equation is given in Equation 2.2. In this equation β_{ij} represents the angle between two column vectors i and j. This angle can be calculated with Equation 2.3. $\mathbf{T_i}$ and $\mathbf{T_j}$ represent the column vectors i and j of the jacobian matrix.

$$LKCI = \sin(\beta_{ij}) \tag{2.2}$$

$$\beta_{ij} = \arccos(\frac{\mathbf{T_i} \cdot \mathbf{T_j}}{|\mathbf{T_i}| \, |\mathbf{T_j}|}) \tag{2.3}$$

Since the Jacobian matrix is position dependent the above introduced LKCI is a local variable. This means that the LKCI value can vary over the workspace of the mechanism. A fully decoupled mechanism has all LKCI values equal to one. If the LKCI value is zero the system is fully coupled (singular points) [26]. Note that different LKCI values between different axis can be present.

Gogu [7] presents a more general cross-coupling index compared to Lee because this one combines the cross coupling between all axis. The one from Lee is only between two axis. Gogu defined it as follows: "The cross-coupling index is a measure of decoupling between all the column vectors of matrix A, and is given by the product of the local cross-coupling indices". Or in formula form as given in Equation 2.4.

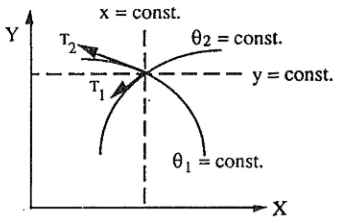

Figure 2.3: Visualization of output coupling. Figure retrieved from [26].

$$\kappa = \prod_{\substack{i=1,n-1 \\ j=1+i,n}} \sin(\beta_{ij}) \tag{2.4}$$

Input decoupling
If an actuator exerts a force on a parallel mechanism to drive the end-effector and if the other actuators don't feel anything of this input than the input is fully decoupled [32], this is called input decoupling. If there is input coupling the actuation of an actuator will cause additional loads on the other actuator(s). This can be an important design criteria when using fragile actuators (e.g. piezo actuators).

2.2. Problem definition

Compliant parallel mechanisms have the potential to outperform serial mechanisms. They have some benefits compared to the serial mechanisms, but they suffer from difficult kinematics. The kinematics are difficult because everything is connected to each other. This can result in cross-coupling errors which makes the control more difficult. Also, parasitic motions can occur for which the control cannot compensate. Therefore, it is important to have suitable strategies to solve these difficult kinematic problems and improves the compliant parallel mechanisms performance. A literature study is performed to answer the following question: What are the strategies to minimize parasitic motions and cross-axis couplings in parallel compliant mechanisms? The available strategies will be compared with each other. The literature study limits itself to positioning mechanisms.

2.3. Search method

To find relevant strategies for parasitic motion and cross-axis coupling compensation different search engines have been used. The used search engines were: Scopus, Google Scholar and Web of Science. Different search terms were combined to find the relevant literature. The search terms were: compliant parallel mechanism (or relevant synonyms) + compensation (or relevant synonyms) + parasitic motion OR cross-coupling (or relevant synonyms). In Scopus and Web of Science articles were selected by checking if these relevant terms occurred in the abstract. For Google Scholar this was not possible and the most relevant articles based on the title and abstract were selected. Also, compensation strategies in rigid body equivalent mechanisms were searched. Another way relevant papers were retrieved was by identifying relevant references in other papers or citations.

2.4. Classification

After and during analysing of the relevant literature it is important to classify the strategies in different classes. This is done in five categories. Sometimes a strategy could also belong to multiple classes. Then the method is classified in the category which corresponds best to the most fundamental way of the achieved compensation. For example, optimization can be used in a method but may not be the most fundamental idea of the strategy. The five different classification classes are summarized below.

1. Symmetry based methods
2. Prevention based methods
3. Compensation based methods
4. Stiffness based methods
5. Optimization based methods

2.5. Criteria based on difference between methods

Once the relevant strategies were found it is important to evaluate them. This evaluation is done based on the following questions:

1. Is the method able to compensate translational and/or rotational parasitic motions?
2. Is the method able to compensate translational and/or rotational cross-couplings?
3. Is the method able to perform instantaneous or continuous compensation?
4. Is the method able to fully compensate the parasitic motion or cross-coupling?

These questions are considered important because of the following reasoning. With the first two questions it can be identified when the strategies can be used. The third question indicates if the strategy can perform compensation over a large range or only locally. The last question indicates if the unwanted motions can be fully eliminated in theory or are reduced.

2.6. Criteria based on performance

Besides the previously mentioned questions the effect on system behaviour is also important. According to Hao and Kong [11] (based on [1, 17]) the precision positioning mechanisms should have ideally: large motion range, well-constrained parasitic motions, minimal cross-coupling, minimal input coupling, minimal lost motion, maximal actuation stiffness and low thermal and manufacturing sensitivities. It is important to design compact mechanisms with good dynamics therefore it is also important to consider the moving mass, overall size and eigenfrequencies. The identified relevant criteria (and commonly presented effects of the methods in literature) for the compensation strategies are listed below. If other relevant effects belong to a certain strategy these will also be considered.

1. Effect on stiffness
2. Effect on eigenfrequency
3. Effect on workspace
4. Effect on mechanism size and volume

3

Existing compensation strategies for parasitic motions and cross-coupling

In literature various methods are used to minimize parasitic motions and cross-couplings. In this chapter these strategies are presented. The strategies are subdivided into multiple classes (symmetry, prevention, compensation, stiffness and optimization). Also, the advantages and disadvantages listed in literature are mentioned. In chapter 4 the strategies are evaluated and compared to each other.

3.1. Symmetry

In this section two strategies are presented which uses rotational or plane symmetry.

3.1.1. Degree of symmetry

One of the most used strategies is mirror symmetry. If a planer mechanism is symmetric about two perpendicular axis the mechanism is output decoupled [5]. According to He et al. [16] the degree of symmetry should be maximized to minimize the parasitic motions. The degree of symmetry is the amount of perpendicular symmetry planes a mechanism has. This is also applicable to 3D mechanisms. The degree of symmetry (DoS) is visualized in Figure 3.1. From this information the first strategy arises:

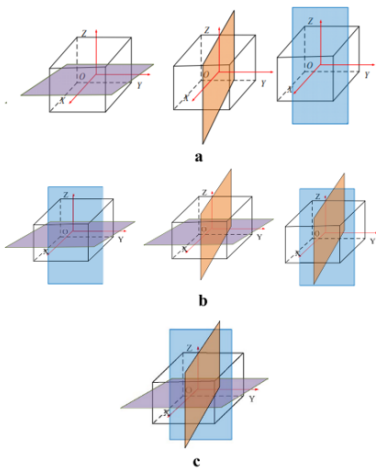

Figure 3.1: Visualization of the degree of symmetry. 1-DoS (a), 2-DoS (b) and 3-DoS (c). Figure retrieved from [16].

Strategy 1: Maximize the degree of symmetry (perpendicular planes of symmetry).

Besides the ability to decouple a design using mirror symmetry has more advantages. If it is applied on the mechanism level (so the limbs are placed mirror symmetric) symmetric designs are dynamically balanced [4], the vibration modes become decoupled [4], the thermal sensitivity decreases [27], it can accommodate higher payloads and the initial stiffness center is in the middle of the design. However, using symmetry will increase the lost motion [9], the actuation stiffness and the footprint/volume of the mechanism.

Note that mirror symmetry can be used on multiple levels in the design (joint, limb, and mechanism). When mirror symmetry is used on the joint level it can potentially reduce the motion range drastically. For example, the compound basic parallelogram mechanism shown in Figure 3.2 has a reduced motion range due to the load stiffening effect [9]. The same holds for mechanism only constructed of basic parallelogram modules. However, the usage of symmetry in this way avoids buckling [13].

The use of mirror symmetry is an instantaneous compensation method. The output-decoupling and parasitic motion effects in [5, 16] are based on the stiffness matrix. The stiffness matrix becomes

diagonal when symmetry is applied and therefore no unwanted motions occur. But this information is position dependent and when a mechanism deforms the symmetry will be lost. For example, in [15] (XY-stage) the cross-coupling is in the initial position almost zero but when the mechanism moves over the X and Y axis the cross-coupling error grows. This is usually not a problem for small range mechanisms but this can become a more severe problem for large motion ranges. In small range motions the mechanism remains almost symmetric.

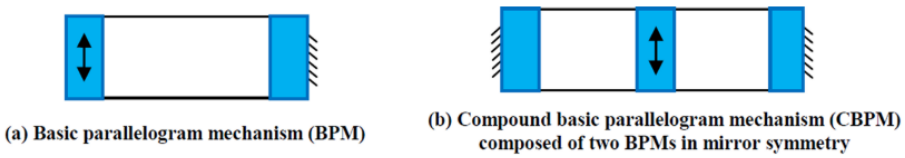

Figure 3.2: Visualization of mirror symmetry which reduces motion range. Figure retrieved from [13].

3.1.2. Symmetric patterns

The influence of rotational symmetry on the output-decoupling for planer mechanisms was studied by Du [5]. It was shown that a rotational symmetry of 3 or $2 * n$ with identical limbs around the end effector results in a diagonal stiffness matrix and is thus free of unwanted motions at its center point. This means that the parasitic motions and cross-couplings are in theory instantaneously eliminated (if the actuation is perfect). This results in the second strategy:

Strategy 2: Place identical limbs in a rotational pattern of 2*n or 3 around the center point of the output stage.

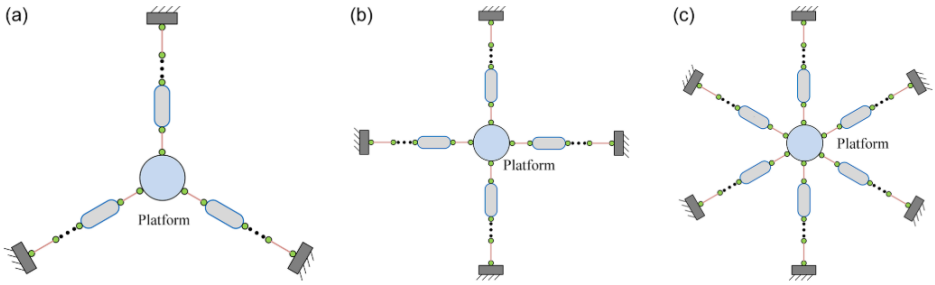

Figure 3.3: Visualization of various output-decoupled rotational patterns. Figure retrieved from [5].

Note that if limbs with a single translational degree of freedom can only be placed in a rotational symmetric pattern of 2. Otherwise the mechanism won't be able to move. The pros and cons of this strategy are identical to the ones from the previously introduced strategy. In Figure 3.3 various symmetric patterns are shown which don't have unwanted motions in their initial position.

3.2. Prevention

There are also methods to prevent parasitic motions. In literature two strategies to prevent parasitic rotations were found.

3.2.1. Actuation in stiffness center

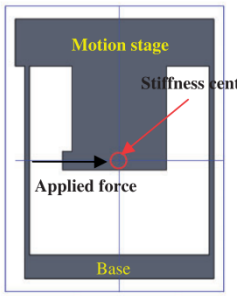

Figure 3.4: Visualization of actuation force through stiffness center. Figure retrieved from [9].

A method to minimize the parasitic rotations is to apply the force through the stiffness center as shown in [9, 12]. This method is most useful for mechanisms with small range of motion because normally the stiffness center shifts when the mechanism deforms. Initially the parasitic rotations are not 'excited' because there is no moment acting on the motion stage. However, once the system deforms the stiffness center shifts. This results in a moment acting on the motion stage leading to a parasitic rotation. An example of a

force which goes through the stiffness center is shown in Figure 3.4. Since this method concerns the placement of the actuation it does not influence other properties (e.g. stiffness, eigenfrequency, etc.) of the mechanism.

Strategy 3: The actuation forces should go through the stiffness center to prevent parasitic rotations.

3.2.2. Actuation space

Using the screw theory actuation spaces can be identified [18]. If the mechanism is actuated in these actuation spaces the parasitic motions are smallest [18]. This method assumes small displacements, linear actuators and parallel mechanisms in which the stage is directly connected to the ground by its flexures [18]. In Figure 3.5 the actuation space is visualized for a 3-DoF rotational mechanism. The actuation spaces can be identified by using the twist-wrench stiffness matrix. Because this matrix links the motions (twist) and the input (wrench) one can determine the ideal actuation positions with minimal parasitic motion. If each wrench (input) placed in the actuation space actuates one unique twist (motion) of the mechanism it is output decoupled [19]. Because this method is based on the stiffness matrix and only applicable for small motions it can only instantaneous compensate the unwanted motions. The method does not (or minimal) effect properties such as stiffness, eigenfrequency and workspace because it only concerns the placement of the actuators and does not change the mechanism constraints. The above information leads to the following strategy:

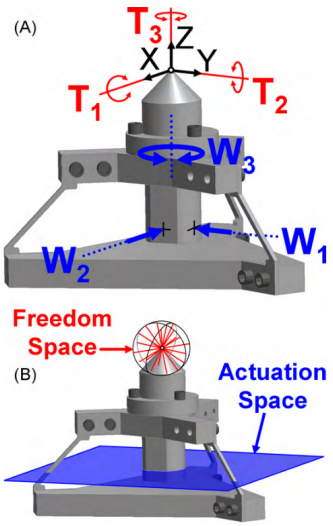

Figure 3.5: Visualization of the actuation space of a 3-DoF rotational mechanism. Figure retrieved from [18].

Strategy 4: Actuate the mechanism in the actuation space with each actuator only actuating one unique motion.

3.3. Compensation

Another approach to compensate the parasitic motions or cross-couplings is to add/use compensation modules in the mechanism. In literature three compensation methods were found. They have in theory the ability to fully compensate the unwanted motions continuously.

3.3.1. Compensation with modules in series

A commonly used method to compensate parasitic motions is to add a module to the design with parasitic motions which behaves similar to the parasitic motions of the original mechanism but in opposite direction [30, 31]. In this way the overall parasitic motion of the system can be eliminated. This strategy works for rotational and translational parasitic motions [30]. This method is used a lot in XY-motion stages in which the compensation module is in series with the original mechanism (for example in [2, 25, 46, 49]). In these designs the double-parallelograms are used, which is shown in Figure 3.6. Some drawbacks of this method when placed in series are a reduced off axis stiffness [13], introduction of non-controllable masses (impacts dynamics) [13] and it results in a bulky design. On the other hand it has the capability of creating a mechanism without parasitic motions and large range of motion. This method helps also reducing the cross-couplings because the individual limbs can be made parasitic motion free.

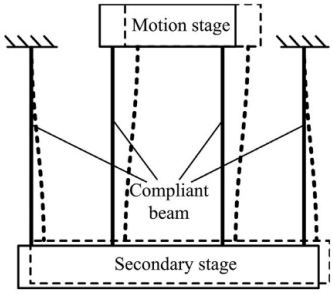

Figure 3.6: Visualization of compensation parasitic motion (motion stage) with another mechanism (secondary stage). Figure retrieved from [46].

Strategy 5: Compensate the overall parasitic motion of a mechanism by placing a module in series with opposite but equal parasitic motion.

3.3.2. Compensation within the mechanism

Another approach to compensate for the parasitic motion is to compensate the overall parasitic motion of the system with parasitic motion in joints [15, 20, 59]. The center shift of cross-spring pivots was used to create a XY-stage [15], 1-DoF translational joint [59] and a 1-DoF RCM (remote center of motion) rotational mechanism [20] with minimized parasitic motions. This approach has the advantage of not introducing uncontrollable-masses, no increase in size and the workspace is not effected. On the other hand, it might be difficult to optimize it in such a way that the unwanted motion over the entire motion range is eliminated. For example, in [59] a 1-DoF linear motion mechanism was constructed but the parasitic motion was not completely eliminated.

Strategy 6: Compensate the overall parasitic motion of a mechanism with the parasitic motion in joints.

In Figure 3.7 a visualization of this strategy is shown on a four bar linkages. On the left a mechanism without compensation is shown. In this mechanism a drop of the stage is shown. On the right the rotation points change in vertical height during the deformation. Due to these changes of the rotation points the output platform remains at a constant height. For this strategy different types of joints could be used as long as they have the desired performance.

Figure 3.7: Visualization of the compensation within the mechanism. On the left without compensation. On the right with compensation (the rotation points change in vertical position during deformation).

3.3.3. Stiffness center shift compensation

As mentioned before the parasitic rotation is dependent on the moment and rotational stiffness. If the applied force does not go through the stiffness center the input force will cause a moment on the end-effector. As a consequence the end-effector will have a parasitic rotation. It is known that the stiffness center shifts when a mechanisms deforms. Liu et al. [40] proposed a method to compensate for this stiffness center shift. Additional modules were added to the design which have a stiffness center shift in the opposite direction as the original mechanism. If these shifts are equal but in opposite direction the overall stiffness center remains stationary. This method is especially useful in large range of motion mechanisms because this method can continuously prevent the unwanted rotation. The benefit of this method is that the parasitic rotation can be prevented without increasing the overall stiffness of the mechanism significantly. The drawback of this strategy is the increase in size of the mechanism.

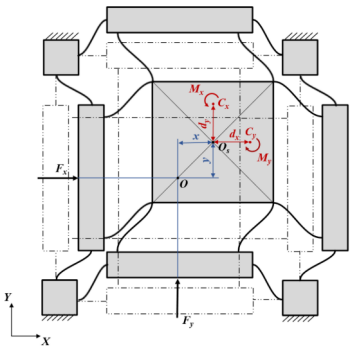

Figure 3.8: Visualization of the stiffness center shift (C_x and C_y). Figure retrieved from [40].

Strategy 7: Compensate the stiffness center shift by adding modules to the design with an equal stiffness center shift but in opposite direction.

3.4. Stiffness

Undesired motions can be minimized by increasing the stiffness in the constraint directions. In this category methods to increase the constraint stiffness are presented.

3.4.1. Rigid connections between non-adjacent legs

In order to lower the parasitic rotations and cross-axis couplings in XY(Z) stages rigid connections between non-adjacent legs are used in [14, 28, 54, 57]. In Figure 3.9 an example of the rigid connections is visualized. The parasitic rotations are better constraint due to the increased rotational stiffness of the end-effector [54]. Also the parasitic rotations of the actuation stages are reduced [14]. Other benefits from the rigid links are the reduced lost motion, thermal sensitivity and buckling is avoided [14]. Because the translational joints are connected to each other one actuator can be used to drive two translational joints. The disadvantages of these rigid links are an increased moving mass (impacts the dynamics), volume of the mechanism and it could lead to difficulties in the manufacturing and assembling process. For 3D printed designs it can be an interesting option to further increase the performance of motion stages. However, support material is probably needed during the printing process. It is important to note that this method can only be used when symmetry is used.

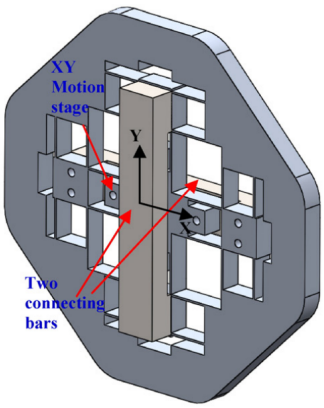

Figure 3.9: Visualization of rigid connections between non-adjacent legs. Figure retrieved from [14].

Strategy 8: Connect non-adjacent intermediate stages with rigid links.

3.4.2. Add extra joints

Another method to increase the stiffness in the undesired motion directions is to add extra joints [36]. For example, in a XY-stage based on 4-PP symmetric configuration a planer joint (E) is added [11]. This planer joint has a low stiffness in the degrees of freedom of the mechanism but helps to increase the stiffness in the other directions (rotations and out of plane direction). Adding extra joints helps not only in constraining the parasitic motions better, but also increases the load-carrying capacity. However, it comes at the cost of increased actuation stiffness, the design becomes more complex and the size/volume is likely to increase.

Strategy 9: Add additional joints to the mechanism.

3.4.3. Overconstraints

Adding overconstraints is a very popular method to better constrain the parasitic motions in mechanisms. For example, in [21, 48] extra flexures are added to the motion stage, in [9, 32, 35, 51] extra flexure beams are added to the double-parallelogram modules and designs using symmetry also introduces overconstraints. Besides better constraining the parasitic motions adding overconstraints also increases load carrying capacity and eigenfrequencies. Also the input decoupling is improved [21]. On the other hand, more powerful actuators are needed to have a similar workspace.

Strategy 10: Add overconstraints.

3.5. Optimization

There are also some optimization based approaches to minimize the errors. These are elaborated in this section.

3.5.1. Placement of constraints

In order to constrain the parasitic rotation in a basic parallelogram mechanism (as shown in Figure 3.2) the spanning size (the distance between the two flexures) can be increased to reduce the unwanted rotation [29, 44]. By increasing the spanning size the reaction forces which withstand the unwanted moment are reduced and therefore the axial deformation of the supporting flexures are minimized. The distance between the flexures can thus be optimized to minimize the undesired rotation. This can be done on joint level or on mechanism level.

By rearranging the limbs of a mechanism the parasitic motions can be reduced [36]. It is thus possible to optimize the limb arrangement for better performance. In [27, 29] the layout of a mechanism (locations of constraint modules) is optimized using the position-space-based reconfiguration approach. This method allows the design to be optimized for different performance parameters (e.g. parasitic motions, cross-couplings, motion range, etc.). The constraint modules are placed at the optimal position within their permitted positions.

Strategy 11: Optimize the placement of the constraints/joints.

3.5.2. Joint optimization

Another approach is to choose a mechanism layout which is in theory fully decoupled and parasitic motion free. When the joints are perfect (no parasitic motions) the overall mechanism is output-decoupled and parasitic motion free. Miao et al. [42] used this approach to design an decoupled 3-PRR mechanism. They optimized the joints to minimize the errors. The benefit from this approach is that known decoupled rigid-body mechanisms can be used to design the compliant mechanism equivalent. In multiple designs the joints are optimized to reduce parasitic motions. For example, the joint parameters were optimized in [6, 8]. There are different methods to create joints with minimized parasitic motions. For example, the topology was optimized in [39] and the shape was optimized in [42, 43].

Strategy 12: Optimize the joints in the mechanism.

3.6. Other design considerations

Manufacturing errors can play a significant role in the unwanted motions [21, 61] therefore it is important to use robust parameters. The kinematics should also be taken into account. With selecting the right mechanism layout with the best kinematics the parasitic motions and cross-couplings can be reduced [11, 36, 49, 55]. Adjusting the preloading on piezo-actuators can also help in reducing cross-couplings [21].

4

Evaluation of existing strategies

In this chapter the strategies presented in chapter 3 will be evaluated. The strengths and weaknesses are presented in tables as well as the similarities and differences between different methods. To do this the criteria presented in chapter 2 are used. After the evaluation possible future challenges and a knowledge gap is presented.

4.1. Comparison of strategies

In Table 4.1 the strategies presented in chapter 3 are compared to each other. This table is constructed with the information presented in the previous chapter. With this table a comparison based on non-physical properties can be made. For example, can it be used for parasitic motions or cross-couplings, can it fully compensate the unwanted motions and is the method able to instantaneous or continuous compensate?

For positioning stages the ideal compensation method should compensate both rotations & translations, have the ability to compensate parasitic motions & cross-couplings and do that in a continuous way with the ability to fully compensate. Only a very few strategies have the potential to do this. These are the compensation by adding an additional mechanism in series, compensate within the mechanism or by optimizing the joints (strategies 5, 6 and 12). Although strategies 5 and 6 have not been used to compensate rotational cross-couplings in the literature (to the best of the authors knowledge) they should have the potential to do so. Strategy 6 and 12 both rely on optimizing the joints and could be considered as the same method. Strategy 6 tries to use the inaccuracies in joints to compensate for the overall unwanted motions while strategy 12 tries to make the joints more precise.

In Table A.1 (Appendix A) the effect of the strategies on other properties are listed. When comparing strategy 5, 6 and 12 it should be noted that strategies 6 and 12 are much better for positioning stages. In chapter 2 it was presented that positioning stages ideally have good dynamics and a large workspace while having minimal errors. The strategy to compensate the unwanted motions by adding an extra module in series (strategy 5) have the problem of introducing underconstrained masses (which also impacts the moving mass), reducing the stiffness and the overall size increases. On the other hand it can result in larger workspaces. Strategies 6 and 12 (joint optimization) do not have these negative effects and the workspace remains the same (if properly designed and optimized). It is important to note that multiple strategies can be used within a design. For example, a lot of XY-stage designs make use of symmetry, overconstraints and the compensation using mechanisms (strategy 1,2, 5 and 10).

4.2. Discussion & future challenges

During the literature study it was observed that one the most promising compensation techniques (strategy 6) is barely used and if used only in translational mechanisms. If it is used cross-pivot joints are optimized. The center shift of cross-spring pivots were used to create a XY-stage [15], 1-DoF translational joint [59] and a 1-DoF RCM (remote center of motion) rotational mechanism [20] with minimized parasitic motions. This can be identified as a knowledge gap. It would be a great addition to the scientific field if there would be a method which can generate different joints within the mechanism and optimize all the joints to compensate for the overall unwanted motions. In other words, if there is a

Strategy (#)	**Parasitic motion**	**Cross-coupling**	**Instantaneous or continuous compensation**	**Possible to instantaneous fully compensate**	**Possible to continuous fully compensate**
Maximize the degree of symmetry (1)	Translations & Rotations	Translations & Rotations	Instananious	Yes	No**
Make use of rotational symmetry (2)	Translations & Rotations	Translations & Rotations	Instananious	Yes	No**
Actuate in stiffness center (3)	Rotations	None	Instantaneous	Yes	No
Actuate in the actuation space (4)	Translations & Rotations	Translations & Rotations	Instantaneous	Yes	No
Compensate with module in series (5)	Translations & Rotations	Translations*	Continuous	Yes	Yes
Compensate within the mechanism (6)	Translations & Rotations	Translations*	Continuous	Yes	Yes
Compensate stiffness center shift (7)	Rotations	None	Continuous	Yes	Yes
Rigid connections (8)	Rotations	Translations	Continuous	No	No
Add additional joints (9)	Rotations	None	Continuous	No	No
Overconstraints (10)	Rotations	None	Continuous	No	No
Optimize the placement of the constraints (11)	Translations & Rotations	Translations	Depends on initial design	Depends on initial design	Depends on initial design
Optimize the joints (12)	Translations & Rotations	Translations & Rotations	Continuous	Yes	Yes

Table 4.1: Classification and comparison of strategies
* it should be possible to use this for rotations as well but this was not found in literature
** only fully compensated in 1 DoF systems or when moving over a single axis

module which you can optimize to synthesize the 'ideal' joint for the mechanism to compensate the overall unwanted motions in the mechanism.

In addition almost none of the strategies is able to perform compensation over an area. Most strategies only compensate at the initial point of the mechanism. In various papers presenting XY-stages when the mechanism is moving towards the limits of its workspace the rate at which the cross-coupling error grows increases [8, 9, 11, 21, 38, 41, 54]. A possible cause for this effect is that most compensation strategies only compensate in the initial position. When a continuous compensation method is used the same effect is present. This could be caused by the continuous compensation method widely used (double parallelogram) which results in poor characteristics and therefore causing new unwanted motions. When the double parallelogram moves the support stiffness drops significantly, resulting in less good constraint parasitic motions.

The most used strategy to continuous compensate parasitic motions in XY-stages is strategy 5. This one is used a lot in XY-positioning stages [2, 3, 9, 10, 25, 32, 35, 38, 40, 41, 46, 49, 54, 56]. In all of these designs translational joints were created as the double parallelograms. In contrast strategy 6 (who uses the joints to compensate) is only used in [15].

In Figure 4.1 and 4.2 the normalized cross-coupling and first eigenfrequency are plotted respectively for designs presenting the cross-coupling, workspace and first eigenfrequency. Therefore, not all strategies presented in the previous chapter can be identified in those figures. From the normalized cross-coupling plot it is observed that different combinations of strategies leads to relative low couplings. However, from the eigenfrequency plot it can be observed that spatial mechanisms have very good dynamics and large workspace. But, these mechanisms are much more difficult to manufacture monolithic compared to planer mechanisms. They can either be manufactured in different subsystems but this can results in assembly errors. Or they can be 3D printed but require support material which could be difficult to remove. The planer mechanism using the strategy to compensate within the original mechanism (strategy 6) has also very good normalized cross-coupling and eigenfrequencies.

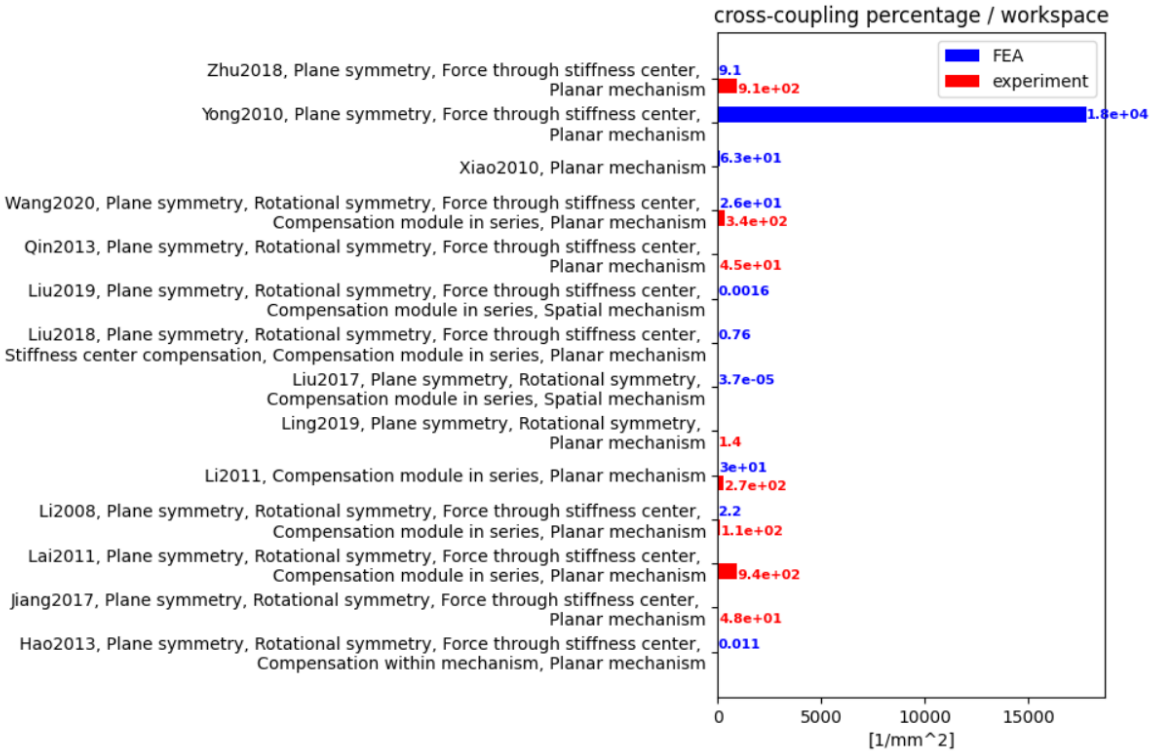

Figure 4.1: Cross-coupling normalized by workspace in XY-stages. The identified used strategies in the design are given on the Y-axis and if it is a planer or spatial mechanism. Note that the overconstraints strategy is left out because all designs use overconstraints. Data retrieved from: Hao2013 [15], Jiang2017 [21], Lai2011 [24, 25], Li2008 [32–34], Li2011 [35], Ling2019 [37], Liu2017 [38], Liu2018 [40], Liu2019 [41], Qin2013 [47], Wang2020 [49], Xiao2010 [50], Yong2010 [53] and Zhu2018 [60].

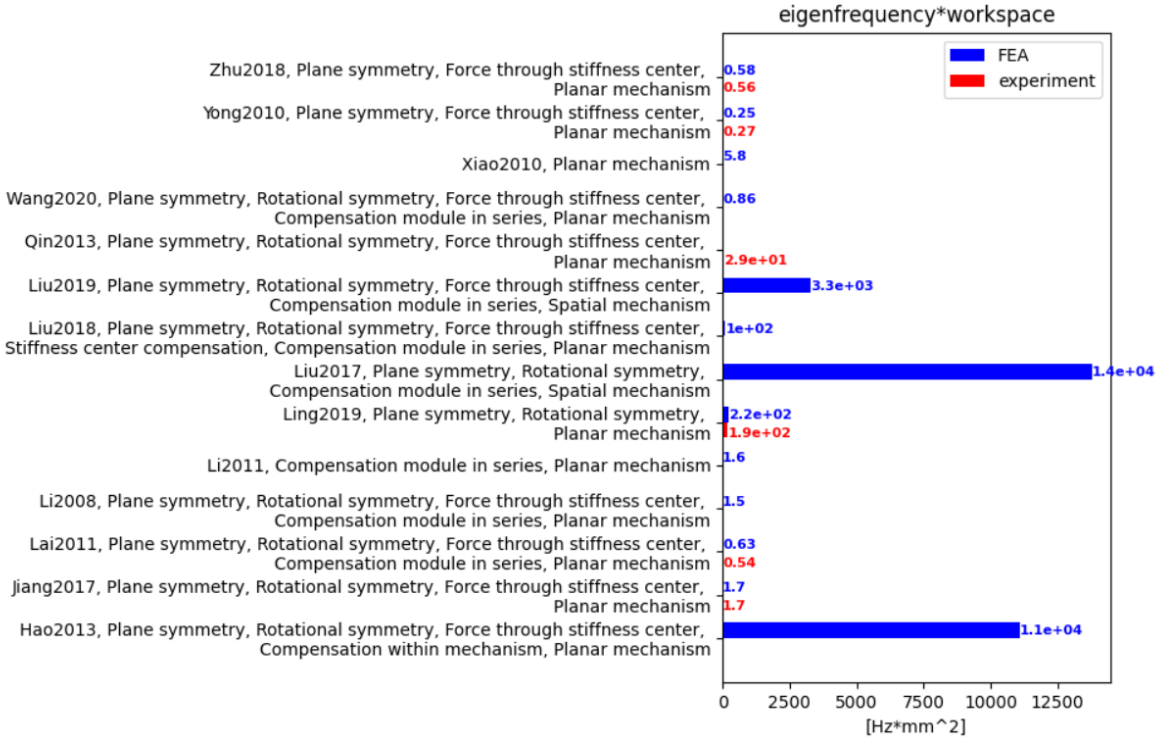

Figure 4.2: Plot of the first eigenfrequency normalized by workspace in XY-stages for different designs. The identified used strategies in the design are given on the Y-axis and if it is a planer or spatial mechanism. Note that the overconstraints strategy is left out because all designs use overconstraints. Data retrieved from: Hao2013 [15], Jiang2017 [21], Lai2011 [24, 25], Li2008 [32–34], Li2011 [35], Ling2019 [37], Liu2017 [38], Liu2018 [40], Liu2019 [41], Qin2013 [47], Wang2020 [49], Xiao2010 [50], Yong2010 [53] and Zhu2018 [60].

4.3. Proposal for new strategy

The goal of this literature study was to find strategies to compensate parasitic motions and cross-couplings in compliant parallel mechanisms. Twelve strategies were found and compared to each other. Only three strategies were identified to be able to fully compensate the unwanted motions continuously. One of them tries to use perfect joints in a mechanisms layout free of unwanted motions. The other two of them relied on compensating the cross-coupling and parasitic motions in the mechanism. The method who compensates the unwanted motions within the mechanism seems to outperform the other compensation method, but is only used with cross-pivots in literature. A method who has the ability to optimize and synthesize joints to compensate for the overall unwanted motions would be an addition to the available literature. This method has the potential to improve the mechanisms performances without impacting other effects (e.g. moving mass, overall dimensions, workspace, etc.) if the correct constraints and objectives are used. This method would be beneficial for both small and large motion ranges because the method has in theory the ability to continuously compensate. Therefore, in this project proposal a method who has the potential to do this is proposed.

Instead of picking joints which are presented in literature one could also generate its own topology/shape. The joints presented in literature are usually designed to be as accurate as possible but for this method non-ideal joints are needed. These joints can be created by a structural optimization method. Therefore, design domains can be assigned at the positions where joints needs to be placed. Besides, joints also part of structures can be optimized to compensate for the unwanted motions.

5

Paper: Optimization of multiple sets of flexures to compensate parasitic motions and cross-couplings in compliant mechanisms with desired stiffnesses and dynamics

Highlights

Optimization of multiple sets of flexures to compensate for parasitic motions and cross-couplings in compliant mechanisms with desired stiffnesses and dynamics

N.K. Meinders

- A new strategy to diminish parasitic motions and cross-couplings in compliant mechanisms with the ability to control stiffnesses and dynamics based on shape optimization of two parallel flexures is presented.
- A constant stiffness linear motion joint is synthesized with a motion range of $\pm 5mm$, maximum parasitic translation of $3.5\mu m$ and a maximum change in x,y and z stiffness of 4.66%.
- A linear guide with well constrained uncontrollable masses is synthesized with a motion range of $\pm 10mm$, maximum parasitic translation of $232nm$ and well constrained uncontrollable masses at a resonance frequency of $113.5Hz$ (1st eigenfrequency at $8.87Hz$).
- A 2-DoF decoupled parallel mechanism is synthesized for a maximum cross-coupling of 0.03% within a workspace of $100mm^2$ and a maximum parasitic rotation of $34\mu rad$.

Optimization of multiple sets of flexures to compensate for parasitic motions and cross-couplings in compliant mechanisms with desired stiffnesses and dynamics

N.K. Meinders[a]

[a]Department of Precision and Microsystems Engineering, Faculty of 3mE, Delft University of Technology, Delft, the Netherlands

ARTICLE INFO

Keywords:
Parasitic motion
Cross-coupling
Controlled stiffness
Controlled dynamics
Shape optimization
Compliant mechanisms

ABSTRACT

A new strategy to compensate parasitic motions and cross-couplings in compliant mechanisms is presented in this paper. Besides diminishing the unwanted motions, the stiffnesses and dynamics of the compliant structures can be controlled. Within a chosen mechanism configuration different design domains are defined for two parallel flexures connecting two parts. These flexures act as joints between the two parts and their shape is optimized. A linear joint with near constant stiffnesses (maximum change of 4.66% in x,y and z stiffness with a motion range of $\pm 5mm$ and $3.5\mu m$ parasitic translation), a linear motion guide with well constraint uncontrollable masses (maximum parasitic motion of $232nm$ with motion range of $\pm 10mm$) and a decoupled 2-DoF parallel mechanism (cross-coupling of 0.03% with a workspace of $100mm^2$ and parasitic rotation of $34\mu rad$) are synthesized using this method. The linear motion guide was experimentally validated using a 3D printed prototype from PLA. This prototype showed a maximum parasitic motion of $16\mu m$. FEA showed that the compliance in the assumed rigid parts causes the difference between the theoretical parasitic motion and the measured parasitic motion.

1. Introduction

In precision positioning mechanisms, compliant mechanisms are often used. These are mechanisms which can move due to elastic deformation of its hinges (lumped compliance) or (parts of its) legs (distributed compliance). They have several advantages over rigid body mechanisms. For example, due to the lack of sliding contact these mechanism have better repeatability (no friction causing backlash), do not require lubrication and don't wear over time. Often they can be manufactured monolithically resulting in less assembly time and errors. Another benefit of compliant mechanisms is their scalability.

Positioning stages can be designed as parallel or serial mechanisms (or a combination of both). The advantages of parallel mechanisms compared to serial mechanisms are a lower moving mass and inertia. Also, the parallel configuration results in increased stiffnesses which makes higher payloads possible. However, parallel mechanisms suffer from a smaller workspace and difficult kinematics. These difficult kinematics origins from parasitic motions in the system. A parasitic motion is a dependent motion which occurs when an independent input motion is given [1]. These are often unwanted motions effecting the precision of systems. In parallel mechanisms multiple legs are connected to the end-effector. Due to parasitic motions in the legs of the mechanism, cross-axis coupling(s) can occur. Cross-axis coupling(s) is/are the movement(s) of the end-effector in other direction(s) than the input motion. For example in an xy-manipulator, if the end-effector moves in x-direction, a cross-coupling error is the small resulting motion in y-direction. These cross-axis couplings can be compensated using control, but this increases the control complexity. The parasitic motions make the mechanism less precise because they can't be compensated. For example, a rotation of an end-effector in a xy-positioning stage. Therefore, it is important to design precision mechanisms with minimal parasitic motions and cross-couplings.

Several strategies are used in literature to minimize the parasitic motions and cross-couplings. The most important ones are shortly introduced here. Some of them directly reduce the cross-axis coupling while others indirectly reduce the coupling error. For example, as a result of parasitic motion free limbs there will be no cross-coupling error in an output-decoupled mechanism configuration. Applying symmetry is a popular method to reduce both types of unwanted motions. By maximizing the degree of symmetry (amount of perpendicular symmetry planes) both parasitic motion and coupling errors can be reduced [2, 3]. Using rotational symmetry decreases the cross-coupling error [3]. A downside of using symmetry is the increase in size of the mechanism. A method to minimize the parasitic rotations is to apply the force through the stiffness center [4, 5]. This works only for the initial position since the stiffness center moves during deformation of the mechanism. Extra compensation modules can be added to make the stiffness center stationary [6]. A commonly used method to compensate parasitic motions is to add a compensation module to the design with similarly behaving parasitic motions as the original mechanism, but in opposite direction [7, 8]. In this way, the overall parasitic motion of the system can be eliminated in theory. For example, this strategy is used in the double parallelogram (shown in Figure 11). However, this method results in reduced off axis stiffness [9], introduction of non-controllable masses (impacts dynamics) [9] and in a bulky design. Another approach to compensate for the parasitic motion is to compensate the overall parasitic motion of the

system with parasitic motion in its joints [10, 11, 12]. For example, the center shift in cross-spring pivots was used to create a 1-DoF translational joint [11]. This approach has the advantage of not introducing uncontrollable masses and no significant increase in size. On the other hand, it might be difficult to optimize it in such a way that the unwanted motion over the entire motion range is eliminated. Adding overconstraints is another widely used method to better constrain the parasitic motions in mechanisms. For example, in [13, 14] extra flexures were added to the motion stage resulting in a better constraint parasitic rotation. Another approach is to choose a mechanism layout which is in theory fully decoupled and parasitic motion free. When the joints are perfect (no parasitic motions) the overall mechanism is output-decoupled and parasitic motion free. Miao et al. [15] used this approach to design a decoupled 3-PRR mechanism. In literature joints are optimized to increase its accuracy, as is done in [16, 17] by optimizing the joint parameters.

From all mentioned strategies only three strategies are in theory able to perform compensation (for translations and rotations) over the entire motion range: adding compensation module, compensation within mechanism and optimizing joints. Symmetry is considered here as an instantaneous compensation method. When an xy-mechanism starts moving over both its axes the symmetry is (partly) lost, resulting in less reduction of its unwanted motions.

In literature various compliant mechanisms have been synthesized using shape optimization of flexures described by parametric curves. For example, non-linear springs [19, 20], path-following mechanisms [21] and output-decoupled mechanisms [22]. Moreover, the motion range of a rotational mechanism was improved by shape optimization [23].

The aim of this paper is to introduce a new compensation strategy which has the ability to perform continuous compensation of parasitic motions and cross-couplings over a large range of motion while having desired stiffnesses and dynamics. Combining the strategies of doing compensation within the mechanism and optimizing the joints with shape optimization of flexures results in a new promising strategy. A mechanism layout could be chosen with fixed joint locations. At these joint locations the shape of the flexures are optimized to compensate for the overall unwanted motions and to control the stiffnesses and dynamics of the mechanism. In this way, one is not dependent on joints with center shift from literature. In literature the strategy of adding a compensation module is widely used (e.g. double parallelogram). However, this results in poor dynamics, reduces stiffnesses and a bulky design. According to Hao et al. [18] most compliant translational joints suffer from a decay of stiffness. This new strategy has the potential to overcome these shortcomings while achieving near zero parasitic motions. This new strategy is presented in combination with three case studies to demonstrate its potential in this paper. This paper limits itself to 2-dimensional translational mechanisms. The case studies are a near constant stiffness linear joint, a linear motion mechanism with well constraint uncontrollable masses and a decoupled xy-stage.

The structure of this paper is as follows. First, some background information on shape optimization is presented, followed by the introduction of the method and the case studies. Afterwards, the results of these case studies are presented and compared with other designs. Then, experimental results of the linear guide are presented followed by a discussion and conclusion.

2. Background

Different methods to optimize the shape of flexures are presented in literature. First, a short overview of different methods will be presented, followed by a description of Bezier curves.

2.1. Shape optimization

Different types of parametric curves are used to synthesize compliant mechanisms. For example, splines [19, 20], Bezier curves [24] and intrinsic functions [23]. When using splines, a curve goes through all the control points. Bezier curves are interpolation curves between all the control points. The shape of intrinsic functions is defined by mathematical formulas (e.g. Fourier series). Some other methods build up on the Bezier curved method, such as wide curves [25] and the beam-based method [26]. In the wide curve theory the width of the flexures is defined by the size of the control points. The beam-based method allows the flexures also to twist and adds additional masses to the flexures. With these masses the dynamics can be controlled. This method is used to design legs between an end-effector and the base, but the legs are not used to actuate the mechanism.

Each method has its own advantages and disadvantages. In this paper, Bezier curves are chosen because this method covers a large design space with a limited number of design variables [24] and some useful constraints to avoid intersections, loops and self-intersections are already presented in literature [25].

2.2. Bezier curves

Bezier curves are parametric curves in which the shape can be changed by changing the location of the control points. The x- and y-coordinates of a Bezier curve are defined by the following equations [25].

$$x(t) = \sum_{i=0}^{m} C_{ix} B_m^i(t) \qquad 0 \le t \le 1 \tag{1}$$

$$y(t) = \sum_{i=0}^{m} C_{iy} B_m^i(t) \qquad 0 \le t \le 1 \tag{2}$$

$$B_m^i(t) = \binom{m}{i} t^i (1-t)^{m-i} \tag{3}$$

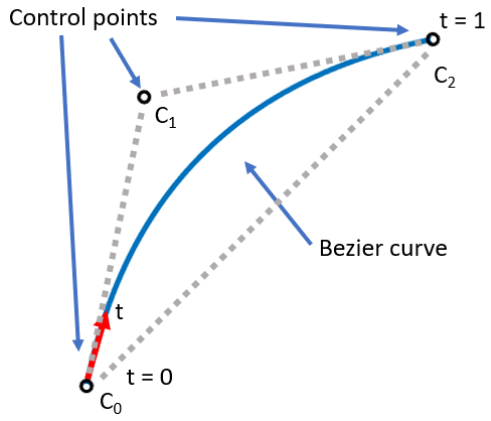

Figure 1: Visualization of a quadratic Bezier curve

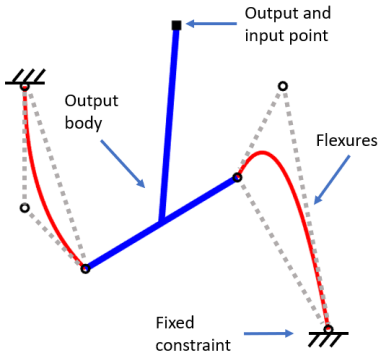

Figure 2: Visualization of model input, output and boundary conditions. The red lines indicates flexures and the blue lines a rigid body. The black circles indicate the control points of the red Bezier curves.

In Equation 1, 2 and 3 m is the order of the bezier curve and $i = 0, 1, ..., m$. C_{ix} and C_{iy} are respectively the x- and y-coordinate of control point i. The parameter t ranges from 0 to 1 and describes where on the curve you are. This is visualized in Figure 1. A Bezier curve goes always through the first and last control point.

3. Method and Case Studies

In this section the method will be introduced and described in detail. Followed by an introduction of the three case studies. Lastly, the constraint and objective functions for the case studies are presented.

3.1. Method description

This method can be used either on a joint level, leg or mechanisms level. Three case studies are used to illustrate the different usages. A brief example is described here for synthesizing a joint. Two parallel flexures are connected to the output body. The coordinates of the output point on the output body is predefined, but the locations where the flexures are connected not. This output body is assumed to be rigid. At the input point a force or displacement can be added. This point is also used to evaluate the displacements and stiffnesses (and rotation if applicable). This is illustrated in Figure 2. For more difficult mechanisms the same method is used, but the parallel flexures are connected to other rigid bodies instead of the ground. This can be seen in the optimization results shown in Figure 9 and 14.

The shape of the flexures are optimized for a specific performance goal. The flexures are modelled using beam elements. Beam elements, which are computationally inexpensive compared to solid elements. This allows for quick model evaluations and relatively short optimization time. If this approach is used on a mechanism level, multiple sets of parallel flexures are modelled at the joint locations of the mechanism. All (or certain) sets of flexures are optimized together to optimize the performance of the entire mechanism. Symmetry of different joints can be used to limit the amount of control points (optimization parameters) needed for the optimization.

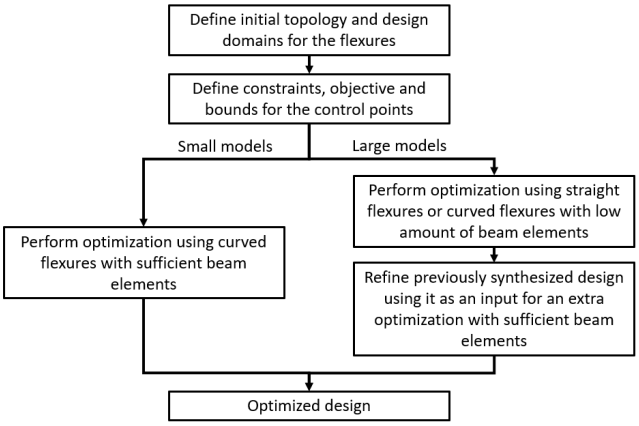

Figure 3: Flow chart of the optimization approach

In Figure 3, a flow chart of the optimization approach is shown. The first step of the method is to define the topology of the overall design and assign design domains for the flexures. The second step is to define the constraints and objective for the optimization algorithm. Additionally, the bounds for the control points need to be chosen. These bounds can be either the entire design domains for the joints or smaller regions of it. If smaller regions are used, one can avoid the flexures intersecting each other or force a design in a certain direction. Practise showed that faster and better optimization results will be synthesized if smart input geometries are used. For example, if a straight line mechanism needs to be synthesized one could set the bounds as a mix between a double parallelogram and Roberts mechanism. This is done in the second case study which will be presented later.

If small models are used, the time to evaluate the model is often small. This allows for a quick optimized design. Sufficient beam elements should be used to model the geometry and its responses accurately. Depending on the amount of flexures a mechanism has, two different

approaches can be used. If larger models are used (e.g. an xy-stage) the time to evaluate the model is relatively long (with sufficient beam elements to model accurately curved flexures). Because many function evaluations needs to happen an efficient model is desired. From a time saving perspective, first a design can be synthesized using straight flexures or curved flexures with a low amount of beam elements. If straight flexures are used, less beam elements are needed for an accurate solution. In this way potential promising configurations can be synthesized relatively quickly. After this optimization, a new optimization can be performed using the previously synthesized mechanism as input. Curvature can be added or refined by the optimizer to further improve the mechanism performance. Using this approach computational time is saved because only at a promising solution an expensive model needs to be evaluated. Additionally, promising configurations can be inserted directly and being optimized directly to bypass the process of finding a promising configuration first.

3.2. Joint input topology

In this paper each joint is represented by two parallel flexures. Instead of having flexures under the rigid body they are also allowed to be partly next to the rigid body. This topology is chosen because having more parallel flexures adds overconstraints and increases the amount of design variables. Moreover, straight line mechanisms (e.g. Roberts mechanism, Watt's linkage or Chebyshev linkage) often have two linkages or flexures connected to an output body. Additionally, adding more flexures increases the chance of having flexures intersecting with each other. Different joint input topologies were tried using this method but resulted in less good optimization results.

3.3. Software

The compliant mechanisms are evaluated in the nonlinear finite element software program SPACAR [27]. This is a program which runs in MATLAB [28]. All inputs (nodes, elements, boundery conditions, etc.) for the SPACAR program are defined in a MATLAB function. In combination with MATLAB's global optimization toolbox [29] the shapes of the flexures are optimized. In SPACAR geometries can be modelled using beam elements. These beam elements can be deformed in elongation, torsion and bending.

3.4. Discretization

Bezier curves are normally continuous, but SPACAR uses straight beam elements. Therefore, the Bezier curve needs to be discretized into smaller segments. The Bezier curve is discretized by sampling n points on the curve. This is done by calculating the x and y coordinate of the curve for different values of t. The values for t are selected by equally spacing n values for t between zero and one. This equally spacing does not result in equally spaced beam elements over the Bezier curve, but the beam elements are more densely spaced at regions where the radius of curvature is small. This is useful to model the curved flexures more accurately. In this paper quadratic Bezier curves are used. Higher order Bezier curves can be used, but require more control points resulting in longer optimizations with potentially even better synthesized mechanisms.

3.5. Assumptions

A couple of assumptions are made in this paper. These are listed below:

(a) No other loads are exerted on the mechanism/joints

(b) Parts connecting flexures are considered rigid

(c) 2D geometries

(d) Material is uniform

(e) The effect of gravity is neglectable

3.6. Optimization algorithm

The surrogate optimization algorithm [29] from MATLAB's global optimization toolbox was used to optimize the shapes. During the optimization the algorithm can be in two different phases. In the random phase the information at different quasirandom points is gathered. In the second phase a surrogate between these points is constructed and based on this surrogate new adaptive samples are taken. If the objective function does not improve anymore, new points will be taken to construct a new surrogate. This algorithm is especially useful for models which have a relatively long run time.

3.7. Case studies introduction

In this paper three different case studies are presented to show the effectiveness of using shape optimization to minimize parasitic motions and cross-couplings in compliant (parallel) mechanisms. Besides minimizing the parasitic motions also other interesting properties can be controlled using the shape optimization. Such as, the stiffnesses or uncontrollable masses. The three case studies are:

(i) A constant stiffness linear joint

(ii) A linear guide with well constrained uncontrollable masses

(iii) A decoupled 2-DoF parallel mechanism

3.8. Constraints

Different constraints can be applied on the different optimizations. These can be subdivided into geometry constraints and output constraints. The geometry constraints can be evaluated before the SPACAR model is evaluated. In contrast, the output constraints require the output of the SPACAR model. In this subsection all constraints for the case studies are given. Not all constraints are used in each case study. The constraints used for each case study is indicated after its name with a i, ii or iii.

3.8.1. Geometry constraints

Besides the bounds for the control points, three other geometry constraints can be used. Constraints can be used to avoid intersections between flexures, self intersections and loops.

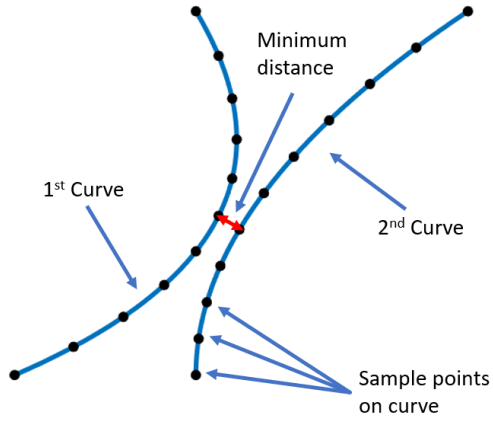

Figure 4: Visualization of the intersection constraint

Intersection detections (case studies i, ii and iii) The shape of the flexures can be changed by moving the control points. In order to create shapes in 2D it is important that those flexures do not cross each other or touch each other during motion. To prevent this from happening a minimum distance (offset) between the curves is defined as a constraint. In Figure 4 this constraint is visualized. On each curve a number of sample points are taken. The distance between all the sample points of the two different curves is calculated. With Equation 4 a scaled constraint is introduced to check if two curves are to close to each other. To ensure the reliability of this constraint enough sample points need to be taken. The amount of sample points doesn't need to be the same as the amount of beam elements. A high number of sample points is recommended.

$$\frac{offset - \min(distance)}{offset} < 0 \tag{4}$$

Self intersections (case studies i, ii and iii) Self intersections can be avoided using the following constraint introduced by Zhou and Ting [25].

$$\max(0.5w - \rho(t)) < 0 \tag{5}$$

$$\rho(t) = \frac{(\dot{x}^2(t) + \dot{y}^2(t))^{2/3}}{|\dot{x}(t)\ddot{y}(t) - \ddot{x}(t)\dot{y}(t)|} \tag{6}$$

In these equations w is the thickness of the flexure, x and y are the coordinates of the curve. This constraint checks if the radius of curvature is bigger than half the width of the flexure. If the radius of curvature is smaller than half the width of the flexure self intersections occur.

Loop constraint In this paper quadratic Bezier curves are used. A quadratic Bezier curve can't make loops with itself. For higher order Bezier curves loops can occur. These loops can be avoided by adding a constraint. For example, a loop constraint to prevent loops in cubic Bezier curves was presented by Zhou [25].

3.8.2. Output constraints

In this subsection all different output constraints are presented. Note that all the constraints are scaled.

Stiffness ratio (case studies i and ii) For a joint or linear guide it is important that the supporting stiffness is higher than the stiffness in the motion direction. According to Hao [18] the stiffness ratio should be higher than 100. The stiffness ratio is defined as the support stiffness divided by the motion stiffness (Equation 7). In Equation 8 the constraint for this stiffness ratio is given. Note that the stiffness ratio varies over the motion range. Therefore, the minimum stiffness ratio of the mechanism is used in this constraint. At different positions in the motion range of the mechanism the stiffness ratio is evaluated.

$$R = \frac{K_y}{K_x} \tag{7}$$

$$\frac{R_{min} - \min(R)}{R_{min}} < 0 \tag{8}$$

Stress constraint (case studies i, ii and iii) The Von Mises stress in the material σ_{mises} should not exceed a maximum defined stress level σ_{max}. This results in the following scaled constraint:

$$\frac{\sigma_{max} - max(\sigma_{mises})}{\sigma_{max}} < 0 \tag{9}$$

Parasitic rotation constraint (case studies ii) The maximum parasitic rotation θ should be smaller than the maximum allowed rotation θ_{max}.

$$\frac{\max(\theta) - \theta_{max}}{\theta_{max}} < 0 \tag{10}$$

Parasitic translation constraint (case study i) The maximum parasitic motion δ in the model should not exceed the set limit δ_{max}.

$$\frac{\max(\delta) - \delta_{max}}{\delta_{max}} < 0 \tag{11}$$

Frequency constraint (case study ii) The second eigenfrequency of the mechanism ω_2 should be higher than the minimum second eigenfrequency $\omega_{2,min}$ set as constraint value.

$$\frac{\omega_{2,min} - \omega_2}{\omega_{2,min}} < 0 \tag{12}$$

Lost motion constraint (case study iii) The lost motion (Equation 13) in a mechanism is defined as the percentage of input motion which is lost. In other words, how good is the input (u_{in}) transmitted to the output (u_{out}). If the lost motion is zero all input motion is transferred to the end-effector. A maximum can be defined as Lm_{max} which results in a constraint on the lost motion Equation 14.

$$Lm = (1 - \frac{u_{in} - u_{out}}{u_{out}})100\% \tag{13}$$

$$\frac{Lm - Lm_{max}}{Lm} < 0 \tag{14}$$

3.9. Objective

For each of the three case studies different objective functions are used. These are introduced in the following subsections.

3.9.1. Constant stiffness linear joint objective

The objective for the first case study is given in Equation 15. This objective consists of a summation of multiple terms. For each stiffness (Kx, Ky, Kz) the difference between the maximum and minimum stiffness is normalized by the maximum stiffness. This is important because all three stiffnesses have different magnitudes. With this objective the optimization algorithm will try to find a solution with all stiffnesses being near constant.

$$\begin{aligned} \text{minimize} \quad & (\frac{K_{x,max} - K_{x,min}}{K_{x,max}} + \\ & \frac{K_{y,max} - K_{y,min}}{K_{y,max}} + \frac{K_{z,max} - K_{z,min}}{K_{z,max}}) \end{aligned} \tag{15}$$

3.9.2. Linear motion mechanism objective

The goal of the linear motion mechanism is to have the center of the topbar move over a near straight line. The objective function (Equation 16) minimizes the parasitic motion δ of the top bar.

$$\text{minimize} \quad \max(\delta) \tag{16}$$

3.9.3. Decoupled xy-stage objective

When optimizing multiple sets of flexures within a mechanism the cross-coupling and parasitic rotation can be minimized (Equation 17). For this optimization the cross-coupling (k) and parasitic rotation (θ) are calculated at multiple points in the workspace. The maximum value of the cross-coupling times the maximum parasitic rotation is minimized.

$$\text{minimize} \quad \max(k)\max(\theta) \tag{17}$$

3.10. Flexure dimensions and material properties

In Table 1 the parameters used to model the flexures are presented. The material PLA is used for case studies i and ii because this material allows for quick and cheap prototyping. The available 3D-printer is able to print flexures with $0.8mm$ thickness. For the decoupled mechanism titanium is used as input material with $0.4mm$ thick flexures. This allows for a better comparison with mechanisms presented in literature.

	PLA	Titanium
flexure thickness [mm]	0.8	0.4
flexure height [mm]	10	10
youngs modulus [GPa]	2.20	110
shear modulus [GPa]	0.759	40
density [kg/m^3]	1240	4000

Table 1: Material properties and flexure dimensions for PLA and titanium

4. Optimization results

In this section the results of the case studies are presented. Each case study is compared with existing joints and mechanisms.

4.1. Constant stiffness linear joint

A linear motion joint with near constant stiffness is synthesized using the optimization method. In Table 2 the values for the constraints are shown and in Table 3 the most important properties of the joint are presented. The maximum allowable stress is chosen as half the yield stress of PLA. The parasitic motion of the joint is shown in Figure 8. The decay of stiffness and stiffnesses are shown in respectively Figure 6 and 7. The optimized geometry (shown in Figure 5) is asymmetric and looks like a Roberts mechanism with curved flexures. Additionally, the bounds for the control points are visualized in this figure. These bounds force the flexures into a similar mechanism as the Roberts mechanisms. These bounds are chosen because the Roberts mechanisms has a near straight line motion over a relatively large range. Moreover, different bounds were tried, but resulted in reduced performance because of the large input motion. For smaller ranges of motion also other geometries showed very good and potentially better results.

Constraint	Value
Minimum distance between flexures	2.5 [mm]
Minimum radius of curvature	0.8 [mm]
Minimum stiffness ratio	500 [$-$]
Maximum stress	25 [MPa]
Maximum parasitic motion	5 [μm]

Table 2: Constraint values for the constant stiffness linear joint

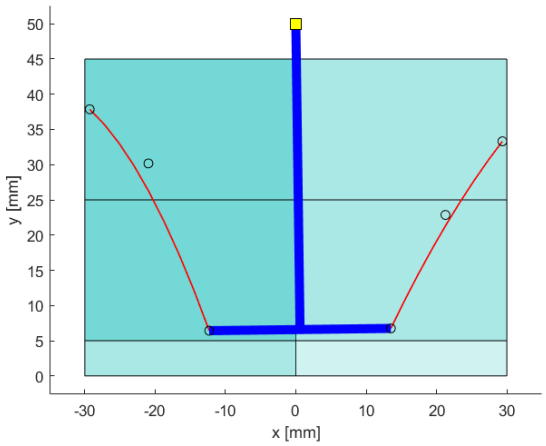

Figure 5: Geometry of the constant stiffness linear joint. The red lines indicate the flexures, the blue lines represent the rigid parts. The boxes represent the bounds for the control points. Note that the boxes are overlapping. The controlpoint locations are indicated with the circles and the yellow square represent the input and output point.

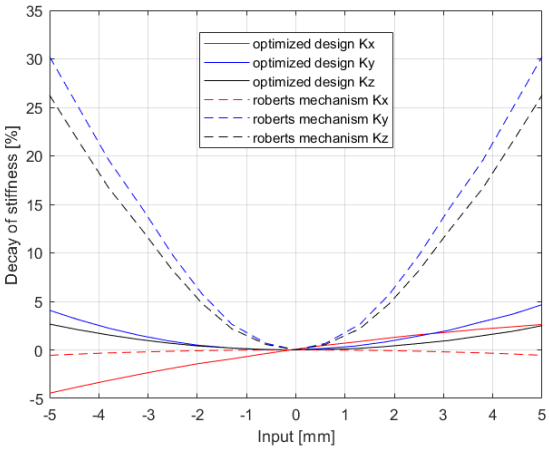

Figure 6: Comparison of the decay of stiffness with respect to the initial position between the constant stiffness linear joint and a Roberts mechanism

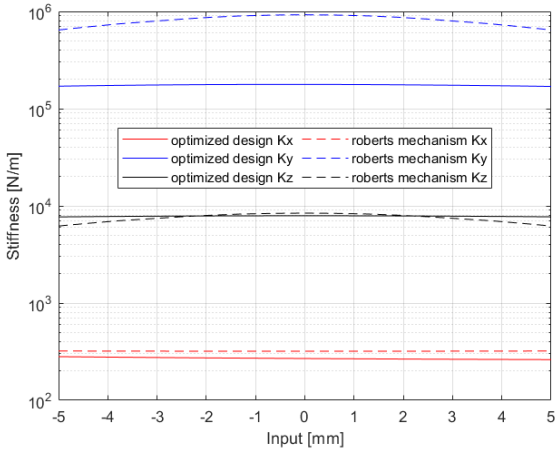

Figure 7: Comparison of the stiffnesses between the constant stiffness linear joint and a Roberts mechanism

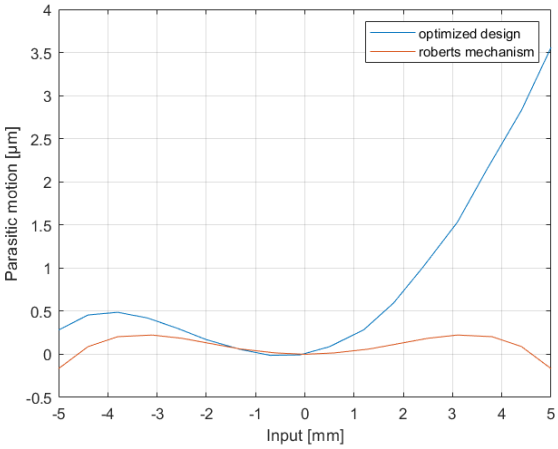

Figure 8: Comparison of the parasitic translation between the constant stiffness joint and a Roberts mechanism

Since the design is asymmetric, the behaviour in terms of stiffness and parasitic motion is also asymmetric. All three different stiffnesses show a little decay of stiffness compared to the neutral position. In fact, the stiffness in x-direction gains some stiffness. In Figure 6 also the decay of stiffness of an optimized Roberts mechanism for minimum parasitic motion is shown. The optimized design shows for K_y a factor 6.5 less decay in support stiffness. The out of plane decay of stiffness is reduced by a factor 9.9. In x-direction the change in stiffness is a factor 8.1 worse compared to a Roberts mechanism. However, the decay in x-direction is still less than 5%.

The magnitudes of the stiffnesses for K_x and K_z are comparable to each other. The support stiffness of the optimized geometry is significantly lower than the Roberts mechanism, but still much higher than K_x or K_z resulting in good stiffness ratios. Additionally, a constraint for a minimum support stiffness could be introduced if higher support stiffnesses are desired. This difference in support stiffness is likely to originate from the added curvature. Adding curvature improves certain performances, but could cost some stiffness.

The parasitic motion for negative inputs is well constraint (maximum of about $0.5\mu m$, which is much smaller than the constraint value) while for the positive inputs the parasitic motion is at maximum $3.56\mu m$. Lastly, the maximum stress in the joint is $19.9MPa$ which is well below the limit set at $25MPa$.

4.2. Linear guide with well constrained uncontrollable masses

In Table 4 the constraint values for the linear motion guide are given. The maximum stress is defined as half the

	Optimized design
Maximum stress [MPa]	19.9
Motion range [mm]	[-5, 5]
Max parasitic motion [μm]	3.56
Maximum change in K_x [%]	4.50
Maximum change in K_y [%]	4.66
Maximum change in K_z [%]	2.65

Table 3: Key properties of the constant stiffness linear joint

Constraint	Value
Minimum distance between flexures	5 [mm]
Minimum radius of curvature	4 [mm]
Minimum stiffness ratio	100 [$-$]
Maximum stress	25 [MPa]
Minimum 2nd frequency in plane	50 [Hz]
Maximum parasitic rotation	200 [μrad]

Table 4: Constraint values for the linear motion guide with well constrained uncontrollable masses

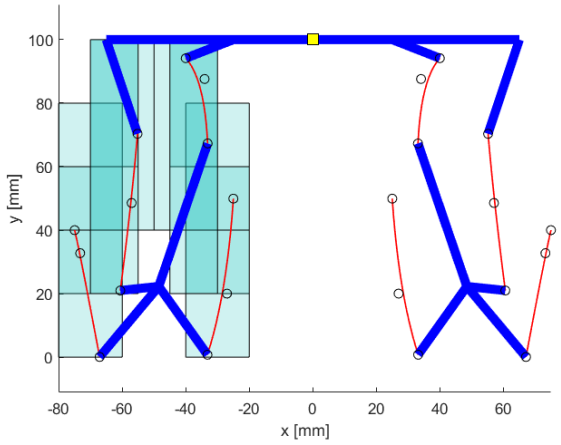

Figure 9: Optimized geometry of the linear motion guide. The red lines indicate the flexures, the blue lines represent the rigid parts. The boxes represent the bounds for the control points. Note that the boxes are overlapping. The controlpoint locations are indicated with the circles and the yellow square represent the input and output point.

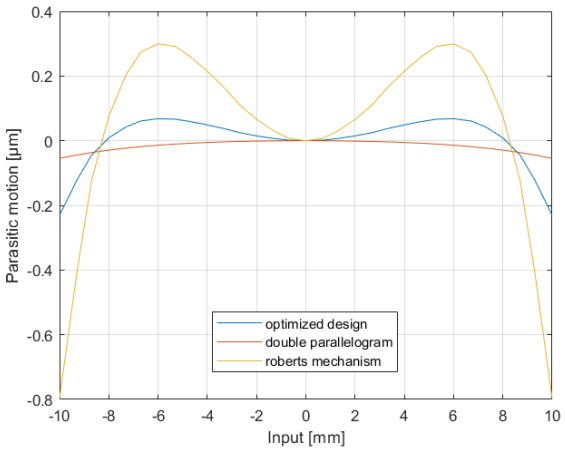

Figure 10: Comparison of parasitic translation between three different linear motion guides

yield stress of PLA. The bounds for the flexures and their optimized configuration are visualized in Figure 9. Note that the mechanism is mirror symmetric to reduce the amount of design parameters. These bounds were chosen with the idea to create a mix between the Roberts mechanism and the double parallelogram. The double parallelogram has very small parasitic motions, but lacks a good constrained middle body. In contrast, the Roberts mechanism has a good constrained middle body, but suffers from parasitic motion. The set bounds resulted for the optimized geometry to be a mix between the Roberts mechanism and the double parallelogram configuration. Because some flexures are angled the middle body is well constrained. During the synthesising process the geometry was optimized for straight flexures first. With an additional optimization the flexures were curved to further improve the performance of the linear motion guide.

The synthesized linear guide is compared with two other linear guides with approximately the same dimensions to benchmark its performance. In Figure 11 a double parallelogram and a linear guide based on Roberts mechanisms are visualized together with the optimized design. The Roberts mechanism was optimized with a similar procedure to find its optimal geometry. The bounds for the width of the Roberts mechanism were chosen to be identical to the bounds for the optimized design. In all designs the blue parts are modelled as 20mm thick beams connecting the flexures. Instead of giving all middle bodies equal weight, it is chosen to give all connecting beams of the intermediate bodies the same cross section. Some designs require bigger middle bodies and therefore using the same cross-section for the middle bodies is deemed as an appropriate comparison method. In this way the eigenfrequencies can be compared in a fair way. The material of all mechanisms is PLA and they have equal flexure thickness and out of plane thickness.

In Table 5 the most important properties of the three designs are summarized. In figures 10, 12 and 13 the comparison plots of the parasitic translation, parasitic rotation and stiffnesses are shown respectively.

The maximum Von Mises stress in the double parallelogram (2.67MPa) is significant lower compared to the other designs (19.2MPa and 20.3MPa). This is partly due to the longer flexures and the lower stiffnesses. The higher stiffness in the two other designs result in significant higher eigenfrequencies. Additionally, the intermediate bodies of the optimized design and Roberts mechanism are much better constrained compared to the double parallelogram. This results in a high uncontrollable mass frequency which is desirable from a control perspective. Their resonance

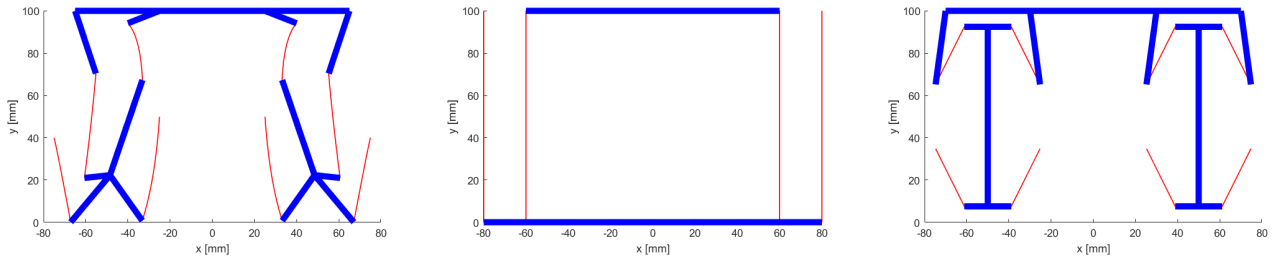

Figure 11: Overview of the different 1 DoF translational mechanism used for comparison. From left to right: optimized geometry, double parallelogram and roberts mechanism.

	Optimized design	Double parallelogram	Roberts mechanism
Maximum stress [MPa]	19.2	2.67	20.3
1st eigenfrequency [Hz]	8.87	2.54	9.57
2nd eigenfrequency [Hz]	29.8 (out of plane)	6.34	28.6 (out of plane)
3rd eigenfrequency [Hz]	96.3 (out of plane)	17.6 (out of plane)	75.6 (out of plane)
uncontrollable mass frequency [Hz]	113.5	6.34	599
motion range [mm]	(-10, 10)	(-10, 10)	(-10, 10)
max parasitic translation [nm]	232	54.5	797
max parasitic rotation [μrad]	134	11.6	99

Table 5: Comparison between the optimized design, double parallelogram and roberts mechanism

frequencies are respectively a factor 17.9 and 94.4 higher compared to the double parallelogram. Besides the extra flexures, the intermediate bodies are better constrained due to the arrangement of the flexures. The angled flexures constrain the middle bodies also in the horizontal direction. The 2nd and 3rd eigenfrequency of the optimized design (29.8Hz and 96.3Hz) are slightly higher as the Robert mechanism (28.6Hz and 75.6Hz), but the uncontrollable mass of the Roberts mechanism (599Hz) is much higher than that of the optimized design (133.5Hz).

The parasitic translation of the optimized design (maximum of 232nm) (Figure 10) is much smaller compared to the Roberts mechanism (maximum of 797nm). However, the double parallelogram has less parasitic motion (maximum of 54.5nm). Additionally, the parasitic rotation (Figure 12) of the double parallelogram (11.6μrad) is much smaller compared to the other designs (99μrad or 134μrad). This can be explained by the much smaller stiffness in x-direction. Therefore, the moment causing the parasitic rotation is much smaller. It is important to mention that the parasitic rotation was not the main objective of the optimization. If a tighter constraint for this rotation was set, the rotation could possibly be smaller but might effect other properties. Furthermore, the mechanisms are not actuated in the stiffness centers which could be a method to reduce the parasitic rotation. Lastly, the legs in the optimized design are placed mirror symmetric which could result in a small parasitic rotation. For example, each leg could have a little difference in parasitic motion when moving to the left or

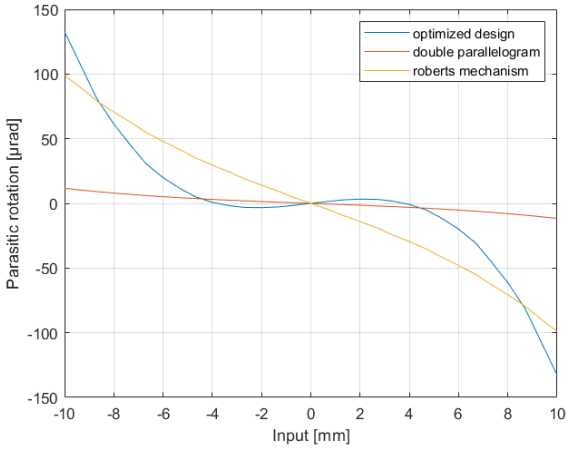

Figure 12: Comparison of parasitic rotation between three different linear motion guides

right. This mirror symmetric placement of the legs also has the potential to compensate for parasitic rotations.

The stiffness in the motion direction (K_x), support stiffness (K_y) and out of plane stiffness (K_z) are plotted in Figure 13. The support stiffness of the double parallelogram drops significantly and at a much higher rate compared to the other designs. Furthermore, the stiffnesses of the optimized design and Roberts mechanism are higher. The longer flexures and lower amount of flexures do probably effect the magnitude of the support stiffness, but not the

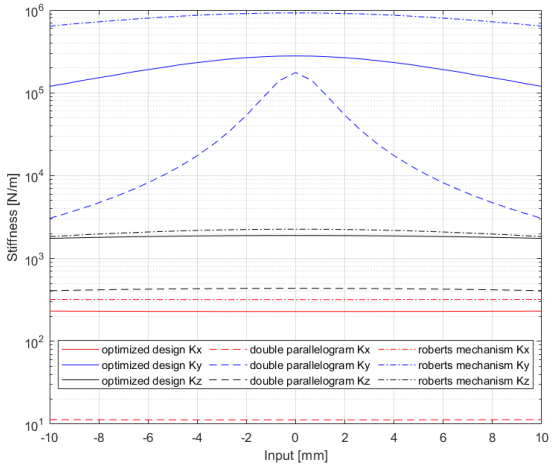

Figure 13: Comparison of stiffnesses between three different linear motion guides

excessive decay of stiffness. The support stiffness of the Roberts mechanism is significantly higher compared to the optimized design. This originates from the curved flexures in the optimized design and its flexure arrangement.

4.3. Decoupled 2-DoF Parallel Mechanism

The last case study is the optimization of a decoupled 2-DoF mechanism. The locations of the start and end points of the flexures from the previously presented case study were used as inputs for this optimization. Consequently, only the middle control points of the flexures needed to be optimized. This approach was chosen because the previous case study showed a flexure configuration with very small parasitic motions and would thus be a useful input to be used in this optimization. By controlling the curvature of the flexures the performance of the mechanism can be tweaked.

This unconventional mechanism layout is used to synthesize a compact mechanism without overconstraints in 2D (according to Grubler's Rule assuming that two parallel flexures represent a joint) and with relatively large range of motion to demonstrate this method's ability. In literature most 2-DoF stages are symmetric resulting in bulky designs, but this helps the decoupling of motions, constraining the parasitic rotation and increases the payload capability. In the synthesized mechanism the parasitic rotation and cross-couplings are reduced by the compensation within the mechanism. In this way the capability of the proposed method can be presented.

Instead of optimizing the mechanism to be output decoupled at its initial position, points at different locations are also considered. These points lie on the x & y axis and at the boundaries of the workspace. The constraint values used are given in Table 6.

In Table 7 the main properties of the 2-DoF mechanism are summarized. In Figure 14 the geometry of the mechanism is shown. All flexures look like straight flexures, but some of them are slightly curved. In comparison, if straight

Constraint	Value
Minimum distance between flexures	2.5 [mm]
Minimum radius of curvature	2 [mm]
Maximum stress	350 [MPa]
Maximum lost motion	1 [%]

Table 6: Constraint values for the decoupled 2-DoF parallel mechanism

flexures were used the maximum cross-coupling is 0.026% (optimized design 0.03%) and parasitic rotation 74μrad (optimized design 34μrad). So, the little cross-coupling is similar and origins from the flexure arrangement and the added little curvature reduced the parasitic rotation a factor 2.17. Additionally, if the curvature of the previous case study was used the cross-coupling is 0.25% and the parasitic rotation is 234μrad. This is much higher compared to the optimized geometries in this mechanism.

In Table 8 the synthesized design is compared with data of other 2-DoF output-decoupled compliant parallel mechanisms. In literature designs with similar workspace were selected to be used in this comparison.

The ratio between footprint and workspace of the optimized design is smaller than the other planar mechanisms. This is mainly due to the compact layout and not using symmetry. The spatial mechanisms have a smaller ratio due to their spatial configurations.

The cross-coupling of the optimized design (0.03%) is much smaller than the other planar designs cross-couplings ranging from 0.17% to 5.7%. Most of the designs in literature use the double parallelograms. These compliant structures lose a lot of their stiffness when they are under large deformations. The previous case study showed that the decay of stiffness of this configuration is much smaller. The cross-coupling is smaller possibly due to better stiffnesses and the optimization approach of minimizing the cross-coupling and parasitic rotation over the workspace.

The parasitic rotation of 34μrad is smaller than the asymmetric design of Hao [5] (62μrad) in which the actuation forces were designed to go through the stiffness center to prevent a parasitic rotation. The planar designs using a symmetric configuration have significantly lower parasitic rotations (between 0.4 and 7μrad). This is due to the symmetric configuration which better constrains the parasitic rotation. However, this symmetry also increases the lost motion percentage of these designs.

5. Experimental

The linear motion mechanism from the second case study is manufactured using a 3D-printer. The nozzle diameter was 0.4 mm and 0.2 mm thick layers of PLA were printed. In Figure 15 the test setup is visualized. A rope connects the 3D printed mechanism with a linear motion stage. Two laser distance sensors were used to measure the input motion and the parasitic motion. A piece of card was

Key properties	Value
Maximum stress	235 [MPa]
Motion range X-axis	[-5, 5] [mm]
Motion range Y-axis	[-5, 5] [mm]
Max cross-coupling	0.03 [%]
Max parasitic rotation	34 [μrad]

Table 7: Properties of the decoupled 2-DoF parallel mechanism

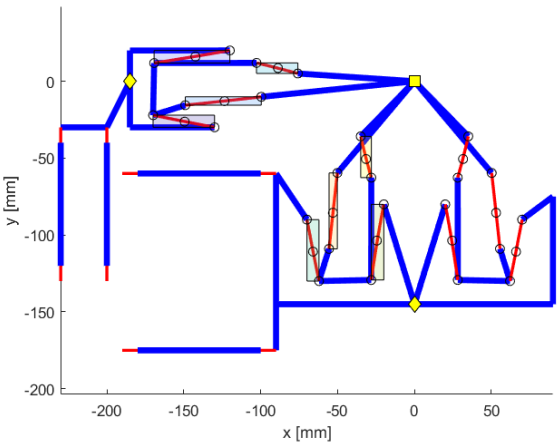

Figure 14: Optimized xy-manipulator. The red lines indicate the flexures, the blue lines represent the rigid parts. The boxes represent the bounds for the control points. The controlpoint locations are indicated with the circles. The yellow diamonds represent the input points and the yellow square the output point.

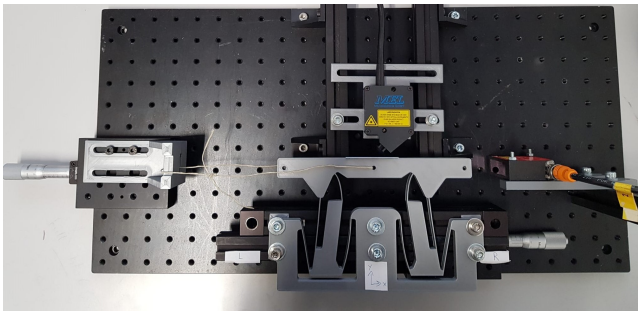

Figure 15: Test setup and the 3D printed prototype

glued on top of the mechanism to have a smooth measuring surface. The measurement data is corrected for angular misalignment errors induced by gluing this smooth surface on the 3D printed part.

In Figure 16 the measured parasitic motion is compared with FEM analysis. Two FEM analyses were performed in COMSOL Multiphysics. In one of these analyses the assumed rigid bodies were modelled as rigid bodies. This resulted in similar parasitic motions as in the optimization model. However, if the compliance of the rigid bodies is taken into account a significant higher parasitic motion is

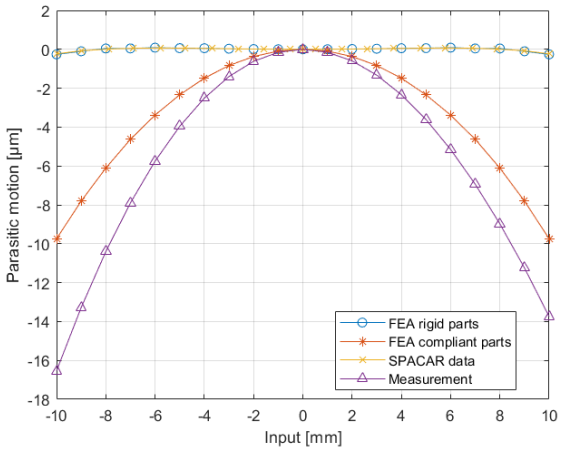

Figure 16: Measured parasitic motion of the linear motion mechanism with well constrained middle bodies (case study ii)

found. This effect was also observable in other compliant mechanisms and can be reduced by using thinner flexures and reducing stresses. A nonlinear FEA analysis in COMSOL showed for the double parallelogram and Roberts mechanism the same phenomenon. The severity of this issue for the double parallelogram was almost neglectable, but for the Roberts mechanism about equally severe as for the optimized design. This is caused by the difference in stress in the flexures at the connection points with the rigid bodies. If the stress is higher at these locations larger tiny deformations will occur resulting in additional parasitic motions. The measured unwanted motion was slightly higher than in the FEM analysis with the compliance of rigid parts taken into account.

6. Discussion

The previously shown optimization results show promising compliant structures in which the unwanted motions are reduced and the stiffness and dynamics were controlled. This method allows the designer to find new topologies of joints satisfying its constraints without being bounded by standard designs in literature. The presented method is a generic method which could also be used to synthesize other types of mechanisms. For example, in this paper only 2-dimensional geometries were synthesized, but the method could be extended to 3-dimensional mechanisms. Additionally, this paper focussed on linear motion mechanisms, but the same method could be used to synthesize rotational or rotational and translational mechanisms. Furthermore, instead of the two parallel flexures other joint input topologies could be used. Moreover, in this paper quadratic Bezier curves were used to model the flexures. Higher order Bezier curves could be used to allow for more complex curved flexures. Lastly, the width of the flexures was kept constant and could be varied as well.

	Optimized design	Yu [30]*	Yu [30]**	Liu [31]	Liu [32]	Hao [5]	Hao [10]	Hao [33]
Footprint / Workspace [−]	640	970	970	100	44	3025	1900	730
Workspace [mm^2]	100	100	100	100	400	16	100	400
Cross-coupling [%]	0.03	[0.17]	[0.29]	0.16	0.015	5.7	1.2	1.6
Parasitic rotation [μrad]	34	7	4	34	n/a	62	0.4	1
Lost motion [%]	0.04	[0.26]	[0.06]	n/a	1.1	n/a	3	4.5
Planar or spatial mechanism	Planar	Planar	Planar	Spatial	Spatial	Planar	Planar	Planar
Symmetric configuation	No	Yes	Yes	Yes	Yes	No	Yes	Yes
Double parallelogram	No	Yes	Yes	Yes	Yes	No***	No	Yes

Table 8: Mechanism comparison with literature data. (Experimental data is given between [ ] and FEA data without [ ]) * design without rigid connections ** design with rigid connections *** double parallelograms were only used to connect the input motion points with the base

The optimization time of this method increases when more beam elements are used to model the flexures more accurately or when more flexures are added to the design. An additional effect of adding more flexures is the increased chance of having flexures intersecting with each other. In this paper, a difference between geometry constraints and output constraints is made. For future research, one could try to create an optimization algorithm in which first the geometry constraints are used to find the regions satisfying the geometry constraints within the original bounds. These regions could then be used for the optimization in which the SPACAR model is evaluated. The evaluation time of the geometry constraints is in the order of milliseconds. In contrast, the time needed to evaluate the SPACAR model ranges between a second and a couple of minutes (depending on model size and amount of beam elements). This could reduce the overall optimization time because only valid potential designs would be evaluated by the computational expensive model.

A large difference between the optimized result and the experiment or FEM analysis with non rigid bodies was found for the parasitic translation ($232nm$, $16\mu m$ and $10\mu m$). It was stated that this difference resulted from the compliance in the rigid bodies. This effect can be significantly reduced by using thinner flexures. When using the same optimized geometry of case study ii, the maximum parasitic motion with $0.4mm$ thick flexures (instead of $0.8mm$) is according to the optimization model $-468nm$ and COMSOL $-2.43\mu m$. This difference is much smaller compared to the difference presented in section 5. Note also the effect on the maximum parasitic motion for the optimization model when using different thicknesses $-468nm$ ($0.4mm$ flexure thickness) and $-232nm$ ($0.8mm$ flexure thickness). With an additional optimization the design with the thinner flexures could possible be improved.

If the method presented in this paper is implemented in another FEA program which can take into account the deformations of the support structures, this method should also be able to compensate for the compliance in the assumed rigid bodies. It was shown that this method is able to compensate for parasitic motions in compliant mechanisms with rigid bodies, so this method should also be able to compensate for other non-idealities causing unwanted motions.

7. Conclusion

This paper presents a new method to synthesize linear motion compliant mechanisms with near zero parasitic motions and cross-couplings. The joints in an original chosen mechanism configuration are replaced by design domains. In these domains the shape of flexures are optimized. The flexures are modelled using Bezier curves. By optimizing the control point locations, the performance of the mechanism can be optimized. With this method the stiffness, dynamics, parasitic motions and cross-couplings of compliant mechanisms can be controlled and optimized. Three case studies were presented showing the capability of this new compensation approach.

The first case study presented a near constant stiffness linear motion joint. The maximum change in stiffness for K_x, K_y and K_z is 4.66% while the maximum parasitic motion in this joint is $3.56\mu m$ over a motion range of $\pm 5mm$.

In the second case study a linear guide with well constrained uncontrollable masses was synthesized. Simulation results showed a maximum parasitic translation of $232nm$ and a motion range of $\pm 10mm$. This is a factor 4.25 more than the popular double parallelogram configuration.

However, the uncontrollable mass frequency is a factor 17.9 higher. Experimental results showed a maximum parasitic translation of $16\mu m$. The difference between the simulation result and the measurement can be explained by the internal compliance of the mechanism.

The final case study presented a non-symmetric xy-stage with minimized cross-couplings and parasitic rotation. At multiple points within the workspace the properties of the mechanism were evaluated. The parasitic rotation was $34\mu rad$ and the cross-coupling 0.03%. This mechanism had smaller cross-couplings than other planer mechanisms with similar workspace. The parasitic rotation was smaller than other asymmetric designs shown in literature, but higher than the designs using a symmetric configuration.

References

[1] Rongfu Lin, Weizhong Guo, and Feng Gao. On parasitic motion of parallel mechanisms. *Proceedings of the ASME Design Engineering Technical Conference*, 5B-2016:1–13, 2016.

[2] Xiao Bing He, Jing Jun Yu, Wan Wan Zhang, and Guang Bo Hao. Effect of degree-of-symmetry on kinetostatic characteristics of flexure mechanisms: A comparative case study. *Chinese Journal of Mechanical Engineering (English Edition)*, 31, 2018.

[3] Y. S. Du, T. M. Li, Y. Jiang, and J. L. Zhang. Output decoupling property of planar flexure-based compliant mechanisms with symmetric configuration. *Mechanical Sciences*, 7(1):49–59, 2016.

[4] Guangbo Hao and Haiyang Li. Design of 3-legged XYZ compliant parallel manipulators with minimised parasitic rotations. *Robotica*, 33(4):787–806, may 2015.

[5] Guangbo Hao. A 2-legged XY parallel flexure motion stage with minimised parasitic rotation. *Proceedings of the Institution of Mechanical Engineers, Part C: Journal of Mechanical Engineering Science*, 228(17):3156–3169, 2014.

[6] Zhiqing Liu, Zhen Zhang, and Peng Yan. A self-adjusting stiffness center design for large stroke compliant XY nanomanipulators. *Mechanical Sciences*, 9(1):41–50, 2018.

[7] S. Z. Li, J. J. Yu, G. H. Zong, and Hai Jun Su. A compliance-based compensation approach for designing high-precision flexure mechanism. *Proceedings of the ASME Design Engineering Technical Conference*, 4(PARTS A AND B):293–301, 2012.

[8] Shouzhong Li and Jingjun Yu. Design principle of high-precision flexure mechanisms based on parasitic-motion compensation. *Chinese Journal of Mechanical Engineering (English Edition)*, 27(4):663–672, 2014.

[9] Guangbo Hao and Haiyang Li. Nonlinear analytical modeling and characteristic analysis of a class of compound multibeam parallelogram mechanisms. *Journal of Mechanisms and Robotics*, 7(4), 2015.

[10] Guangbo Hao, Qiaoling Meng, and Yangmin Li. Design of large-range XY compliant parallel manipulators based on parasitic motion compensation. *Proceedings of the ASME Design Engineering Technical Conference*, 6 A(August 2014), 2013.

[11] Hongzhe Zhao, Shusheng Bi, and Jingjun Yu. A novel compliant linear-motion mechanism based on parasitic motion compensation. *Mechanism and Machine Theory*, 50:15–28, 2012.

[12] Tonglong Huo, Jingjun Yu, Hongzhe Zhao, Haoran Wu, and Yuan Zhang. A family of novel RCM rotational compliant mechanisms based on parasitic motion compensation. *Mechanism and Machine Theory*, 156:104168, 2021.

[13] Georg Schitter, Philipp J. Thurner, and Paul K. Hansma. Design and input-shaping control of a novel scanner for high-speed atomic force microscopy. *Mechatronics*, 18(5-6):282–288, 2008.

[14] Yao Jiang, Tiemin Li, Liping Wang, and Feifan Chen. Systematic design method and experimental validation of a 2-DOF compliant parallel mechanism with excellent input and output decoupling performances. *Applied Sciences (Switzerland)*, 7(6), 2017.

[15] Yang Miao, Du Zhijiang, Sun Lining, and Dong Wei. Optimal design, modeling and control of a long stroke 3-PRR compliant parallel manipulator with variable thickness flexure pivots. *Robotics and Computer-Integrated Manufacturing*, 60(December 2018):23–33, 2019.

[16] Abdullah T. Elgammal, Mohamed Fanni, Manar Lashin, Mahmoud Magdy, and Abdelfatah M. Mohamed. Parametric design and analysis of a new 3D compliant manipulator for micromanipulation. *IEEE/ASME International Conference on Advanced Intelligent Mechatronics, AIM*, pages 1197–1202, 2017.

[17] G. Hao. Towards the design of monolithic decoupled XYZ compliant parallel mechanisms for multi-function applications. *Mechanical Sciences*, 4(2):291–302, 2013.

[18] Guangbo Hao, Haiyang Li, Xiuyun He, and Xianwen Kong. Conceptual design of compliant translational joints for high-precision applications. *Frontiers of Mechanical Engineering*, 9(4):331–343, 2014.

[19] Christine Vehar Jutte and Sridhar Kota. Design of nonlinear springs for prescribed load-displacement functions. *Journal of Mechanical Design, Transactions of the ASME*, 130(8):0814031–08140310, 2008.

[20] Christine Vehar Jutte and Sridhar Kota. Design of single, multiple, and scaled nonlinear springs for prescribed nonlinear responses. *Journal of Mechanical Design, Transactions of the ASME*, 132(1):0110031–01100310, 2010.

[21] Ashok Kumar Rai, Anupam Saxena, and Nilesh D. Mankame. Unified synthesis of compact planar path-generating linkages with rigid and deformable members. *Structural and Multidisciplinary Optimization*, 41(6):863–879, 2010.

[22] Minh Tuan Pham, Song Huat Yeo, Tat Joo Teo, Pan Wang, and Mui Ling Sharon Nai. A Decoupled 6-DOF Compliant Parallel Mechanism with Optimized Dynamic Characteristics Using Cellular Structure. *Machines*, 9(1):5, jan 2021.

[23] Chao-Chieh Lan and Yung-Jen Cheng. Distributed Shape Optimization of Compliant Mechanisms Using Intrinsic Functions. *Journal of Mechanical Design*, 130(7):1–10, 2008.

[24] Dong Xu and G. K. Ananthasuresh. Freeform skeletal shape optimization of compliant mechanisms. *Journal of Mechanical Design, Transactions of the ASME*, 125(2):253–261, 2003.

[25] Hong Zhou and Kwun-Lon Ting. Shape and Size Synthesis of Compliant Mechanisms Using Wide Curve Theory. *Journal of Mechanical Design*, 128:551–558, 2006.

[26] Minh Tuan Pham, Song Huat Yeo, Tat Joo Teo, Pan Wang, and Mui Ling Sharon Nai. Design and Optimization of a Three Degrees-of-Freedom Spatial Motion Compliant Parallel Mechanism with Fully Decoupled Motion Characteristics. *Journal of Mechanisms and Robotics*, 11(5):1–8, 2019.

[27] J. B. Jonker and J. P. Meijaard. SPACAR Computer Program for Dynamic Analysis of Flexible Spatial Mechanisms and Manipulators. In *Multibody Systems Handbook*, pages 123–143. Springer Berlin Heidelberg, Berlin, Heidelberg, 1990.

[28] *MATLAB (Version 9.8 (R2020a))*. The MathWorks Inc., Natick, Massachusetts, 2021.

[29] *Global Optimization Toolbox (Version 4.3)*. The MathWorks Inc., Natick, Massachusetts, 2021.

[30] Jingjun Yu, Yan Xie, Zhenguo Li, and Guangbo Hao. Design and experimental testing of an improved large-range decoupled XY compliant parallel micromanipulator. *Journal of Mechanisms and Robotics*, 7(4):1–6, 2015.

[31] Zhiqing Liu, Zhen Zhang, and Peng Yan. A spatial design of a large stroke compliant XY nanomanipulator with cross-coupling error reduction. *Proceedings of MARSS 2019: 4th International Conference on Manipulation, Automation, and Robotics at Small Scales*, (1), 2019.

[32] Hua Liu, Shixun Fan, Xin Xie, Zhiyong Zhang, and Dapeng Fan. Design and modeling of a novel monolithic parallel XY stage with centimeters travel range. *Advances in Mechanical Engineering*, 9(11):1–17, 2017.

[33] Guangbo Hao and Xianwen Kong. A Novel Large-Range XY Compliant Parallel Manipulator With Enhanced Out-of-Plane Stiffness. *Journal of Mechanical Design*, 134(6):1–9, jun 2012.

6

Testing and comparison with FEA

In this chapter the final test results are presented. Additionally, a detailed analysis of the test setup and the prototype are given. Multiple testing iterations led to the testing results presented in this chapter. Some of the testing iterations are presented in Appendix G. Before the test results are presented first some difficulties needed to be overcome for a successful experiment are elaborated.

6.1. Testing difficulties

The prototype is manufactured out of PLA using a PRUSA 3D printer. The part is printed using a $0.4mm$ nozzle diameter with 100% infill and a layer thickness of $0.2mm$. Due to the 3D printing there are some difficulties resulting in possible measurement errors. These are listed below and are further elaborated below.

1. Manufacturing tolerances
2. Surface roughness
3. Material properties
4. Warping

According to PRUSA the 3D printers have a tolerance of $0.1mm$ on the Z-axis and $0.3mm$ on the X and Y axis [45]. If additional calibrations are done the printers can be more accurate. It is unknown if the used printers are additional calibrated. These achievable tolerances are significant higher compared to the predicted parasitic motion.

Additionally, the first layers of the flexures are printed about 50% thicker as the other layers of the flexures. The first layers are about $1.2mm$ while the other layers of the flexures are about $0.80mm$ thick. Which is also the designed thickness. The first layers are probably thicker because they are printed on the heated print bed, while the other layers are printed on top of each other. This heated print bed is needed for a good adhesion between the print bed and the 3D printed part.

Another difficulty is the surface roughness of the prototype. For this experiment measurements are performed in the micrometer range. However, the part is not flat due to all the layers printed on top of each other and being slightly misaligned. In order to have a smooth measuring surface some additional parts needs to be glued on top of the part. This resulted in some other measurement difficulties and is explained later in more detail.

Thirdly, PLA is not the stiffest material and because the support stiffness is not constant due to its own weight the test piece would sag about $4\mu m$. Which is significant to the amount of parasitic motion is expected to be measured. Therefore, it is chosen to position the part horizontal instead of vertical. There will still be some displacement due to its own weight, but it will be less severe compared to a vertical placement of the part.

Finally, the 3D printed part can be warped due to the printing process. Different parts of the geometry are printed at different times leading to an uneven cooling pattern. This can lead to thermal stresses in the material and cause warping. The part was printed with a 100% infill to give the assumed rigid parts maximum stiffness. As a consequence the part is more prone to warping. Also, large prints are more prone to warping compared to smaller parts.

6.2. Measurement surface

Something flat needs to be glued onto the 3D printed mechanism because the 3D printed part is not flat. In Figure 6.1 the surface from the 3D printed part is shown. Between all layers are valleys which are significantly bigger as the expected parasitic motions. In Figure 6.2 the glued flat surface is shown.

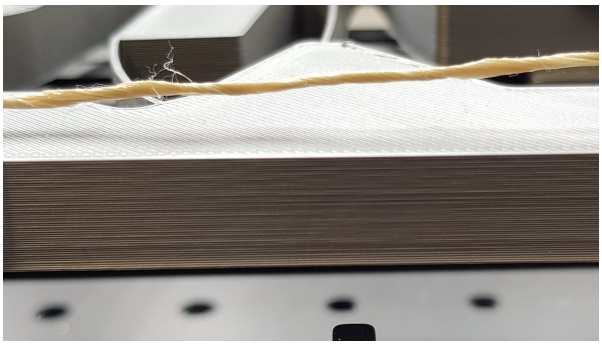

Figure 6.1: The surface of the 3D printed part. Due to the different layers placed on top of each other during the printing process a rough surface is manufactured.

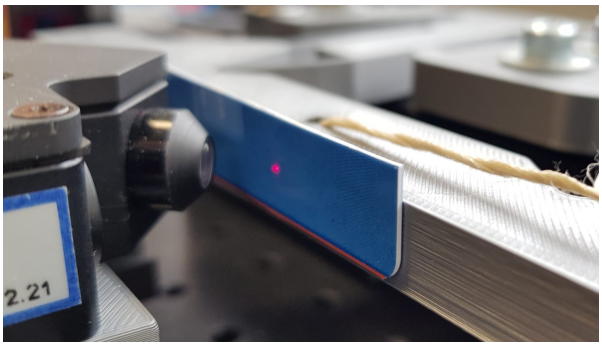

Figure 6.2: The assumed flat part glued onto the 3D printed part.

6.3. Measurement errors

In Figure 6.3 the ideal test setup situation is shown. In reality the test setup contains multiple errors. The most important ones are visualized in Figure 6.4. In the list below the different errors are indicated and elaborated.

1. Manufacturing error: the 3D printing process creates an irregular surface with ups and downs resulting in a non-flat surface. Also, the surface could be warped.
2. Surface error: The glued strip on the 3D printed part can be glued on it under an angle and the surface itself can also have some roughness. Though, the roughness is much smaller as the ones resulting from the 3D printing process. Additionally, the strip could also be warped.
3. Alignment error: The 3D printed parts is mounted on top of a linear stage. It is unlikely that they are aligned perfectly because they are bolted on top of each other.

6.4. Measurement setup and procedure

In Figure 6.5 the test setup is shown. The test setup is build using standard parts of Thorlabs. Two different laser distance sensors are used. The one used to measure the input (red) has a measuring range of $20mm$ and a resolution of $4\mu m$. The sensor used to measure the parasitic motion (MEL) has a measuring range of $0.5mm$ and a theoretical resolution of $500nm$. Both sensors were connected to a DAQ from national instruments and using labVIEW the data was recorded. The labVIEW program

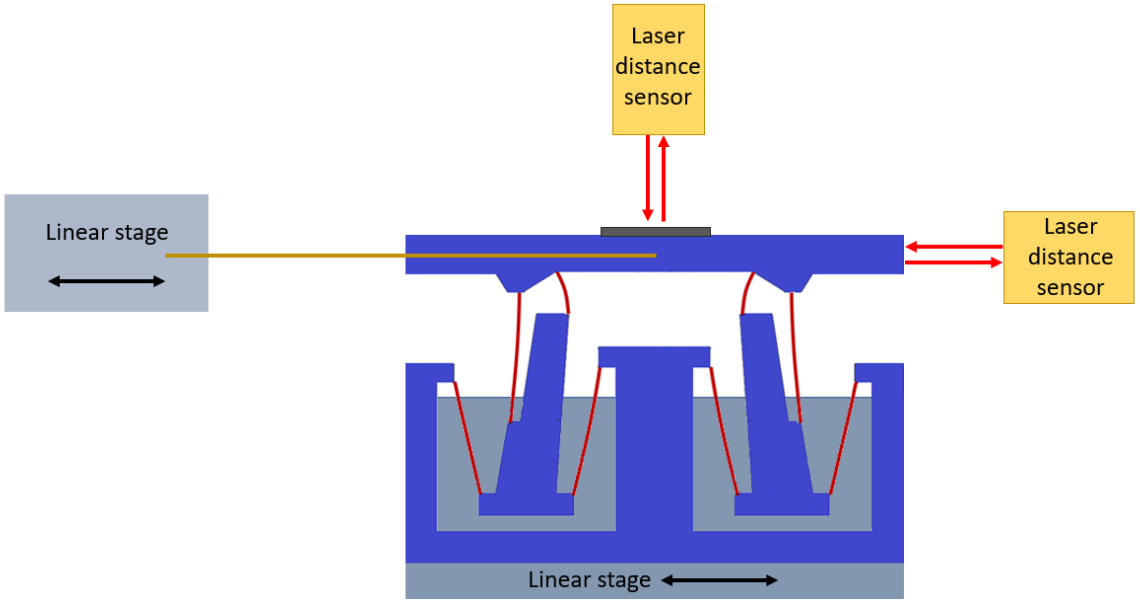

Figure 6.3: Ideal test setup

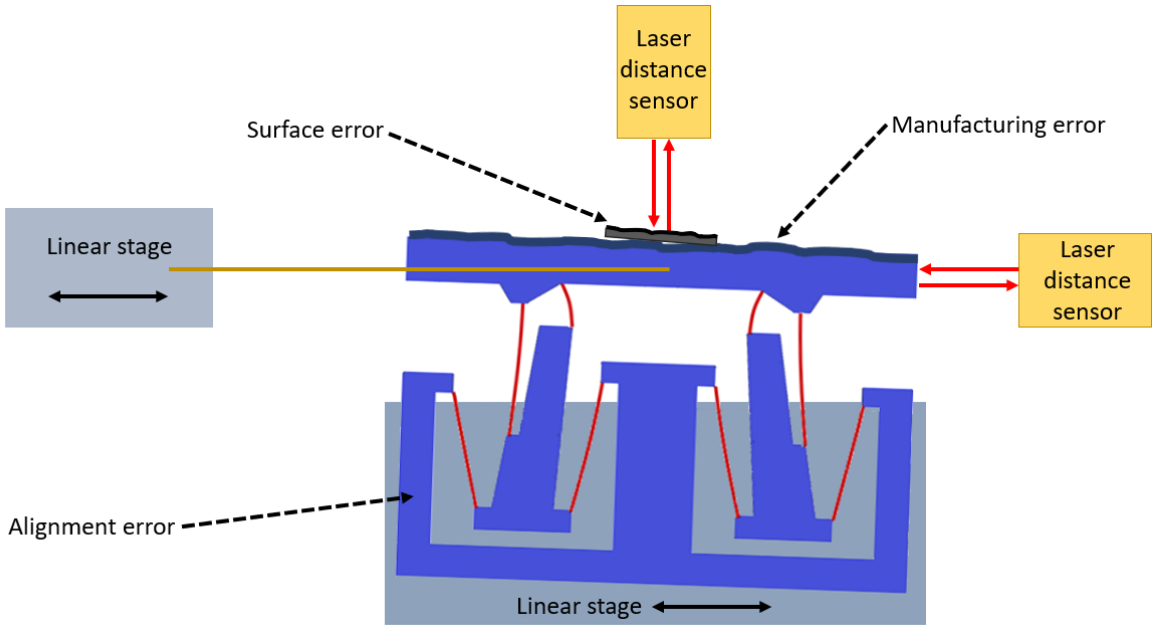

Figure 6.4: Test setup with indicated errors

saves the data at a rate of $500Hz$ with a resolution of $14\mu m$ and $1\mu m$ respectively. The data was post processed using Matlab.

There are multiple ways to correct/eliminate for the measurement errors. One of these methods is to measure the alignment error and surface error. This can be done by performing multiple measurements. These are listed below.

1. Compliant measurement: The linear stage on which the mechanism is mounted is kept at a fixed location. By moving the other linear stage tension can be put on the rope. Due to this tension the mechanism will undergo a compliant motion. The compliant measurement is the measurement of the distance between the laser distance sensor and the part glued onto mechanism.

2. Surface scan measurement: The rope is disconnected from the mechanism. The linear stage at

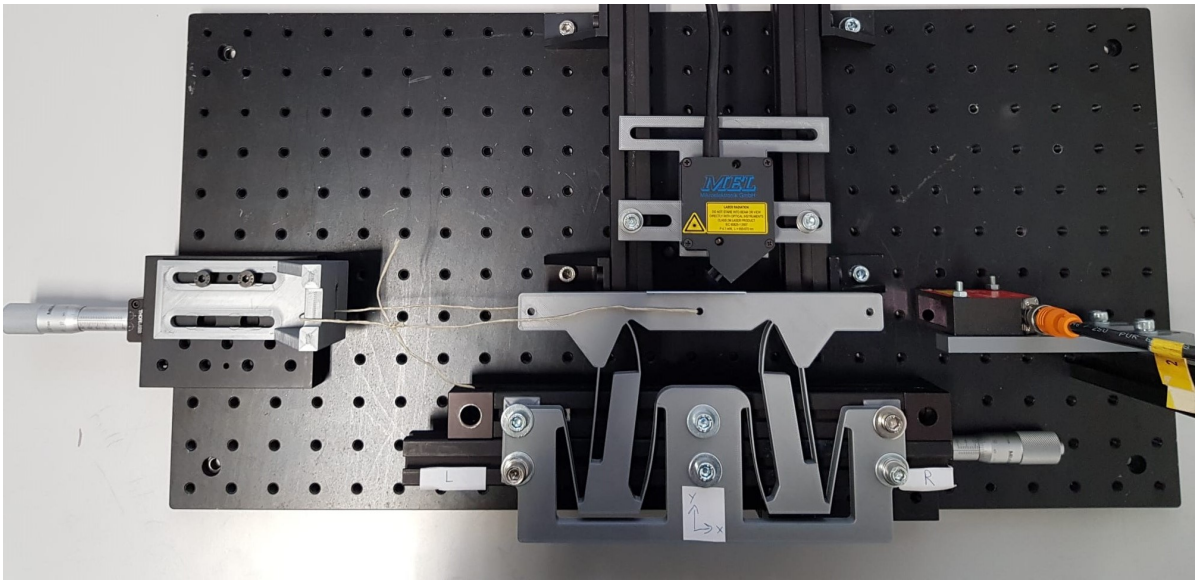

Figure 6.5: Test setup

which the mechanism is mounted is moved left or right. Again the distance between the sensor and the glued part is measured.

3. Alignment measurement: In this measurement the rope is again disconnected. The linear stage at which the mechanism is mounted is moved left and right. The distance between the sensor and the part is measured. Note that this measurement needs to be performed before the flat strip is glued onto the mechanism.

In Equation 6.1, 6.2 and 6.3 the measured properties for the compliant measurement, surface scan measurement and alignment measurement are given respectively.

$$\text{Compliant measurement} = \text{Parasitic motion} + \text{Surface error} + \text{Manufacturing error} \tag{6.1}$$

$$\text{Surface scan measurement} = \text{Surface error} + \text{Alignment error} + \text{Manufacturing error} \tag{6.2}$$

$$\text{Alignment measurement} = \text{Alignment error} + \text{Manufacturing error} \tag{6.3}$$

In Equation 6.4 the calculation of the parasitic motion is shown. Note that the manufacturing error cannot be eliminated using this test setup. Note that any internal manufacturing errors are not taken into account in this analysis. An internal manufacturing error could be a slight offset of a flexure.

$$\begin{aligned}\text{Parasitic motion} + \text{Manufacturing error} = \text{Compliant measurement} - \\ \text{Surface scan measurement} + \text{Alignment measurement}\end{aligned} \tag{6.4}$$

6.5. Measurement data and post processing

In Figure 6.6, 6.7 and 6.8 the alignment measurement, surface scan and compliant motion scan are plotted respectively. In all plots some fitted lines are indicated. Also, the plotted data shows many outliers. These outliers are probably from the not completely flat measurement surface. Additionally, the linear guides were by hand actuated which could induce external vibrations. It is assumed that the average between these ups and downs gives a good representation of the real situation. Also, their are some clear trends visible in the data. These trends are visualized by fitting polynomials to the data. In Figure 6.7 and 6.8 around $x = -5mm$ one big outlier can be identified. This is probably caused by a scratch in the measurement surface.

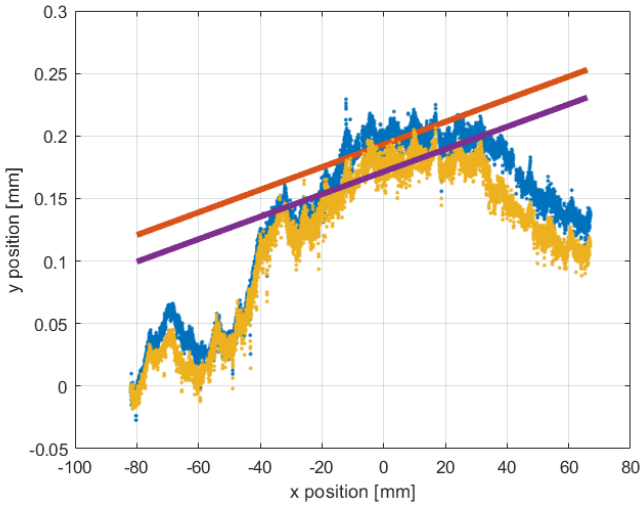

Figure 6.6: The alignment measurement. The lines are fitted between $-20mm$ and $20mm$. The slope of the lines indicate an alignment error of approximately $0.05°$.

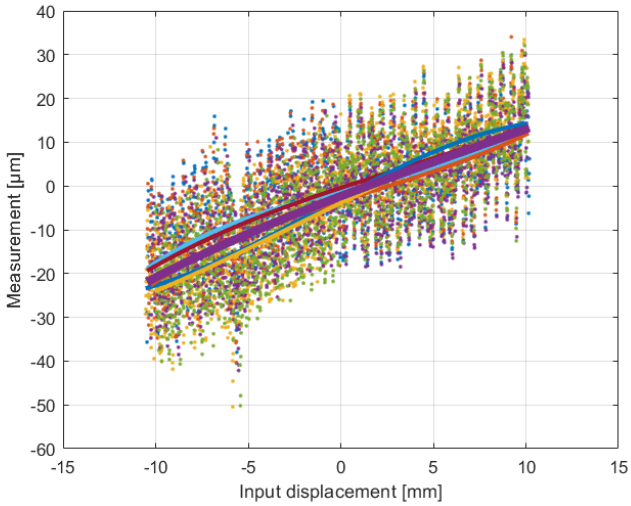

Figure 6.7: The surface scan measurement. Five different sets of data are plotted. The purple line indicates the average polynomial fit of all data sets. The order of the polynomial is three.

With the gathered data and the previously introduced equations the parasitic motion of the mechanism can be calculated. The results are plotted in Figure 6.9. In this plot the influence of the order of the fitted polynomials is also given. A first order polynomial clearly does not work. Which makes sense because it is a straight line and the expected parasitic motion has a parabolic shape. The other polynomials are very similar to each other. If the order of the polynomials is higher a higher sensitivity to measurement errors is expected.

The parasitic motion does not seem to be symmetrical. Several reasons which could have caused this are listed below.

1. Alignment measurement: the final compliant motion is very sensitive to the measured alignment error. A slightly higher or lower estimated alignment error directly impacts the final result. The alignment measurement consisted of multiple measurements at different positions along the 3D printed part. Since, the linear stages and sensors have limited ranges the measurement needed to be repeated multiple times. The sensor needed to be moved to a new position to perform the next part of the measurement. Connecting these datasets together could have resulted in

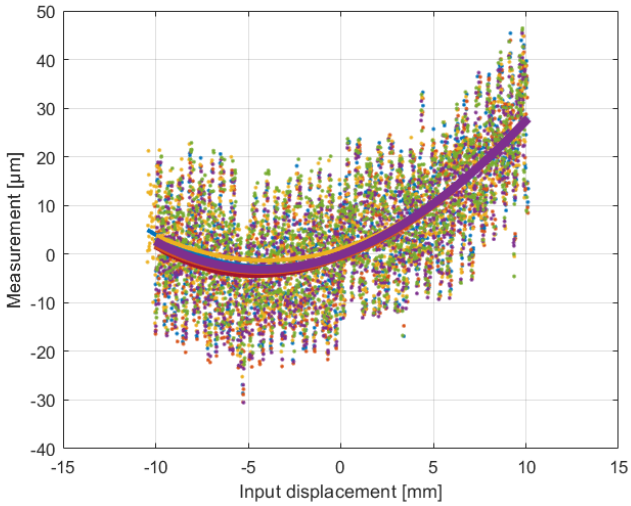

Figure 6.8: The compliant motion scan measurement. Five different sets of data are plotted. The purple line indicates the average polynomial fit of all data sets. The order of the polynomial is three.

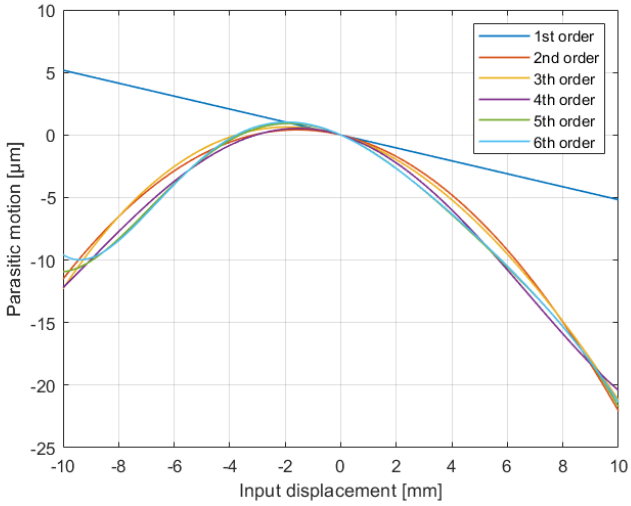

Figure 6.9: The measured parasitic motion after correcting the data. Different order of polynomials are plotted to indicate the effect of higher order fittings.

small errors. Additionally, the 3D printed part was mounted on a linear motion stage. These linear motion stages are never perfect and could also introduce some error resulting in a larger or smaller alignment error.

2. Rotational stiffness of the linear stage: the rotational stiffness of the linear motion stage is not infinite. When doing the compliant motion a tiny rotation could occur. Resulting in a tiny rigid body rotation of the 3D printed part during the measurement. This could also lead to some error. The measurement point of the 3D printed part is not placed directly above the linear stage but at an offset. This amplifies the error induced by the tiny rotation of the linear motion stage.

3. Internal manufacturing error: The 3D printed part is never perfectly printed which could cause some errors.

Another way of interpreting the data is to only consider the compliant motion scan. Since the mechanism is symmetrical the parasitic motion should also be symmetrical. This property can be used to compensate for the surface error of the measurement (Assuming that the glued part is flat and not sig-

nificantly warped). The derivative of the fitted data should be zero at the initial position. In reality this derivative is not zero, indicating there is a angular error (the angle at which the flat surface is glued on the 3D printed prototype). This error can be compensated by correcting for this angle. This is shown in Equation 6.5. Applying this method results in the measured parasitic motion shown in Figure 6.10. Using this method measurement errors during the alignment and surface scan measurement are not present.

$$\text{Parasitic motion} = \text{Compliant measurement} - \frac{dy}{dx}\text{Compliant measurement(initial position)} * \text{position} \tag{6.5}$$

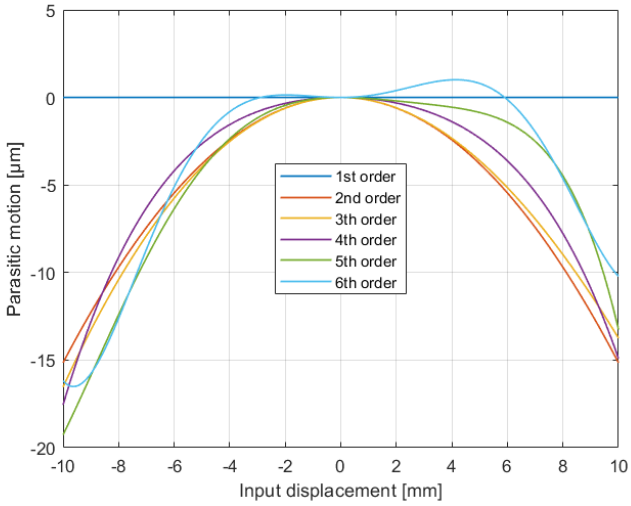

Figure 6.10: The measured parasitic motion after correcting the data using the symmetry property. Different order of polynomials are plotted to indicate the effect of higher order fittings.

6.6. Difference between test results and SPACAR results

The measured parasitic motion differs quite a lot from the SPACAR result. In order to better understand the differences between the SPACAR results and the experimental results a non-linear 2D finite element analysis is performed. Fourth order elements are used in COMSOL Multiphysics for this analysis.

In Figure 6.11 the displacement is plotted. The color scale is adjusted to visualize the small displacements in the base of the mechanism. These deformations of the base are in the order of a micrometer and most severe at the connections between the flexures and the assumed rigid parts. The deformations in the moving bodies are not visible in this figure, but it is more than likely that the tiny deformations are also present in these bodies. All these small deformations are not taken into account in the SPACAR optimization model and can explain the large difference between the test results and the SPACAR model.

If the same COMSOL model is evaluated, but now with the assumed rigid bodies modelled rigidly the small deformations are not present. This results in a very similar parasitic motion compared to the SPACAR data. In Figure 6.12 the parasitic motion data from the FEA analysis with and without rigid bodies and SPACAR is shown. When the bodies are assumed to be rigid the SPACAR and COMSOL Multiphysices model data matches almost perfectly. However, when the small deformations are taken into account a significant difference can be identified. For future designs one could take these effects into account or design a stiffer surrounding structure. Also, if thinner flexures are used this effect will be smaller. The flexures exert a force on the 'rigid bodies' and if the flexures are smaller these forces and thus deformations will be smaller.

Similar effects can be observed when for example a double parallelogram mechanism or Roberts mechanism is modelled in both software packages. However, for the double parallelogram this issue is almost neglectable, but for the Roberts mechanism about equally severe as for the optimized design.

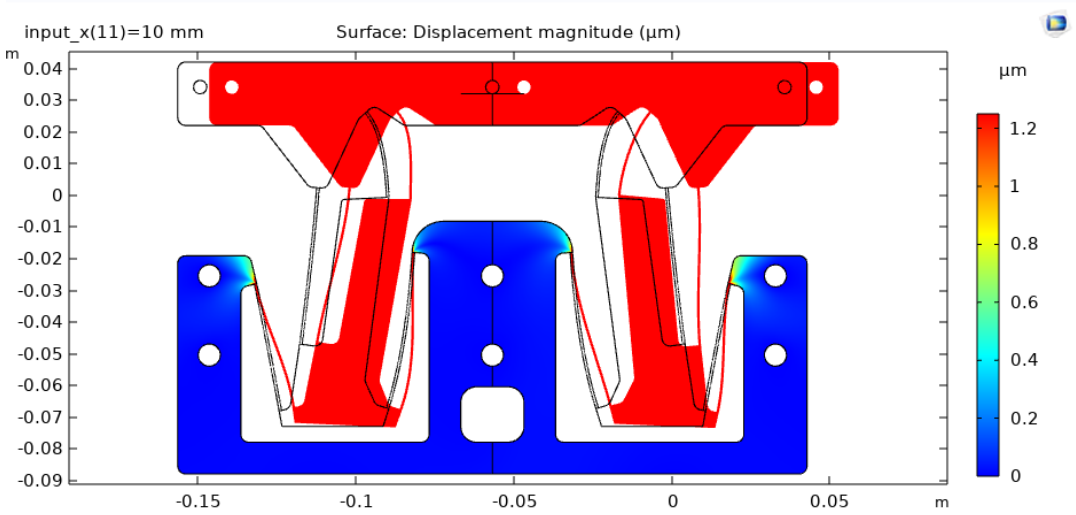

Figure 6.11: Comsol displacements plot with the bodies not rigid modelled

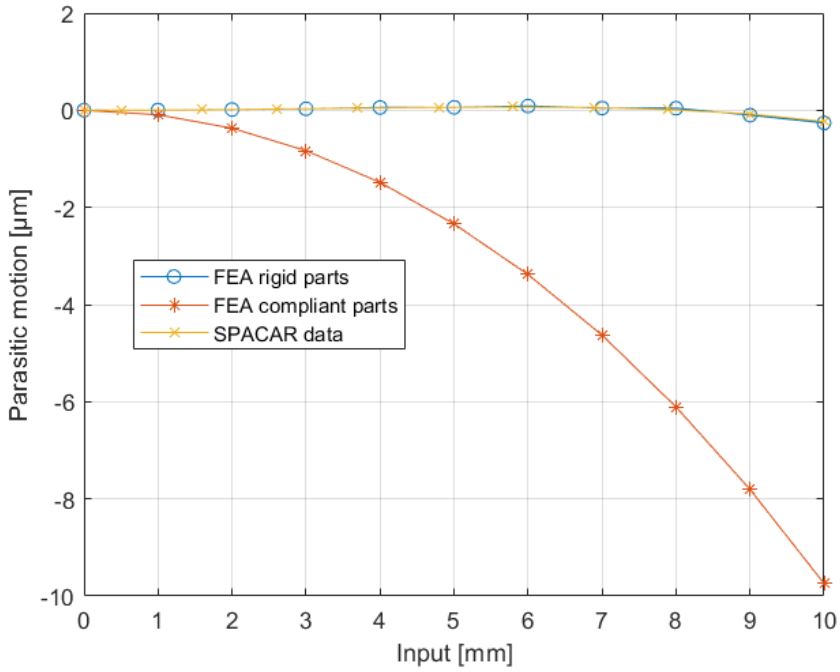

Figure 6.12: Comparison between SPACAR and COMSOL Multiphysics parasitic motion data

Due to the much lower stress in the double parallelogram this effect is much smaller. More about this can be read in Appendix H.

In Figure 6.13 the measured parasitic motion is compared with the FEA data. The measured parasitic motion is bigger as all FEA analysis. The magintude of the measurement is in the same order as FEA with compliant parts. Several hypothesis for this difference are elaborated in the list below.

1. Support stiffness: the 3D printing process can result in lower stiffness as desired which lead to bigger displacement at the supports causing more parasitic motion.

2. Measurement inaccuracies: Several things have been done to perform the measurement. For example, something flat is glued on top of the mechanism. This flat part could also have been slightly warped resulting in a measurement error. Also, the alignment of the sensor with the part might have a small impact on the measurement. Thirdly, it is assumed that the part does not

move in the out of plane direction when pulling on the rope. This out of plane movement could also be a source of error.

3. Manufacturing errors: For some of the manufacturing errors was accounted, but any internal error could not be corrected. For example, a slightly longer flexure or a warped base structure leading to misaligned flexures.

4. Stiffness of linear stage: the 3D printed part was mounted on top of a linear stage. This linear stage does not have infinite rotational stiffness. When pulling on the rope this stage could also have rotated slightly. This tiny rotation can result in some measurement error.

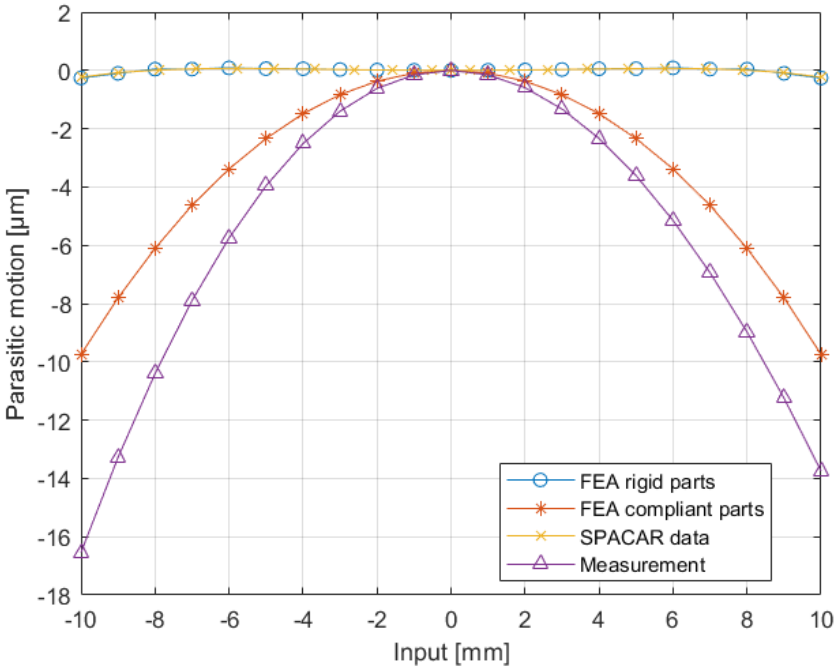

Figure 6.13: Comparison of measurement with FEA-analysis

7

Conclusion and recommendations

This report consisted of two parts. During the first part of the report the following research question was used: What are the strategies to minimize parasitic motions and cross-axis couplings in parallel compliant mechanisms? Twelve different strategies were found in literature and compared with each other. Only three strategies were identified to have the theoretical ability to fully compensate for translational and rotational parasitic motion and cross-couplings in a continuous manner. These three strategies are listed below:

1. Compensate the overall parasitic motion of a mechanism by placing a module in series with opposite but equal parasitic motion
2. Compensate the overall parasitic motions in a mechanism by using parasitic motion in its joints
3. Optimize the joints in a mechanism

From these three strategies the use of the first one results in mechanisms with decreased stiffness, uncontrollable masses, increased moving mass and increased size. The second strategy is currently barely used and if it is applied correctly it doesn't effect the systems performance in theory significantly. The last strategy is currently used to design perfect joints (no unwanted motions). In this way a mechanism configuration without unwanted motions can be used. A combination of the latter two strategies from the literature study were combined resulting in a new compensation strategy for the parasitic motions and cross-couplings.

The second part of the report focussed on this new strategy. In a mechanism certain joints can be replaced by a design domain. In these design domains joints can be synthesized using shape optimization of two parallel flexures. By optimizing the joints the overall unwanted motions of the mechanism can be compensated. This method can be used on joint, guide or mechanism level as shown in the case studies. Based on the literature study and the optimization results shown in this report the following conclusions were made:

1. In theory the parasitic motions and/or cross-couplings can be almost completely compensated
2. This method allows for synthesizing new types of joints and variants/mixtures of current joint designs
3. The stiffnesses and stiffness ratio's of compliant structures can be controlled while compensating unwanted motions
4. Intermediate bodies can be properly constrained avoiding uncontrollable masses at low eigenfrequencies
5. The compensation can be achieved over a large range of motion

Several recommendations are listed on the next page. These recommendations are based on the optimization experience and finite element comparison. The second recommendation is based on information presented in Appendix E.

1. Take the deformations of the support structure of rigid bodies into account during optimization.
2. Although branches didn't reduce the parasitic motions they could be used to reduce stress at the connections with rigid parts. Adding branches at both ends of the flexures might reduce the tiny deformations in the assumed rigid structures. This could reduce the parasitic motions of the compliant mechanisms in the real world.
3. The best optimization results are achieved when using smart input geometries. It is recommanded to choose the inputs carefully to find good optimized geometries.
4. Start the optimization with straight flexures. This results in quicker optimized designs and with small unwanted motions. If needed curvature can be added to these straight flexures to improve performance.

Bibliography

[1] Shorya Awtar and Alexander H. Slocum. Constraint-based design of parallel kinematic XY flexure mechanisms. *Journal of Mechanical Design, Transactions of the ASME*, 129(8):816–830, 2007. ISSN 10500472. doi: 10.1115/1.2735342.

[2] Kee Bong Choi and Doo Hyeong Kim. Monolithic parallel linear compliant mechanism for two axes ultraprecision linear motion. *Review of Scientific Instruments*, 77(6), 2006. ISSN 00346748. doi: 10.1063/1.2207368.

[3] Kee Bong Choi, Jae Jong Lee, Gee Hong Kim, and Seiichi Hata. Mechanical performances of a piezo-driven stage with 4-PP compliant guide mechanism. *ICCAS-SICE 2009 - ICROS-SICE International Joint Conference 2009, Proceedings*, pages 5529–5532, 2009.

[4] Bingxiao Ding and Yangmin Li. Design and analysis of a decoupled XY micro compliant parallel manipulator. *2014 IEEE International Conference on Robotics and Biomimetics, IEEE ROBIO 2014*, pages 1898–1903, 2014. doi: 10.1109/ROBIO.2014.7090613.

[5] Y. S. Du, T. M. Li, Y. Jiang, and J. L. Zhang. Output decoupling property of planar flexure-based compliant mechanisms with symmetric configuration. *Mechanical Sciences*, 7(1):49–59, 2016. ISSN 2191916X. doi: 10.5194/ms-7-49-2016.

[6] Abdullah T. Elgammal, Mohamed Fanni, Manar Lashin, Mahmoud Magdy, and Abdelfatah M. Mohamed. Parametric design and analysis of a new 3D compliant manipulator for micromanipulation. *IEEE/ASME International Conference on Advanced Intelligent Mechatronics, AIM*, pages 1197–1202, 2017. doi: 10.1109/AIM.2017.8014181.

[7] Grigore Gogu. *Structural Synthesis of Parallel Robots*, volume 149 of *Solid Mechanics and its Applications*. Springer Netherlands, Dordrecht, 2008. ISBN 978-1-4020-5102-9. doi: 10.1007/978-1-4020-5710-6. URL http://link.springer.com/10.1007/978-1-4020-5710-6.

[8] G. Hao. Towards the design of monolithic decoupled XYZ compliant parallel mechanisms for multi-function applications. *Mechanical Sciences*, 4(2):291–302, 2013. ISSN 21919151. doi: 10.5194/ms-4-291-2013.

[9] Guangbo Hao. A 2-legged XY parallel flexure motion stage with minimised parasitic rotation. *Proceedings of the Institution of Mechanical Engineers, Part C: Journal of Mechanical Engineering Science*, 228(17):3156–3169, 2014. ISSN 20412983. doi: 10.1177/0954406214526865.

[10] Guangbo Hao and Xianwen Kong. Conceptual design and modelling of a self-Adaptive compliant parallel gripper for high-precision manipulation. *Proceedings of the ASME Design Engineering Technical Conference*, 4(PARTS A AND B):161–167, 2012. doi: 10.1115/DETC2012-70045.

[11] Guangbo Hao and Xianwen Kong. A Novel Large-Range XY Compliant Parallel Manipulator With Enhanced Out-of-Plane Stiffness. *Journal of Mechanical Design*, 134 (6):1–9, jun 2012. ISSN 1050-0472. doi: 10.1115/1.4006653. URL https://asmedigitalcollection.asme.org/mechanicaldesign/article/doi/10.1115/1.4006653/432450/A-Novel-LargeRange-XY-Compliant-Parallel.

[12] Guangbo Hao and Haiyang Li. Design of 3-legged XYZ compliant parallel manipulators with minimised parasitic rotations. *Robotica*, 33(4):787–806, may 2015. ISSN 0263-5747. doi: 10.1017/S0263574714000575. URL https://www.cambridge.org/core/product/identifier/S0263574714000575/type/journal{_}article.

[13] Guangbo Hao and Haiyang Li. Nonlinear analytical modeling and characteristic analysis of a class of compound multibeam parallelogram mechanisms. *Journal of Mechanisms and Robotics*, 7(4), 2015. ISSN 19424310. doi: 10.1115/1.4029556. URL http://asmedigitalcollection.asme.org/mechanismsrobotics/article-pdf/7/4/041016/6253583/jmr{_}007{_}04{_}041016.pdf.

[14] Guangbo Hao and Jingjun Yu. Design, modelling and analysis of a completely-decoupled XY compliant parallel manipulator. *Mechanism and Machine Theory journal*, 102:179–195, 2016. doi: 10.1016/j.mechmachtheory.2016.04.006. URL http://dx.doi.org/10.1016/j.mechmachtheory.2016.04.006.

[15] Guangbo Hao, Qiaoling Meng, and Yangmin Li. Design of large-range XY compliant parallel manipulators based on parasitic motion compensation. *Proceedings of the ASME Design Engineering Technical Conference*, 6 A(August 2014), 2013. doi: 10.1115/DETC2013-12206.

[16] Xiao Bing He, Jing Jun Yu, Wan Wan Zhang, and Guang Bo Hao. Effect of degree-of-symmetry on kinetostatic characteristics of flexure mechanisms: A comparative case study. *Chinese Journal of Mechanical Engineering (English Edition)*, 31, 2018. ISSN 21928258. doi: 10.1186/s10033-018-0235-4.

[17] Thomas R Hicks and Paul D Atherton. *The Nanopositioning Book*. Queensgate Instruments Ltd, Devon, UK, 1997.

[18] Jonathan B. Hopkins and Martin L. Culpepper. A screw theory basis for quantitative and graphical design tools that define layout of actuators to minimize parasitic errors in parallel flexure systems. *Precision Engineering*, 34(4):767–776, 2010. ISSN 01416359. doi: 10.1016/j.precisioneng.2010.05.004. URL http://dx.doi.org/10.1016/j.precisioneng.2010.05.004.

[19] Jonathan B. Hopkins and David McCalib. Synthesizing multi-axis flexure systems with decoupled actuators. *Precision Engineering*, 46:206–220, 2016. ISSN 01416359. doi: 10.1016/j.precisioneng.2016.04.015. URL http://dx.doi.org/10.1016/j.precisioneng.2016.04.015.

[20] Tonglong Huo, Jingjun Yu, Hongzhe Zhao, Haoran Wu, and Yuan Zhang. A family of novel RCM rotational compliant mechanisms based on parasitic motion compensation. *Mechanism and Machine Theory*, 156:104168, 2021. ISSN 0094114X. doi: 10.1016/j.mechmachtheory.2020.104168. URL https://doi.org/10.1016/j.mechmachtheory.2020.104168.

[21] Yao Jiang, Tiemin Li, Liping Wang, and Feifan Chen. Systematic design method and experimental validation of a 2-DOF compliant parallel mechanism with excellent input and output decoupling performances. *Applied Sciences (Switzerland)*, 7(6), 2017. ISSN 20763417. doi: 10.3390/app7060591.

[22] Christine Vehar Jutte and Sridhar Kota. Design of nonlinear springs for prescribed load-displacement functions. *Journal of Mechanical Design, Transactions of the ASME*, 130(8): 0814031–08140310, 2008. ISSN 10500472. doi: 10.1115/1.2936928.

[23] Christine Vehar Jutte and Sridhar Kota. Design of single, multiple, and scaled nonlinear springs for prescribed nonlinear responses. *Journal of Mechanical Design, Transactions of the ASME*, 132(1):0110031–01100310, 2010. ISSN 10500472. doi: 10.1115/1.4000595.

[24] Lei-Jie Lai, Guo-Ying Gu, and Li-Min Zhu. Design and control of a decoupled two degree of freedom translational parallel micro-positioning stage. *Rev. Sci. Instrum*, 83:45105, 2012. doi: 10.1063/1.3700182. URL https://doi.org/10.1063/1.3700182.

[25] Leijie Lai, Guo Ying Gu, Pengzhi Li, and Limin Zhu. Design of a decoupled 2-DOF translational parallel micro-positioning stage. *Proceedings - IEEE International Conference on Robotics and Automation*, pages 5070–5075, 2011. ISSN 10504729. doi: 10.1109/ICRA.2011.5979723.

[26] Ming-yih Lee. Development of Kinematic / Kinetic Performance Tools in Synthesis of ulti-DOF Mechanisms. *Transactions of the ASME*, 115:462–471, 1993.

[27] Haiyang Li and Guangbo Hao. Position-space-based design of a symmetric spatial translational compliant mechanism for micro-/nano-manipulation. *Micromachines*, 9(4):1–18, 2018. ISSN 2072666X. doi: 10.3390/mi9040189.

[28] Haiyang Li, Guangbo Hao, and Richard C. Kavanagh. A new XYZ compliant parallel mechanism for micro-/nano-manipulation: Design and analysis. *Micromachines*, 7(2), 2016. ISSN 2072666X. doi: 10.3390/mi7020023.

[29] Haiyang Li, Guangbo Hao, and Richard C. Kavanagh. Position-Space-Based Compliant Mechanism Reconfiguration Approach and Its Application in the Reduction of Parasitic Motion. *Journal of Mechanical Design, Transactions of the ASME*, 138(9):1–13, 2016. ISSN 10500472. doi: 10.1115/1.4033988.

[30] S. Z. Li, J. J. Yu, G. H. Zong, and Hai Jun Su. A compliance-based compensation approach for designing high-precision flexure mechanism. *Proceedings of the ASME Design Engineering Technical Conference*, 4(PARTS A AND B):293–301, 2012. doi: 10.1115/DETC2012-71018.

[31] Shouzhong Li and Jingjun Yu. Design principle of high-precision flexure mechanisms based on parasitic-motion compensation. *Chinese Journal of Mechanical Engineering (English Edition)*, 27 (4):663–672, 2014. ISSN 10009345. doi: 10.3901/CJME.2014.0415.076.

[32] Yangmin Li and Qingsong Xu. Design of a new decoupled XY flexure parallel kinematic manipulator with actuator isolation. *2008 IEEE/RSJ International Conference on Intelligent Robots and Systems, IROS*, pages 470–475, 2008. doi: 10.1109/IROS.2008.4650580.

[33] Yangmin Li and Qingsong Xu. Design and analysis of a totally decoupled flexure-based XY parallel micromanipulator. *IEEE Transactions on Robotics*, 25(3):645–657, 2009. ISSN 15523098. doi: 10.1109/TRO.2009.2014130.

[34] Yangmin Li and Qingsong Xu. Development and assessment of a novel decoupled XY parallel micropositioning platform. *IEEE/ASME Transactions on Mechatronics*, 15(1):125–135, 2010. ISSN 10834435. doi: 10.1109/TMECH.2009.2019956.

[35] Yangmin Li and Qingsong Xu. A novel piezoactuated XY stage with parallel, decoupled, and stacked flexure structure for micro-/nanopositioning. *IEEE Transactions on Industrial Electronics*, 58(8):3601–3615, 2011. ISSN 02780046. doi: 10.1109/TIE.2010.2084972.

[36] Rongfu Lin, Weizhong Guo, and Feng Gao. On parasitic motion of parallel mechanisms. *Proceedings of the ASME Design Engineering Technical Conference*, 5B-2016:1–13, 2016. doi: 10.1115/DETC2016-59859.

[37] Mingxiang Ling, Junyi Cao, Zhou Jiang, Minghua Zeng, and Qisheng Li. Optimal design of a piezo-actuated 2-DOF millimeter-range monolithic flexure mechanism with a pseudo-static model. *Mechanical Systems and Signal Processing*, 115:120–131, 2019. ISSN 10961216. doi: 10.1016/j.ymssp.2018.05.064. URL https://doi.org/10.1016/j.ymssp.2018.05.064.

[38] Hua Liu, Shixun Fan, Xin Xie, Zhiyong Zhang, and Dapeng Fan. Design and modeling of a novel monolithic parallel XY stage with centimeters travel range. *Advances in Mechanical Engineering*, 9(11):1–17, 2017. ISSN 16878140. doi: 10.1177/1687814017729624.

[39] Min Liu, Jinqing Zhan, and Xianmin Zhang. Topology optimization of distributed flexure hinges with desired performance. *Engineering Optimization*, 52(3):405–425, 2020. ISSN 10290273. doi: 10.1080/0305215X.2019.1595612.

[40] Zhiqing Liu, Zhen Zhang, and Peng Yan. A self-adjusting stiffness center design for large stroke compliant XY nanomanipulators. *Mechanical Sciences*, 9(1):41–50, 2018. ISSN 2191916X. doi: 10.5194/ms-9-41-2018.

[41] Zhiqing Liu, Zhen Zhang, and Peng Yan. A spatial design of a large stroke compliant XY nanomanipulator with cross-coupling error reduction. *Proceedings of MARSS 2019: 4th International Conference on Manipulation, Automation, and Robotics at Small Scales*, (1), 2019. doi: 10.1109/MARSS.2019.8860928.

[42] Yang Miao, Du Zhijiang, Sun Lining, and Dong Wei. Optimal design, modeling and control of a long stroke 3-PRR compliant parallel manipulator with variable thickness flexure pivots. *Robotics and Computer-Integrated Manufacturing*, 60(December 2018):23–33, 2019. ISSN 07365845. doi: 10.1016/j.rcim.2019.05.014.

[43] Van Khien Nguyen, Duy Luong Tuong, Huy Tuan Pham, and Huy Hoang Pham. Design and Optimization of a New Hollow Circular Flexure Hinge for Precision Mechanisms. *Applied Mechanics and Materials*, 889(c):337–345, 2019. doi: 10.4028/www.scientific.net/amm.889.337.

[44] Zongyue Ni, Dawei Zhang, Yingjun Wu, Yanling Tian, and Ming Hu. Analysis of parasitic motion in parallelogram compliant mechanism. *Precision Engineering*, 34(1):133–138, 2010. ISSN 01416359. doi: 10.1016/j.precisioneng.2009.05.001.

[45] PRUSA KNOWLEGDE BASE. FAQ - Frequently Asked Questions Retrieved, 2021. URL https://help.prusa3d.com/en/article/faq-frequently-asked-questions{_}1932{#}:{~}:text=Accordingtoourtesting{%}2Cthe,mmonXandY.

[46] Ke qi Qi, Ya lin Ding, Yang Xiang, Chao Fang, and Yang Zhang. A novel 2-DOF compound compliant parallel guiding mechanism. *Mechanism and Machine Theory*, 117:21–34, 2017. ISSN 0094114X. doi: 10.1016/j.mechmachtheory.2017.06.017.

[47] Yanding Qin, Bijan Shirinzadeh, Yanling Tian, and Dawei Zhang. Design issues in a decoupled XY stage: Static and dynamics modeling, hysteresis compensation, and tracking control. *Sensors and Actuators, A: Physical*, 194:95–105, 2013. ISSN 09244247. doi: 10.1016/j.sna.2013.02.003.

[48] Georg Schitter, Philipp J. Thurner, and Paul K. Hansma. Design and input-shaping control of a novel scanner for high-speed atomic force microscopy. *Mechatronics*, 18(5-6):282–288, 2008. ISSN 09574158. doi: 10.1016/j.mechatronics.2008.02.007.

[49] Fujun Wang, Xiaolu Zhao, Zhichen Huo, Beichao Shi, Cunman Liang, Yanling Tian, and Dawei Zhang. A 2-DOF nano-positioning scanner with novel compound decoupling-guiding mechanism. *Mechanism and Machine Theory*, 155, 2020. doi: 10.1016/j.mechmachtheory.2020.104066. URL www.elsevier.com/locate/mechmachtheory.

[50] Xiaohui Xiao, Lizhi Pan, Pinkuan Liu, Xuemei Tong, and Caiyu Yin. Comprehensive optimization of an XY nano positioning stage with flexure-hinges and lever mechanisms. *2010 IEEE Nanotechnology Materials and Devices Conference, NMDC2010*, pages 368–373, 2010. doi: 10.1109/NMDC.2010.5652301.

[51] Bao Yang, Chi Zhang, Hongtao Yu, Miao Yang, Guilin Yang, and Silu Chen. *Design and analysis of a planar 3-DOF large range compliant mechanism with leaf-type flexure*, volume 11740 LNAI. Springer International Publishing, 2019. ISBN 9783030275259. doi: 10.1007/978-3-030-27526-6_35. URL http://dx.doi.org/10.1007/978-3-030-27526-6{_}35.

[52] Qing Yao, J. Dong, and P. M. Ferreira. Design, analysis, fabrication and testing of a parallel-kinematic micropositioning XY stage. *International Journal of Machine Tools and Manufacture*, 47 (6):946–961, 2007. ISSN 08906955. doi: 10.1016/j.ijmachtools.2006.07.007.

[53] Yuen Kuan Yong, Kexiu Liu, and S. O.Reza Moheimani. Reducing cross-coupling in a compliant XY nanopositioner for fast and accurate raster scanning. *IEEE Transactions on Control Systems Technology*, 18(5):1172–1179, 2010. ISSN 10636536. doi: 10.1109/TCST.2009.2033201.

[54] Jingjun Yu, Yan Xie, Zhenguo Li, and Guangbo Hao. Design and experimental testing of an improved large-range decoupled XY compliant parallel micromanipulator. *Journal of Mechanisms and Robotics*, 7(4):1–6, 2015. ISSN 19424310. doi: 10.1115/1.4030467.

[55] Yuan Yun and Yangmin Li. Performance analysis and optimization of a novel large displacement 3-DOF parallel manipulator. *2008 IEEE International Conference on Robotics and Biomimetics, ROBIO 2008*, pages 246–251, 2009. doi: 10.1109/ROBIO.2009.4913011.

[56] Zhen Zhang, Binbin Liu, Peng Wang, and Peng Yan. Design of an additive manufactured XY compliant manipulator with spatial redundant constraints. *Chinese Control Conference, CCC*, 2016-Augus:9149–9154, 2016. ISSN 21612927. doi: 10.1109/ChiCC.2016.7554814.

[57] Zhen Zhang, Zhiqing Liu, and Peng Yan. Design of a flexure-based XY positioning stage with balanced axial forces on decoupling modules. *IEEE 3M-NANO 2016 - 6th IEEE International Conference on Manipulation, Manufacturing and Measurement on the Nanoscale*, 1:83–88, 2017. doi: 10.1109/3M-NANO.2016.7824921.

[58] Zhen Zhang, Xiaodong Yang, and Peng Yan. Large dynamic range tracking of an XY compliant nanomanipulator with cross-axis coupling reduction. *Mechanical Systems and Signal Processing*, 117:757–770, 2019. ISSN 10961216. doi: 10.1016/j.ymssp.2018.08.014. URL https://doi.org/10.1016/j.ymssp.2018.08.014.

[59] Hongzhe Zhao, Shusheng Bi, and Jingjun Yu. A novel compliant linear-motion mechanism based on parasitic motion compensation. *Mechanism and Machine Theory*, 50:15–28, 2012. ISSN 0094114X. doi: 10.1016/j.mechmachtheory.2011.11.009.

[60] Wu Le Zhu, Zhiwei Zhu, Ping Guo, and Bing Feng Ju. A novel hybrid actuation mechanism based XY nanopositioning stage with totally decoupled kinematics. *Mechanical Systems and Signal Processing*, 99:747–759, 2018. ISSN 10961216. doi: 10.1016/j.ymssp.2017.07.010.

[61] Zhiwei Zhu, Suet To, Xiaoqin Zhou, Rongqi Wang, and Xu Zhang. Characterization of spatial parasitic motions of compliant mechanisms induced by manufacturing errors. *Journal of Mechanisms and Robotics*, 8(1):1–9, 2016. ISSN 19424310. doi: 10.1115/1.4030586.

A

Comparison table

Strategy (#)	Effect on stiffness	Effect on eigenfrequency	Effect on moving mass	Effect on workspace	Effect on size / volume	Other effects
Maximize the degree of symmetry (1)	Increases	Increases	Increases	Could decrease	Increases	• Dynamically balanced • Less thermal sensitive • Increased lost motion
Make use of rotational symmetry (2)	Increases	Increases	Increases	Could decrease	Increases	• Dynamically balanced • Less thermal sensitive • Increased lost motion
Actuate in stiffness center (3)	Not effected	Not effected	Not effected	Not effected	Not effected	
Actuate in the actuation space (4)	Not effected	Not effected	Not effected	Not effected	Not effected	
Compensate with module in series (5)	Decreases	Decreases	Increases	Increases	Increases	
Compensate within the mechanism (6)	Depends on optimization	Depends on optimization	Not effected	Not effected	Not effected	
Compensate stiffness center shift (7)	Small effect	Depends on added joint	Depends on added joint	Not effected	Increases	
Rigid connections (8)	Increases	Unknown	Increases	Could decrease	Minimal increase	• Reduced lost motion • Less thermal sensitive • Actuator drives multiple joints • Avoids buckling • Symmetry is needed
Add additional joints (9)	Increases	Depends on added joint	Depends on added joint	Not effected	Increases	
Overconstraints (10)	Increases	Increases	Not effected	Not effected	Not effected	• Reduced input coupling
Optimize the placement of the constraints (11)	Depends on optimization	Depends on optimization	Depends on optimization	Depends on optimization	Depends on optimization	
Optimize the joints (12)	Depends on optimization	Depends on optimization	Not effected	Not effected	Not effected	

Table A.1: Classification and comparison of strategies

B

Overview of the iterative process

The goal of this appendix is to give a short overview of the process towards the final geometries. Different iterations on the optimization inputs and goals were made. In the beginning of this project the idea was to synthesize networks of flexures to compensate for the overall parasitic motions.

Before starting to optimize these networks two mirror symmetrical flexures were optimized. These flexures were positioned under the rigid body. These geometries showed good compensation of parasitic motions, but suffered from poor stiffnesses and stiffness ratios. In Appendix C a promising optimization result is shown and additional information is presented.

Then networks were optimized which were also positioned under the rigid part of the structure. More about these networks can be read in Appendix D. In short, the synthesized networks can compensate for the parasitic motion but have poor stiffness ratios. Also, the stresses were high and the optimization time was quite long.

After these networks again two parallel flexures were optimized. But, now also allowed to have their flexures positioned (partly) above the rigid bodies. This method of two parallel flexures showed very good and promising results. Both in terms of parasitic motions as well as for the stiffnesses. At the beginning compliant structures were synthesized with relative small ranges of motion. This resulted in a couple of new geometries. Then the motion range was started to be increased to find the limits of this method. This resulted in geometries slowly converging to configurations similar as the Roberts mechanism, but with added curvature.

The next step in the process was to check if adding branches could further reduce the parasitic motions. In literature branches are sometimes used during shape optimization. More about this can be read in Appendix E. The added branches didn't reduce the parasitic motions further but didn't cost stiffness either. In the branches itself the stress was low.

After the branches the effect of adding more flexures was investigated. In Appendix F some optimization results of 3 or 4 parallel flexures are shown and discussed. Again, the parasitic motions were not further decreased.

The previous synthesized designs were all joints. These compliant structures could be placed symmetrical in a final mechanism. Apart from only synthesizng joints with this method also legs could be synthesized. One of the synthesized legs was presented in the paper (chapter 5). Although the optimization time was quite long the final theoretical result was very good. Over a long range of motion the parasitic translational motion was very good compensated.

The final step was to synthesize complete mechanism. By optimizing the legs or joints within an initial defined topology the overall unwanted motions were compensated.

C

Optimization of two parallel flexures under the rigid body

In Figure C.1 a typical optimization result of an optimization with two parallel flexures under the rigid body is shown. Note that each parallel flexure consist of two Bezier curves in series. This optimization result has an motion range of $\pm 5mm$ due to its symmetric geometry. In the list below some conclusions on this type of input geometry are given.

1. The parasitic motions can be reduced significantly
2. The stiffnesses are small due to the curvature
3. The stiffness ratio's are low

Having two Bezier curves in series allows the optimizer to find geometries which have small parasitic motions. Because the flexures needed to be positioned under the rigid body the flexures needed to be shaped in a way that they can extend to compensate for the parasitic motion. This resulted in designs with a high amount of curvature. For the parasitic motions this works fine, but too much curvature impacts the stiffness a lot. Consequently this resulted in designs with poor stiffnesses and stiffness ratios.

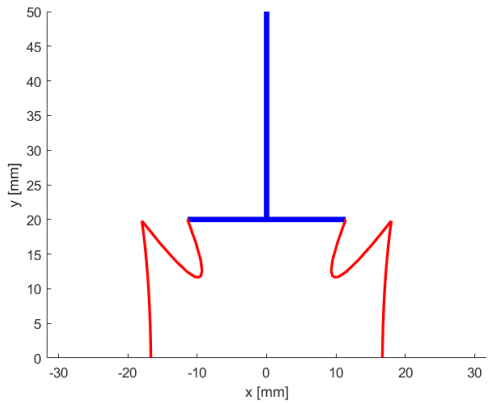

(a) Geometry

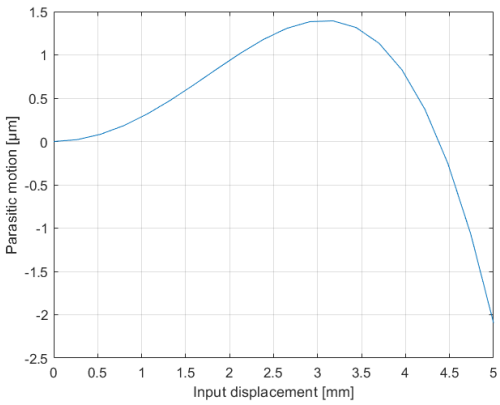

(b) Parasitic motion

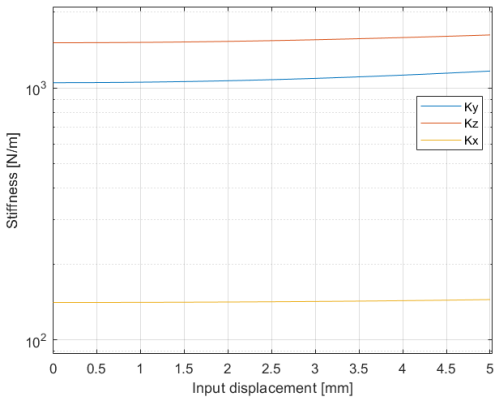

(c) Stiffnesses

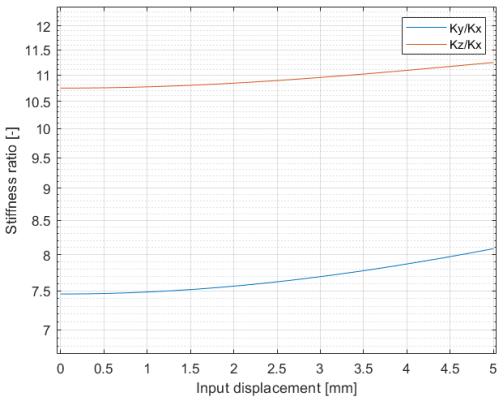

(d) Stiffness ratio

Figure C.1: Optimization of two parallel flexures under the rigid body. Optimized for minimal parasitic motion.

Flexure thickness	0.4 mm
Youngs modulus	3.5 GPa
Shear modulus	2.4 GPa
Max stress	21.8 MPa

Table C.1: Flexure thickness, material and maximum stress of optimization result visualized in Figure C.1.

D

Optimization of networks

Different networks of flexures were optimized. Some of the better optimization results are shown in Figure D.1, D.2 and D.3. These networks were synthesized using a genetic algorithm. From this optimization results some conclusion were drawn. These are listed below and will be further elaborated.

1. Networks can be used to create a near zero parasitic motion joint
2. Networks have a poor stiffness ratio (Ky/Kx)
3. Optimization time increases when networks with increased complexity are used as input
4. In a network there is more chance for self contact/intersections

The optimization results show parasitic motions in the micron range with a relative large input displacement range. In comparison, if the network would have been replaced by a cross-hinge the parasitic motion is about $260\mu m$. This shows that the networks can reduce the parasitic motions significantly. However, the stiffnesses of these networks are poor. Especially the stiffness ratio (Ky/Kx) is not good. These poor stiffnesses can be explained by the geometry of the joints. To have little parasitic motion the flexures are curved in a a specific way. If flexures are curved too much the stiffnesses will also drop significantly. This is happening in these networks. Additionally the support stiffness (Ky) of these networks is in the order of $10^4 N/m$, while a cross-pivot hinge has a support stiffness in the order of $10^5 N/m$ with the same material and flexure thickness. Furthermore, the optimization time of these networks is quite long. A lot of control points are needed to describe the shape of the flexures in the networks. Although symmetry is used there are still a significant amount of control points needed. More design variables results in an increased optimization time and complexity. Additionally, if more flexures are present in the networks more beam elements are needed to describe these networks accurately. This results in a longer model evaluation time. Lastly, there is also some space needed to move for the joint. If there are more flexures there is also more space needed to avoid self intersections. For example, in Figure D.3 the end points of the flexures are quite close to the rigid parts which could lead to difficulties in implementing this geometry into a physical prototype.

There are also some important remarks concerning these networks. These are listed below. It should be noted that these networks were synthesized at the beginning of the project. During the project a lot of knowledge have been gained and changes to the design area were made. With the current knowledge other networks could have been used as input geometry. For example, parts of the networks could have been partly above the rigid body or a bigger design area could be used. Initially the idea was to have small joints performing the compensation.

1. The behaviour of networks depends on the initial network configuration. Other network layouts of which the author didn't know or thought may have more potential to be successful. For determining the input configuration inspiration was gathered from literature and from a brainstorm session.
2. The space assigned to the networks is small resulting in high stresses.

3. The ratio between design space and input motion might be to high. The flexures undergo quite some deformation resulting in high stresses.

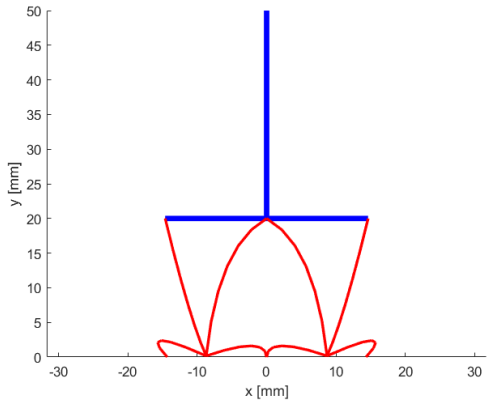

(a) Geometry

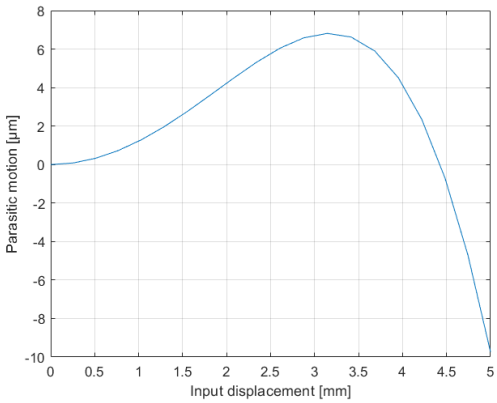

(b) Parasitic motion

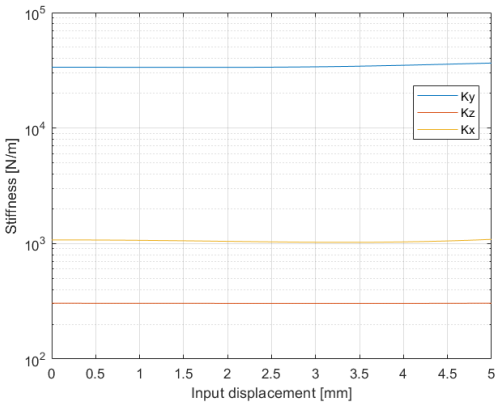

(c) Stiffnesses

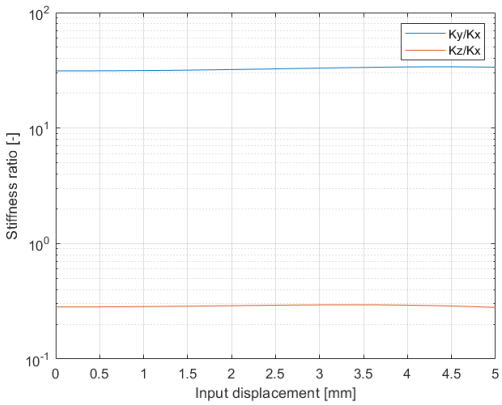

(d) Stiffness ratio

Figure D.1: Optimization of a network of flexures. In this network intersections were tried to be avoided while having small parasitic motions.

Flexure thickness	0.5 mm
Youngs modulus	3.5 GPa
Shear modulus	2.4 GPa
Max stress	38.6 MPa

Table D.1: Flexure thickness, material and maximum stress of optimization result visualized in Figure D.1.

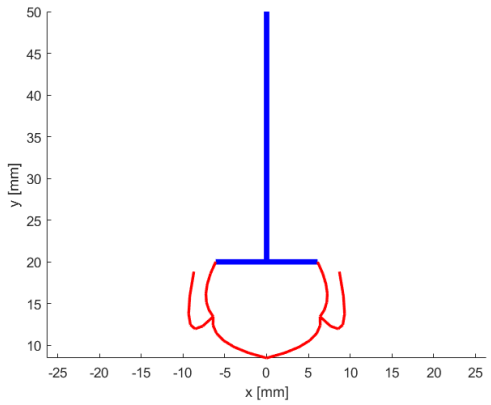

(a) Geometry

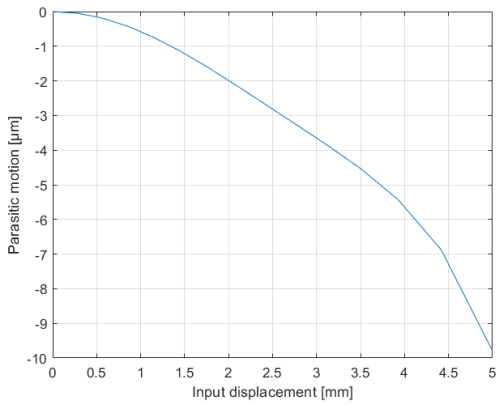

(b) Parasitic motion

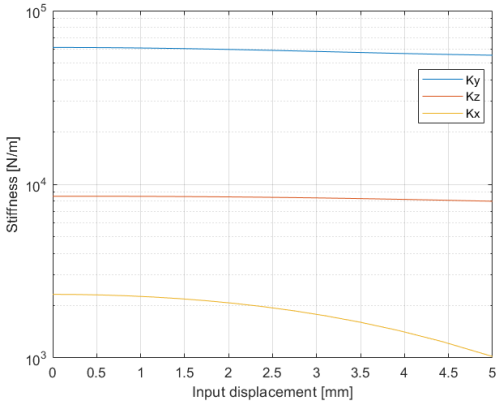

(c) Stiffnesses

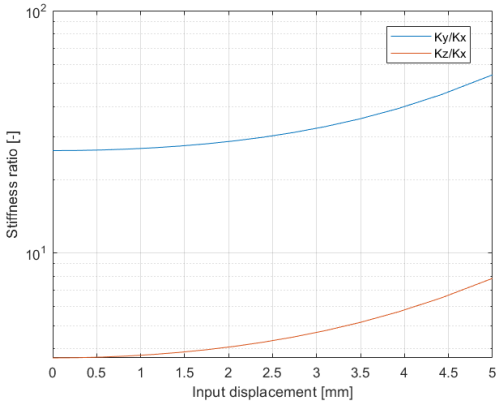

(d) Stiffness ratio

Figure D.2: Optimization of a network of flexures. This network was only optimized for small parasitic motion with a minimum support stiffness of $5 * 10^4 N/m$. Other constraints were not taken into account.

Flexure thickness	0.5 mm
Youngs modulus	3.5 GPa
Shear modulus	2.4 GPa
Max stress	144 MPa

Table D.2: Flexure thickness, material and maximum stress of optimization result visualized in Figure D.2.

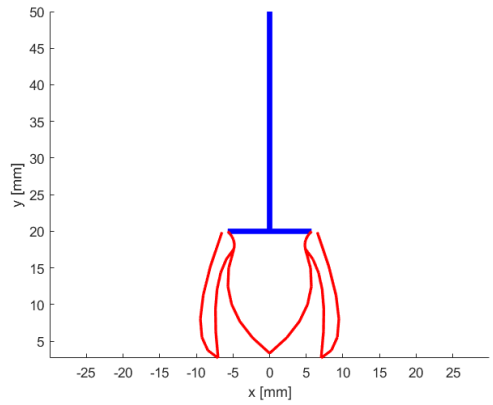

(a) Geometry

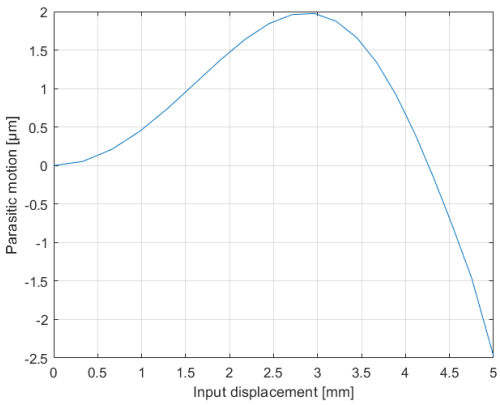

(b) Parasitic motion

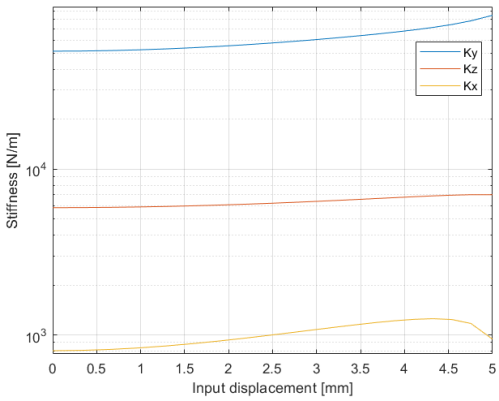

(c) Stiffnesses

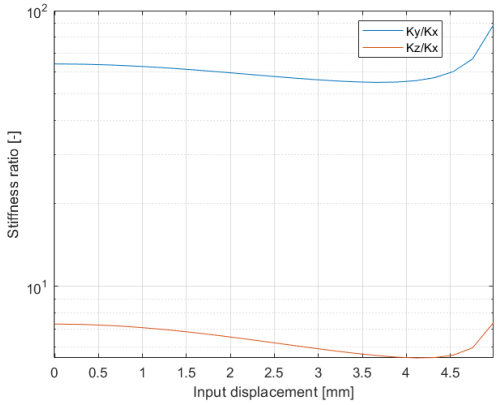

(d) Stiffness ratio

Figure D.3: Optimization of a network of flexures. This network was only optimized for small parasitic motion with a high stiffness ratio. Other constraints were not taken into account.

Flexure thickness	0.5 mm
Youngs modulus	3.5 GPa
Shear modulus	2.4 GPa
Max stress	74.7 MPa

Table D.3: Flexure thickness, material and maximum stress of optimization result visualized in Figure D.3.

E

Optimization of branches

In literature also flexures with branches are optimized [22, 23] during shape optimization. During this project also branches were optimized to find out if they could help with reducing the parasitic motion in the mechanisms. Two parallel flexures connected to an output body are used as initial topology. These two parallel flexures are positioned similar to a Roberts mechanism. Either one or two branches are added to the end of the two parallel flexures. Each branch consist of two flexures. In Figure E.1 at one flexure a branch is added. Two branches are added in Figure E.2 and in Figure E.3 a benchmark design without branches is shown. Al flexures are optimized using the genetic algorithm and can be curved. From these results the following conclusions were drawn:

1. Adding branches does not further reduce the parasitic motion compared to the benchmark optimization
2. More control points needs to be optimized resulting in longer optimization times
3. In the branches itself the von Mises stress is small
4. The stiffnesses are little effected by the branches compared to the benchmark design

Comparing all three designs the maximum parasitic motion is comparable. All are within $10\mu m$ over a motion range of $\pm 10mm$. Since, more flexures are needed to be optimized also more control points are needed to describe the shapes. As a consequence the optimization time does increase. The benefit of these branches is the small stress in the branches. If it is needed to have small stress concentrations at locations where flexures are connected to rigid bodies branches could be added. A low stress in these branches also indicates small motion is happening. Therefore, the main parasitic motion compensation is coming from the geometry and the bending of the non-branch flexures. The branches in the optimized geometries have an almost straight flexure in vertical direction. This is probably for having maximal support stiffness in the vertical direction. The other flexures are curved and constraining the motion in horizontal direction of the vertical flexures. An other benefit of these branches is the potential to decrease the size of the moving mass in mechanisms. The results in Figure E.2 shows that regions of the rigid structure needed to connect the flexures can be replaced by branches. This can reduce the amount of connecting structure needed resulting in a more lightweight design.

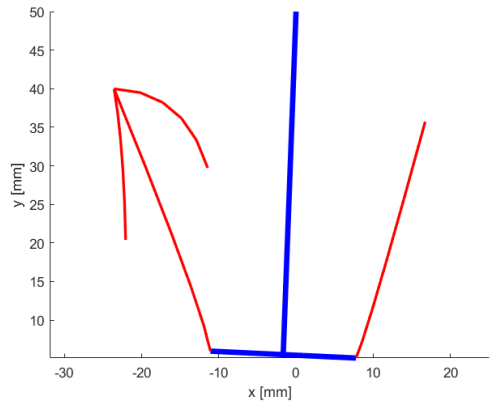

(a) Geometry

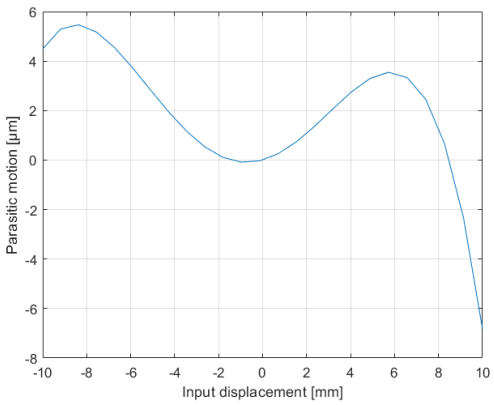

(b) Parasitic motion

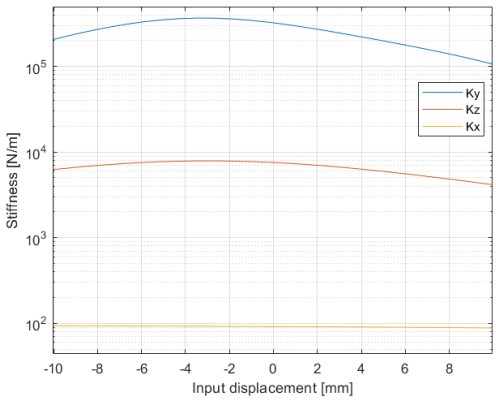

(c) Stiffnesses

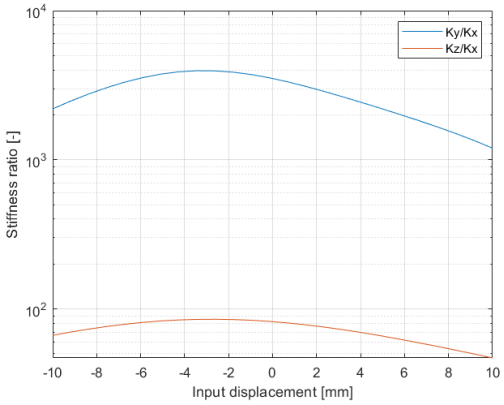

(d) Stiffness ratio

Figure E.1: Optimization of two parallel flexures with a branch on one side. Optimized for minimal cross-coupling (parasitic motion divided by input displacement). Geometry constraints on radius of curvature and distance between flexures. Minimum stiffness ratio > 200 and maximum stress $< 40MPa$

Flexure thickness	0.5 mm
Youngs modulus	3.5 GPa
Shear modulus	2.4 GPa
Max stress	36.0 MPa

Table E.1: Flexure thickness, material and maximum stress of optimization result visualized in Figure E.1.

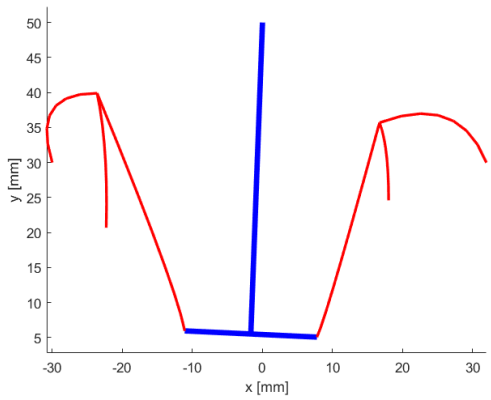

(a) Geometry

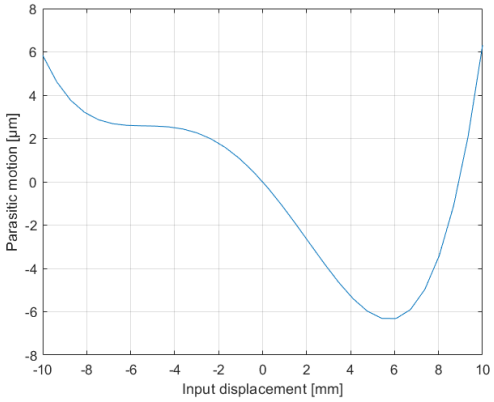

(b) Parasitic motion

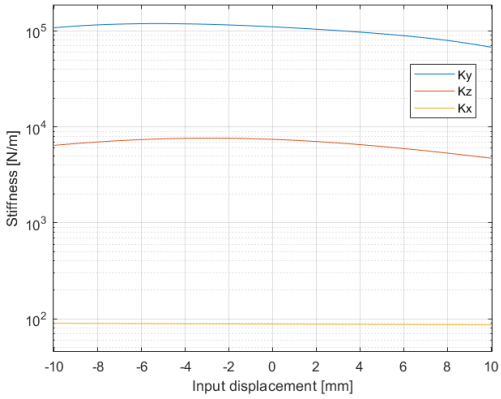

(c) Stiffnesses

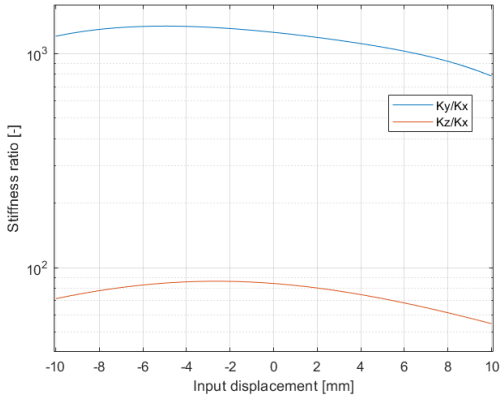

(d) Stiffness ratio

Figure E.2: Optimization of a network of two parallel flexures with at two sides a branch. Optimized for minimal parasitic motion. Geometry constraints on radius of curvature and distance between flexures. Minimum stiffness ratio > 750 and maximum stress $< 40MPa$

Flexure thickness	0.5 mm
Youngs modulus	3.5 GPa
Shear modulus	2.4 GPa
Max stress	33.7 MPa

Table E.2: Flexure thickness, material and maximum stress of optimization result visualized in Figure E.2.

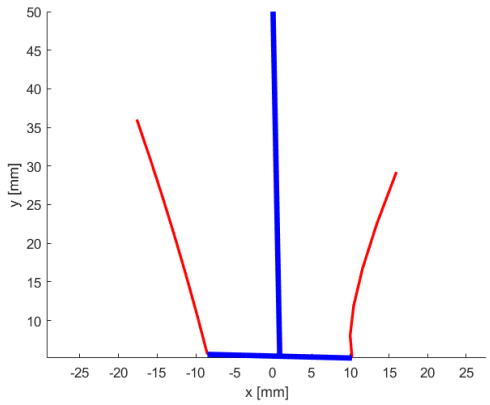

(a) Geometry

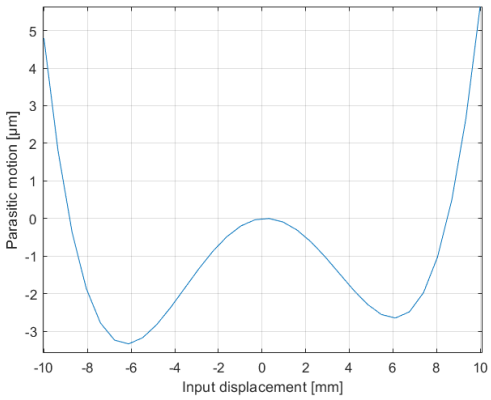

(b) Parasitic motion

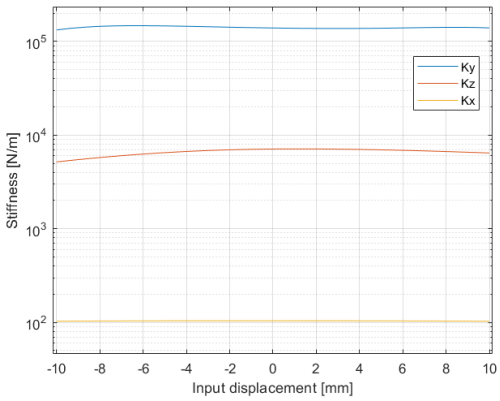

(c) Stiffnesses

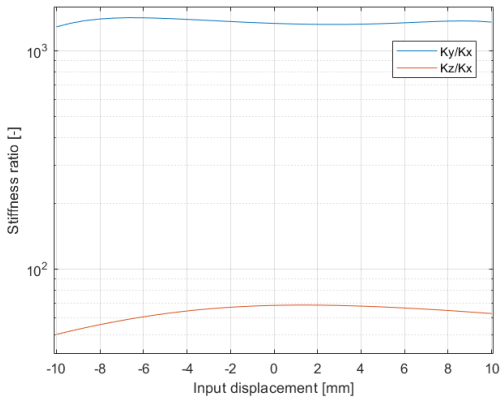

(d) Stiffness ratio

Figure E.3: Optimization of two parallel flexures. Optimized for minimal cross-coupling (parasitic motion divided by input displacement). Geometry constraints on radius of curvature and distance between flexures. Minimum stiffness ratio > 850 and maximum stress $< 40MPa$

Flexure thickness	0.5 mm
Youngs modulus	3.5 GPa
Shear modulus	2.4 GPa
Max stress	36.6 MPa

Table E.3: Flexure thickness, material and maximum stress of optimization result visualized in Figure E.3.

F

Optimization of multiple parallel flexures

In Figure F.1, F.2, F.3, F.4 and F.5 five different optimization results of multiple parallel flexures connected to a rigid body are shown. All of these examples have an input motion of $\pm 5mm$ except for the last one which has an input motion of $\pm 2.5mm$. Again from these optimization results some conclusions were drawn. These are listed below and will be further elaborated and discussed after the enumeration.

1. From the synthesized geometries it is difficult to create a rigid body connecting all flexures without interfering with a flexure or support structure
2. There is a higher risk of finding structures which can self-intersect when deforming
3. Multiple parallel flexures can be used to compensate for the parasitic motions
4. The parasitic motions of these structures are not better than other synthesized structures with less flexures
5. Multiple parallel flexures do not necessary increase the stiffnesses.

When optimizing multiple parallel flexures many flexures are shaped and curved around each other. This can lead to situations in which no 2D rigid body can be synthesized without intersecting with the flexures. For example, the result shown in Figure F.4. Creating a connecting structure between the flexures for three parallel flexures is possible but will result in complex geometries. For these geometries it might be difficult to keep its rigidity. Additionally there is the risk of synthesizing structures which intersect with each other. In chapter 5 (paper) a constraint to avoid this is presented. The optimized geometries show that structures with small parasitic motions can be synthesized. However, these are not better in terms of unwanted motions compared to the constant stiffness joint presented in the paper (chapter 5) or the benchmark result for two parallel flexures without branches shown in Figure E.3. Lastly, adding more flexures might seem to be a good idea to increase the stiffnesses. However, due to a lot of curvature added to these flexures the stiffnesses of the individual flexures drops. Also, having more flexures can lead to higher stiffnesses in the motion direction. Normally the flexures do have little stiffness in the motion direction. But, now more flexures are added which is at the risk of decreasing the stiffness ratio (Ky/Kx). This stiffness ratio is important if mechanisms are needed in which the transmission of input motion and output motion needs to be high.

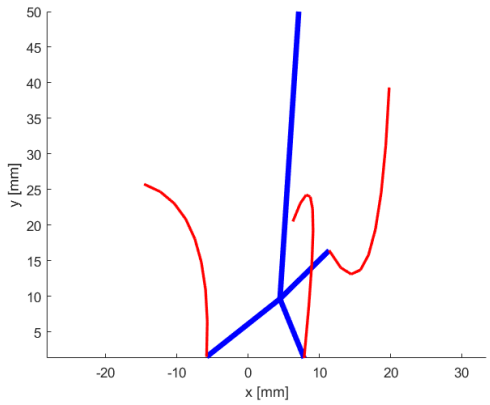

(a) Geometry

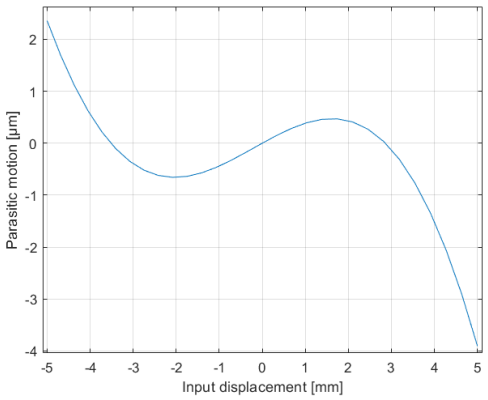

(b) Parasitic motion

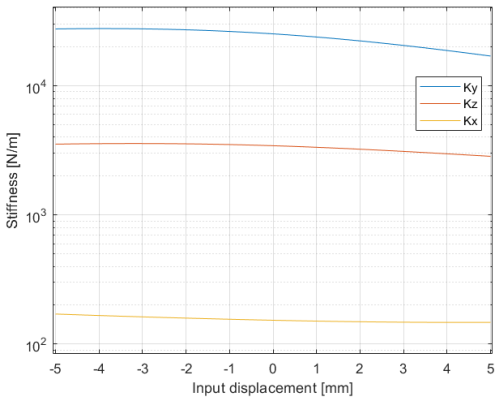

(c) Stiffnesses

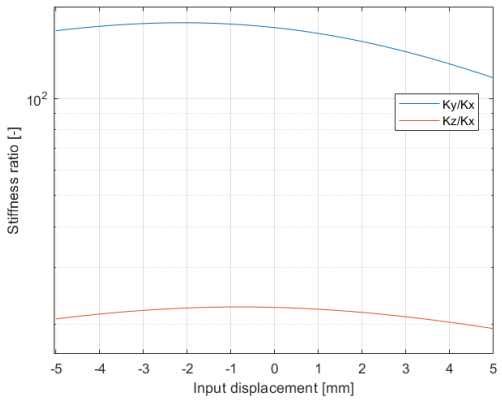

(d) Stiffness ratio

Figure F.1: Optimization of a three parallel flexures. Optimized for minimal cross-coupling (parasitic motion divided by input displacement). Minimum stiffness ratio > 100 and maximum stress $< 40MPa$

Flexure thickness	0.5 mm
Youngs modulus	3.5 GPa
Shear modulus	2.4 GPa
Max stress	21.4 MPa

Table F.1: Flexure thickness, material and maximum stress of optimization result visualized in Figure F.1.

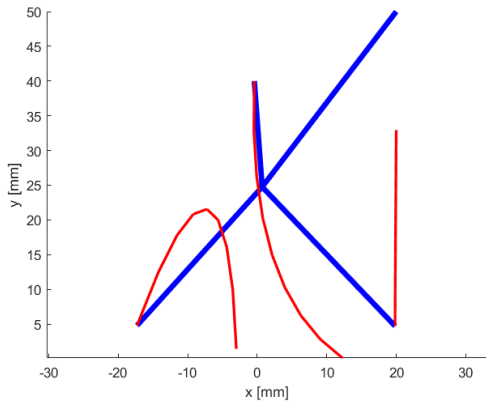

(a) Geometry

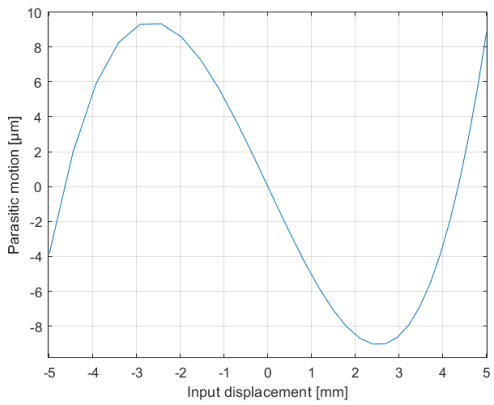

(b) Parasitic motion

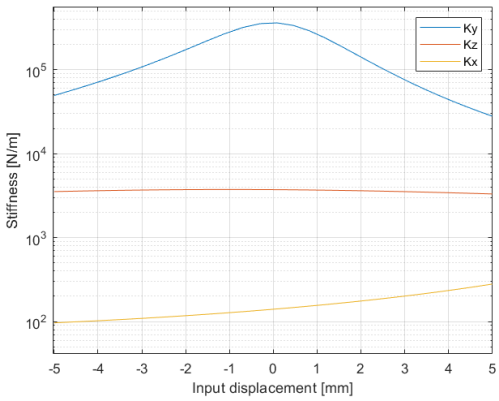

(c) Stiffnesses

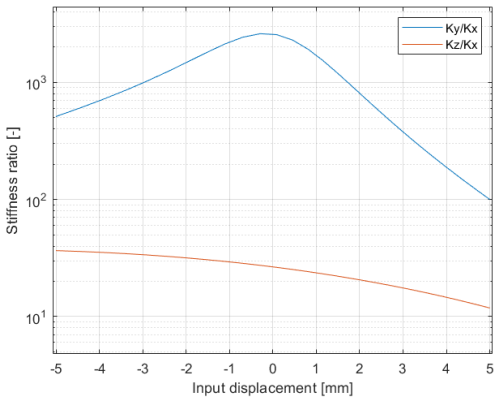

(d) Stiffness ratio

Figure F.2: Optimization of a three parallel flexures. Optimized for minimal parasitic motion. Minimum stiffness ratio > 100 and maximum stress $< 40MPa$

Flexure thickness	0.5 mm
Youngs modulus	3.5 GPa
Shear modulus	2.4 GPa
Max stress	19.4 MPa

Table F.2: Flexure thickness, material and maximum stress of optimization result visualized in Figure F.2.

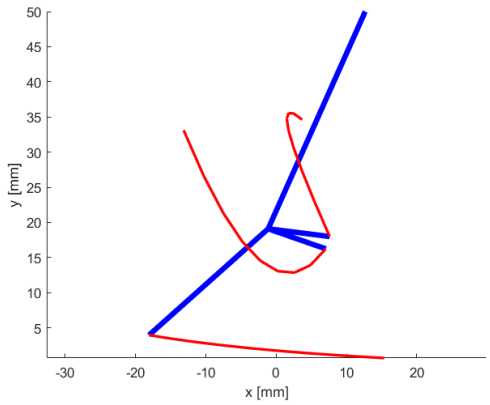

(a) Geometry

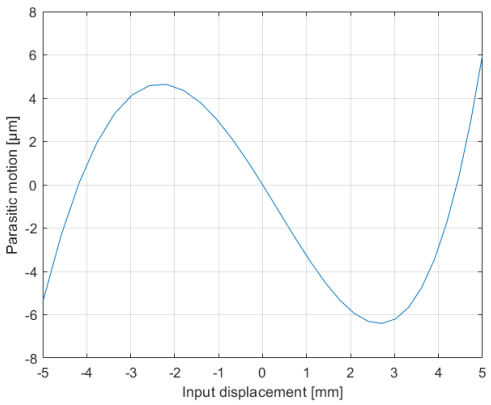

(b) Parasitic motion

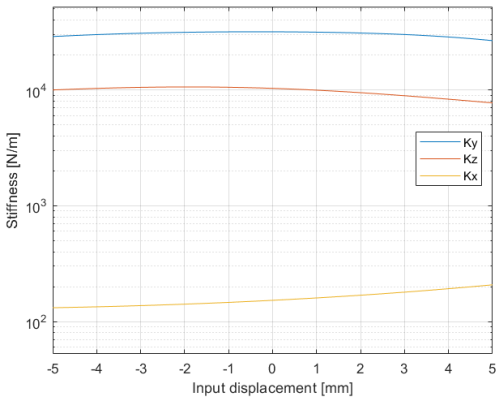

(c) Stiffnesses

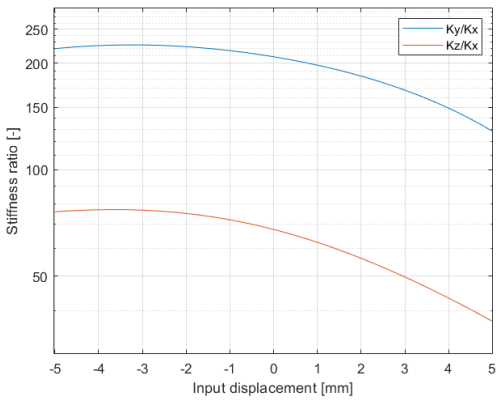

(d) Stiffness ratio

Figure F.3: Optimization of a three parallel flexures. Optimized for minimal parasitic motion. Minimum stiffness ratio > 100 and maximum stress $< 40MPa$

Flexure thickness	0.5 mm
Youngs modulus	3.5 GPa
Shear modulus	2.4 GPa
Max stress	26.9 MPa

Table F.3: Flexure thickness, material and maximum stress of optimization result visualized in Figure F.3.

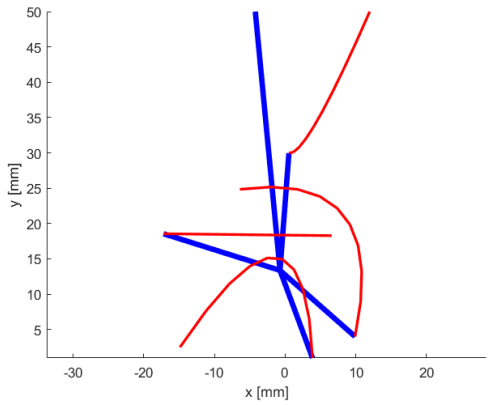

(a) Geometry

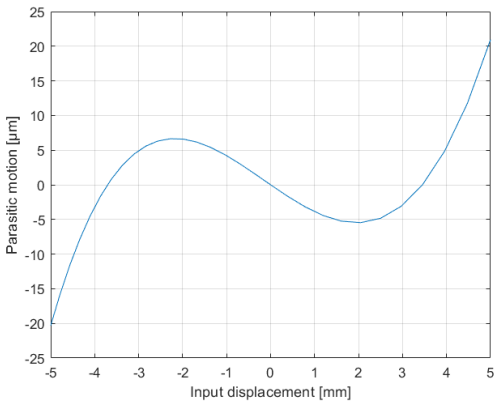

(b) Parasitic motion

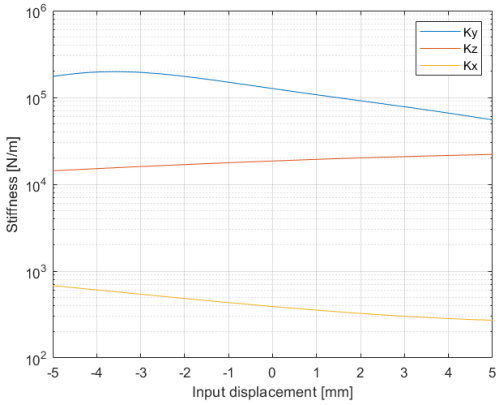

(c) Stiffnesses

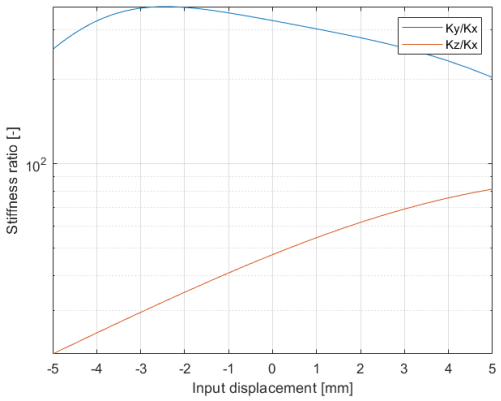

(d) Stiffness ratio

Figure F.4: Optimization of a four parallel flexures. Optimized for minimal cross-coupling (parasitic motion divided by input displacement). Minimum stiffness ratio > 200 and maximum stress $< 40MPa$

Flexure thickness	0.5 mm
Youngs modulus	3.5 GPa
Shear modulus	2.4 GPa
Max stress	41.3 MPa

Table F.4: Flexure thickness, material and maximum stress of optimization result visualized in Figure F.4.

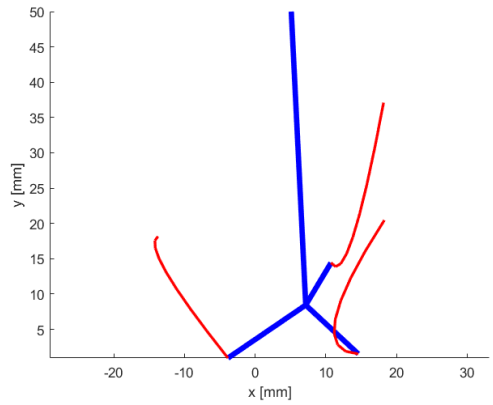

(a) Geometry

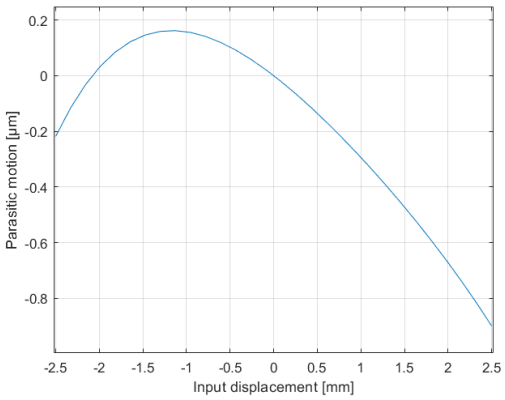

(b) Parasitic motion

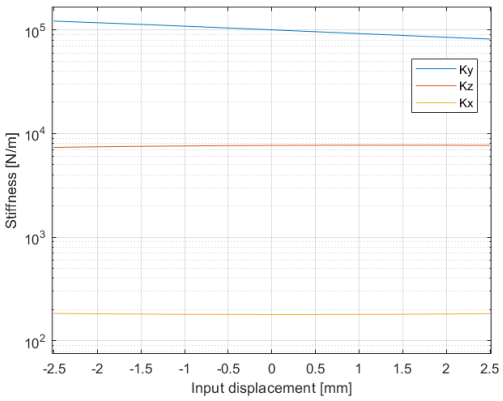

(c) Stiffnesses

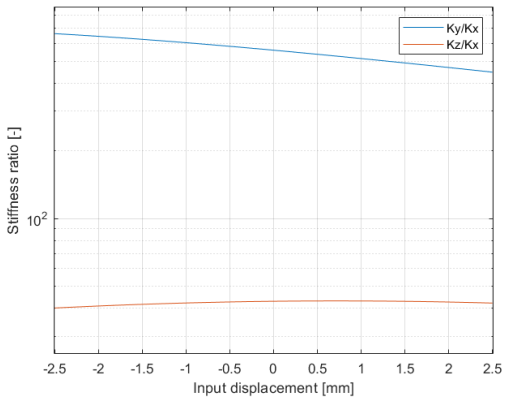

(d) Stiffness ratio

Figure F.5: Optimization of a three parallel flexures. Optimized for minimal parasitic motion. Minimum stiffness ratio > 100 and maximum stress $< 40MPa$

Flexure thickness	0.5 mm
Youngs modulus	3.5 GPa
Shear modulus	2.4 GPa
Max stress	10.1 MPa

Table F.5: Flexure thickness, material and maximum stress of optimization result visualized in Figure F.5.

G

Test setup iterations

In this appendix some information about the testing phase is presented. The testing phase turned out to be quite difficult to perform reliable measurements. In this appendix it is tried to give some more insight in what caused these difficulties and what steps were needed towards a successful measurement.

G.1. Measurement surfaces

Different measurement surfaces were used throughout the project. In Figure G.1 six different surfaces are shown. It was difficult to find a flat surface compatible with the laser distance sensor. This sensor had issues when the measurement surface is too shiny. This resulted in fluctuating measurement signals going up and down several tens of micrometers while the mechanisms and test setup were not moving or vibrating. A short summery of the experience with the different measurement surface is given below:

1. The 3D printed surface (Figure G.1a) was not flat enough resulting in inaccurate measurements.
2. The stainless steel strip (Figure G.1b) was too shiny resulting in a fluctuating measurement signal.
3. The encoder ruler (Figure G.1c) provided by the PME department of the TU Delft was warped and had some scratches. This resulted in measurement difficulties. Also, it was quite shiny causing the laser distance sensor to not give a steady signal.
4. The silicon wafer (Figure G.1d) was too reflective. This resulted in a non-consisted measurement signal. Also, the less reflective side of the wafer was used. However, this one was also too shiny. Later on the wafer was used to paste a sticker on it.
5. The measurement surface of the sticker (Figure G.1e) was quite flat (not perfectly) and the laser was able to give a proper signal.
6. The card (Figure G.1f) performed quite good. The laser sensor gave a consisted signal and looked more flat as the sticker. This made the card the best option for the final measurements.

G.2. Different test setup configurations

In Figure G.2 different test setups used throughout the project are shown. They are shortly introduced and discussed in the following enumeration.

1. The layout of the test setup shown in Figure G.2a is one of the initially used test setups. On the left side of the figure a part with a notch hinge is mounted on a linear stage. Using this linear stage the part can push on the mechanism causing the compliant part to undergo a near straight line motion. At two sides of the part the parasitic motion is measured. It was expected that at the sides the parasitic motion is largest due to parasitic rotation present. The idea was that this would reduce the influence of measurement errors. Using Equation G.1 the parasitic motion of the middle point could be measured.

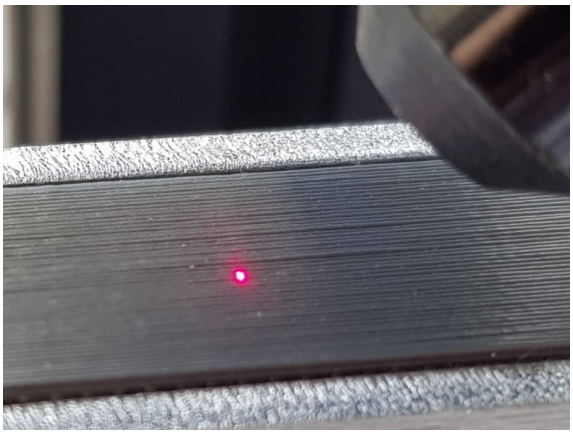

(a) 3D printed surface

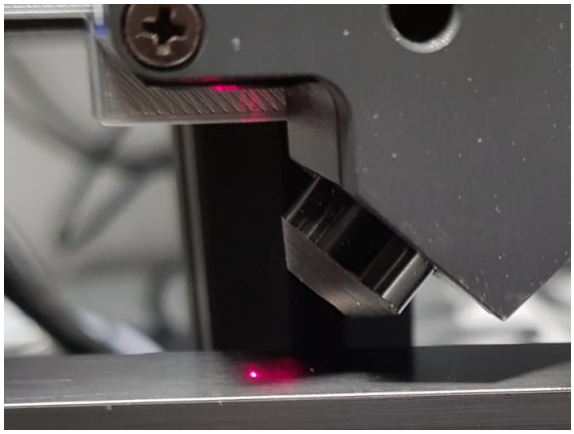

(b) Stainless steal strip

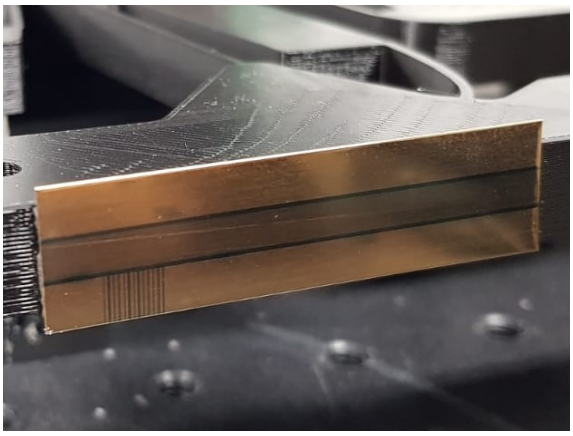

(c) Encoder ruler

(d) Silicon wafer

(e) Sticker pasted on a silicon wafer

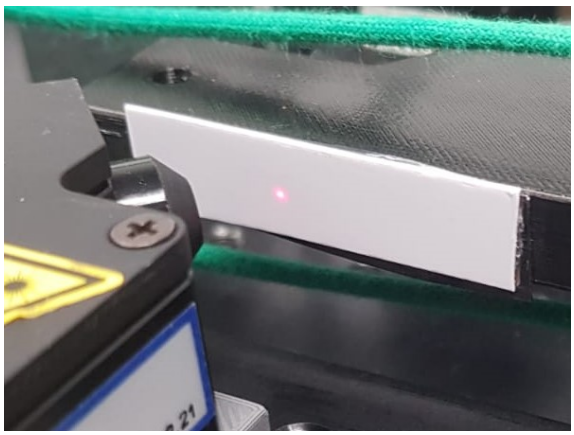

(f) Card

Figure G.1: An overview of the different surfaces used for the parasitic motion measurements

2. Instead of moving the top part of the compliant mechanism also the base can be moved. If the top part is fixed in horizontal direction the same parasitic motions can be measured. In Figure G.2b this is shown. The black part on the right of the figure prevents the designed moving part of the mechanism to move. The leaf spring in this part allows the part to still move in vertical direction. The curved surface allows the part to rotate. In this way only the horizontal position is constrained. The base is mounted on a linear stage which was used for the input motion. The benefit of this layout is that the surface error is eliminated. The measurement surface stays at the same

horizontal position, but can still move in the parasitic motion direction (vertical). This layout is still prone to the alignment error presented in chapter 6. Also, this setup is prone to the parasitic motion in the linear stage used for the input motion.

3. Figure G.2c shows a similar layout of the previously discussed test setup shown in Figure G.2a. Instead of pushing the prototype a rope is used to pull on it. The rope is made as long as possible to minimize the angle of the rope with the horizontal axis. In this way an unwanted force in vertical direction is minimized. Also, visible in this figure is the linear motion stage to perform the surface scan and alignment measurement discussed in chapter 6.

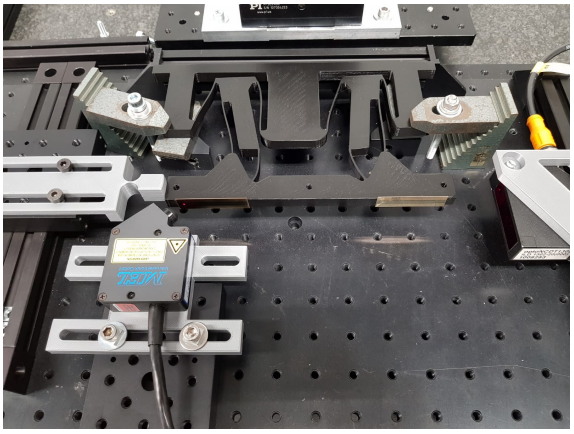

(a) Test setup layout in which the compliant motion is pushed by a part to perform the compliant motion. Note that the part is in a compliant motion.

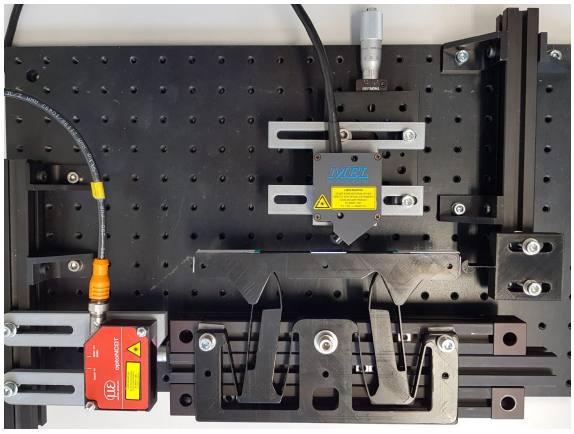

(b) The top bar of the mechanism is kept in place by the part on the right of the mechanism. By moving the base the compliant motion is performed.

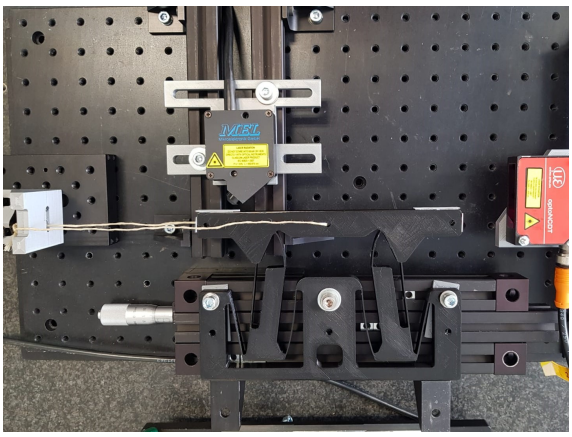

(c) Test setup in which the topbar of the mechanism is moved around by pulling on the rope.

Figure G.2: An overview of the different test setup layouts used

The two test setups using contact gave less good results as the one using the rope. Therefore, the test setup with the rope was used for the final test setup. Also, there was a method available to determine the parasitic motions without doing all the measurement to compensate for the measurement errors. The results of the final measurement setup were presented in chapter 6.

G.3. Testing results for measurement at two sides

In this section the final test results of the measurement at two sides is presented. The measured parasitic motion is slightly different as the one measured using the middle measurement (chapter 6), but shows that it is more than likely that the measured parasitic motion is in this order of magnitude. It is also used to illustrate how the parasitic motion in most of the experiments was measured. Additionally, the parasitic rotation can be measured using this test setup and will be presented in this section.

In Figure G.3 a schematic overview of the test setup is shown with some of the errors present. These errors were discussed in chapter 6. A rope connects the linear stage which can move in horizontal direction and the mechanism. The experiments is conducted in two parts because only two laser sensors were available. The vertical sensor is positioned as far as possible to the sides of the mechanism because there the biggest displacements are expected (which is easier to measure than very small displacements). The displacements are expected to be largest because it contains also a displacement caused by the parasitic rotation. By using the measurement at both sides this parasitic rotation error can be eliminated in the measurement of the parasitic motion.

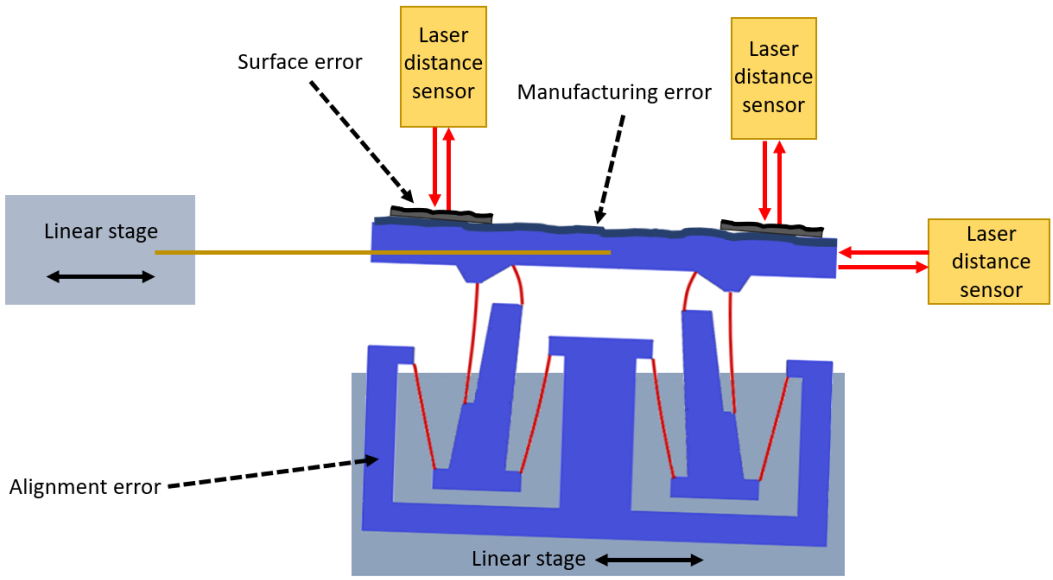

Figure G.3: Visualization of errors

To calculate the parasitic motion of the point of interest (black dot) the Equation G.1 is used. In Figure G.4 the important parameters to calculate the unwanted motions are visualized. Also, the point of interest is visualized in this figure. To calculate the parasitic rotation Equation G.2 is used. La is the distance between the sensors measuring the parasitic motion. Lm is the distance between the left sensor and the point of interest. La and Lm are also visualized in Figure G.4.

$$\text{Parasitic motion} = \frac{\text{Measurement sensor 1.2} - \text{Measurement sensor 1.1}}{\text{La}}\text{Lm} + \text{Measurement sensor 1.1} \tag{G.1}$$

$$\text{Parasitic rotation} = \text{atan}\left(\frac{\text{Measurement sensor 1.2} - \text{Measurement sensor 1.1}}{\text{La}}\right) \tag{G.2}$$

Different measurements can be performed to eliminate most of the errors. These measurements are the so called compliant measurement, surface scan measurement and alignment measurement. The compliant measurement the base of the mechanism is fixed and the top part is forced to translate by pulling on the rope using the linear stage. During the surface scan measurement the rope is disconnected from the mechanism and the base is translated using the linear stage. During this measurement the surface of the glued parts is scanned. The alignment measurement is very similar to the surface scan measurement but is performed without the glued parts. In this way the alignment error can be measured. In Figure G.3 the errors from the test setup are visualized. Note that the sources of error are enlarged in this figure for explanation purposes. The errors are explained in more detail in chapter 6.

The alignment measurement is shown in Figure G.5. In Figure G.6 and G.7 the surface scan, compliant motion and the corrected data are plotted for respectively the measurement performed on the left and right side. With this data the parasitic translation and rotation are calculated and plotted in Figure G.8 and G.9 respectively. The parasitic motions can be calculated in three different ways. The parasitic motion can be calculated using both measurements or using one of the measurements. Since,

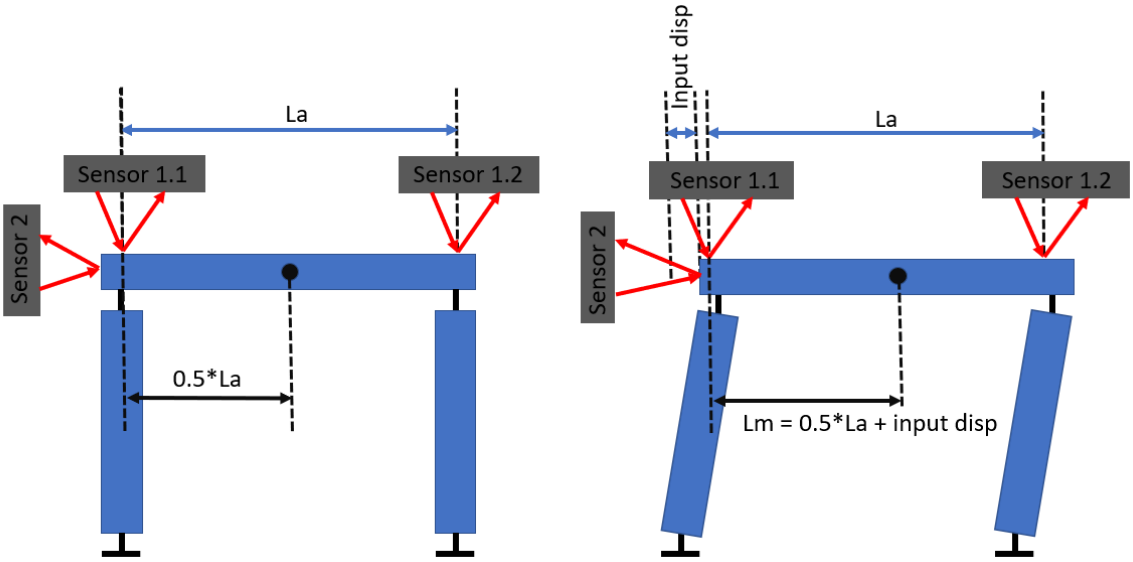

Figure G.4: Measurement evaluation

the mechanism is symmetric the measurement of for example, the right side can be mirrored to the left side. In the figure it can be seen that all different evaluation methods results in slightly different results. But, all of them are in the same order of magnitude. With a more high-end prototype it is expected that better measurements can be done. For example, one machined using wiring edm and with a polished surface finish. Then there is no need to perform all types of error compensations which should result in better measurement results.

The data of this measurement is very similar to the parasitic motion measured in chapter 6. The measurement based on both measurement surfaces is almost identical. The difference between the measured parasitic motion based on the left and right surface origins from the fact that both corrected data plots are not perfectly symmetrical. This could be caused by some measurement errors. The parasitic rotation of the three evaluation methods are much more similar, but higher than the FEA analysis showed. The parasitic rotation of the SPACAR FEA analysis and the comsol analysis with rigid parts are almost identical. If the compliance of the support structures is taken into account a slight deviation is visible.

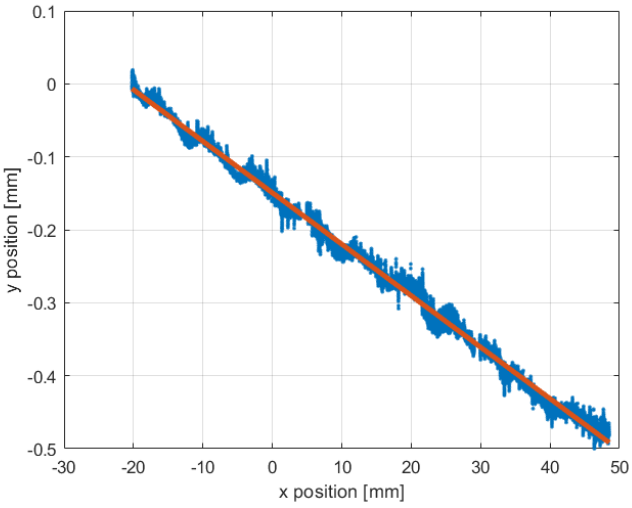

Figure G.5: Alignment measurement

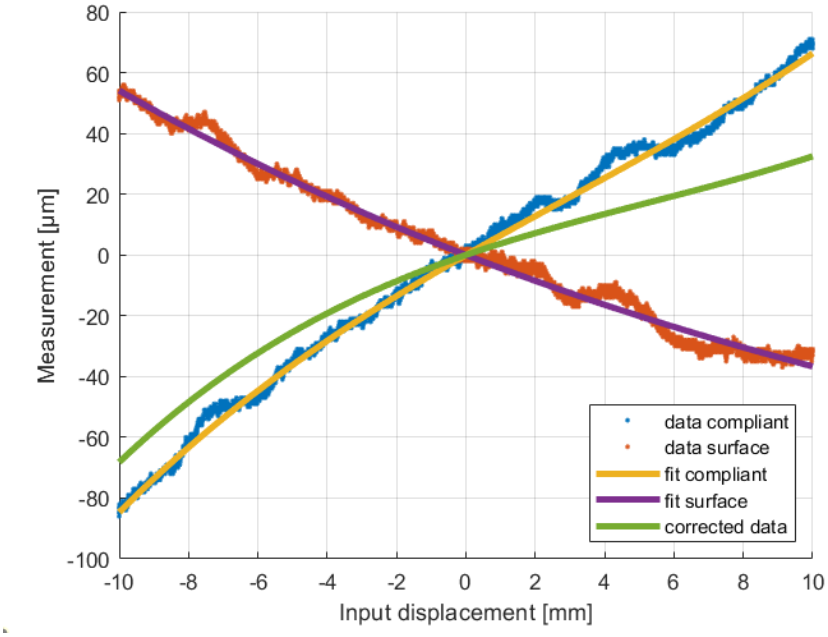

Figure G.6: Measurements performed on the left side of the prototype.

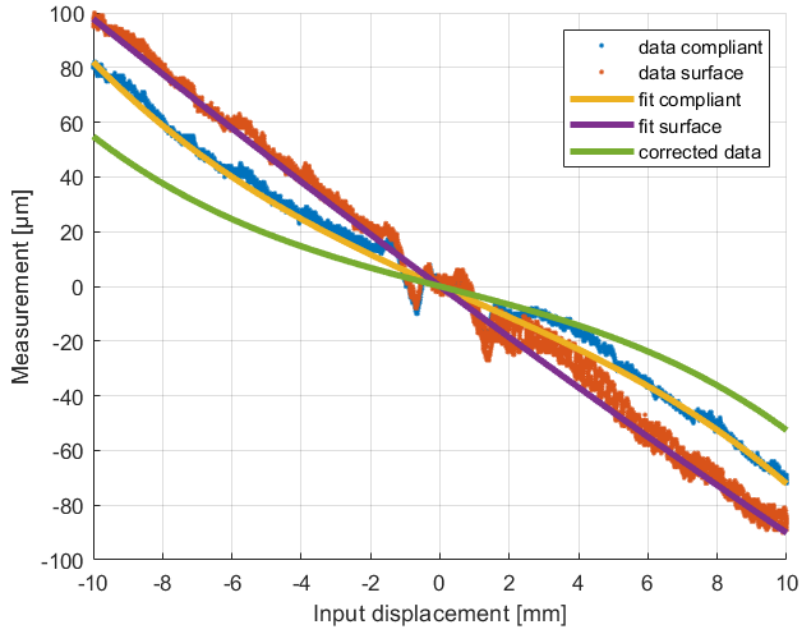

Figure G.7: Measurements performed on the right side of the prototype.

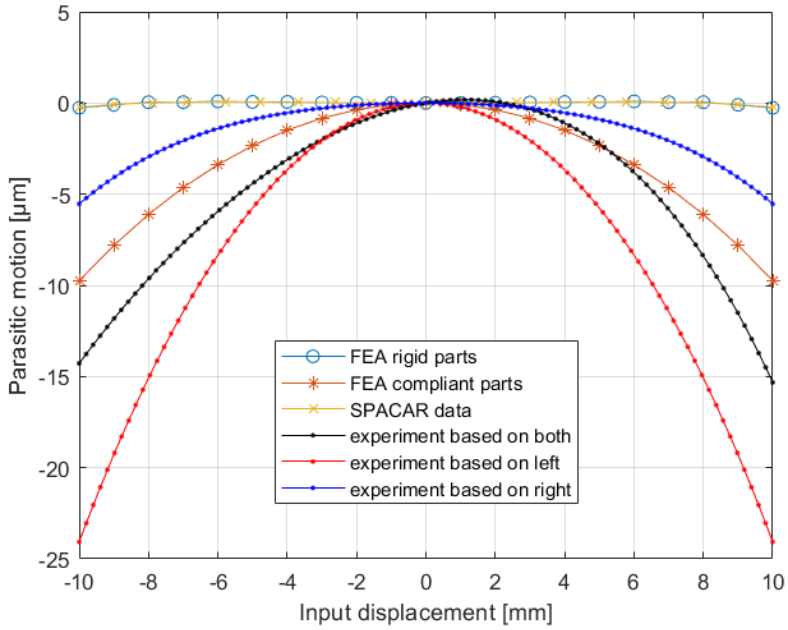

Figure G.8: Experimental and FEA parasitic translation results

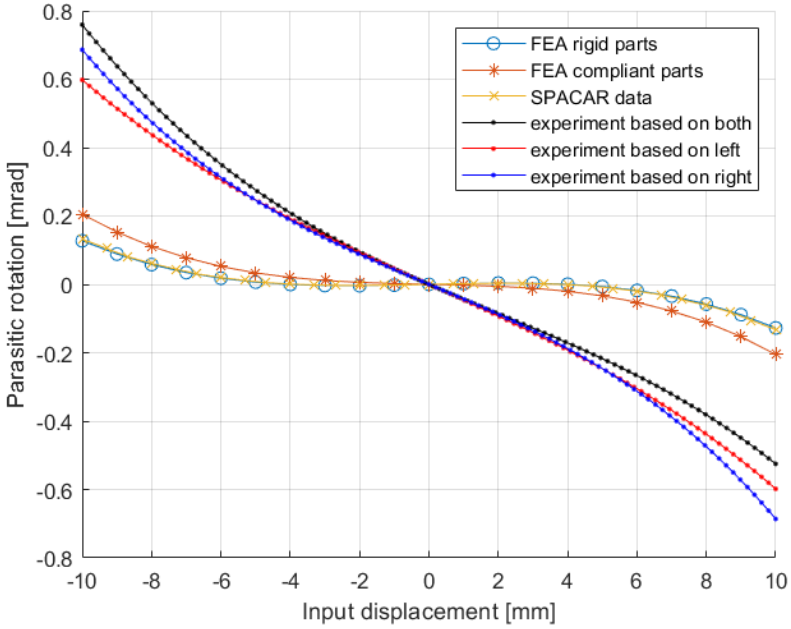

Figure G.9: Experimental and FEA parasitic rotation results

H

Effect of compliance of the base and moving bodies on parasitic motion

In this appendix some results of a nonlinear FEA in COMSOL multiphysics are presented. This is done to show the effect of taking the compliance of assumed rigid bodies into account. The used material during these simulations is PLA. The flexure thickness is $0.8mm$ for the Roberts mechanisms and the double parallelogram mechanisms. The optimized design has a flexure thickness of $0.4mm$. In chapter 6 the same analysis was performed for this optimized design with $0.8mm$ thick flexures.

In the designs with higher stresses in the flexures (Roberts and the optimized design) the effect on the parasitic motion of the compliance in the support structures is large (Figure H.2 and 6.12). For the double parallelogram the stresses are smaller and the effect on the parasitic motion is much smaller (Figure H.4). When the flexure thickness is reduced from $0.8mm$ to $0.4mm$ (Figure H.6) the parasitic motion is much closer to a simulation using rigid bodies. The stress in the flexures is reduced and thus the assumed rigid bodies deform much less (Figure 6.11 compared with Figure H.5).

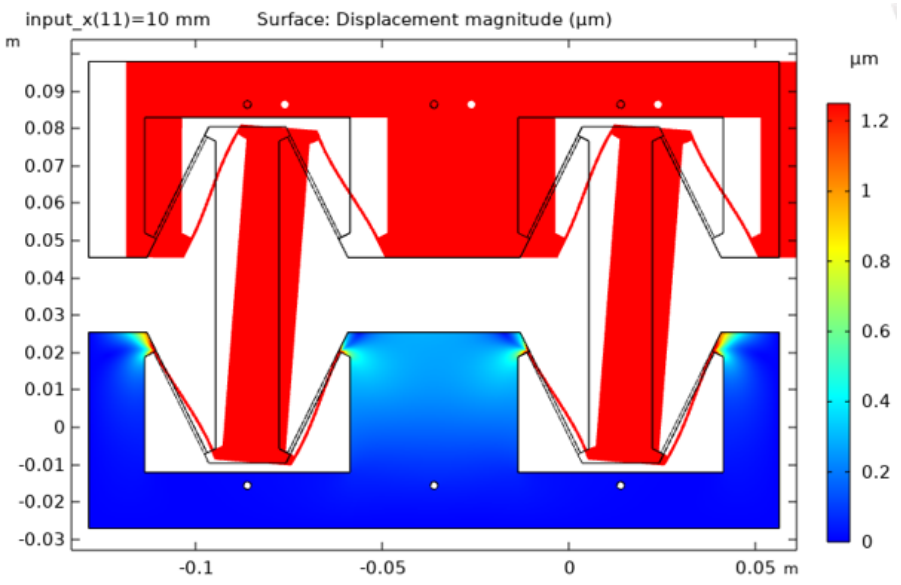

Figure H.1: Nonlinear FEA of a Roberts mechanism taking the compliance of the base and moving bodies into account.

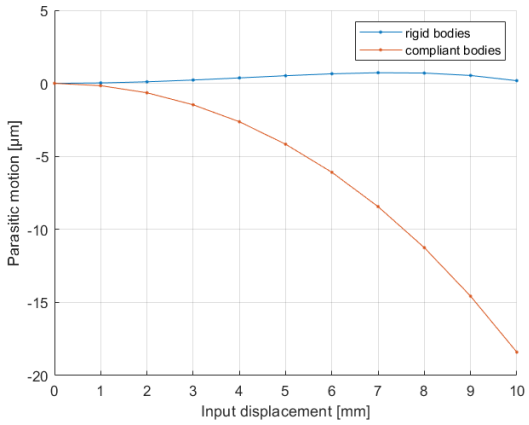

Figure H.2: Parasitic motion of a Roberts mechanism with rigid bodies and non-rigid bodies

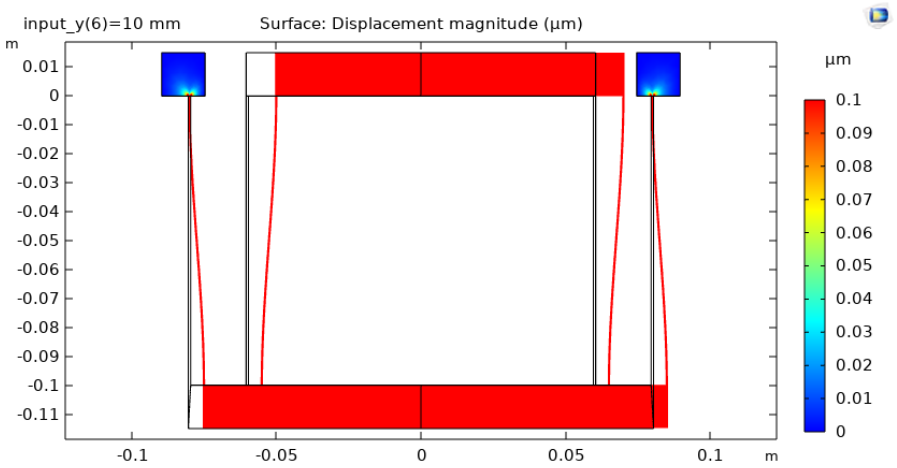

Figure H.3: Nonlinear FEA of a double parallelogram mechanism taking the compliance of the base and moving bodies into account.

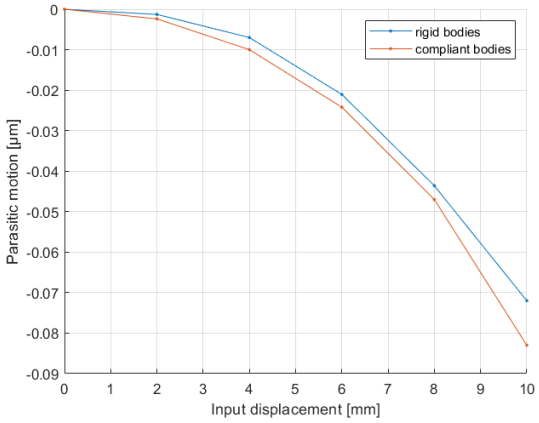

Figure H.4: Parasitic motion of a double parallelogram mechanism with rigid bodies and non-rigid bodies

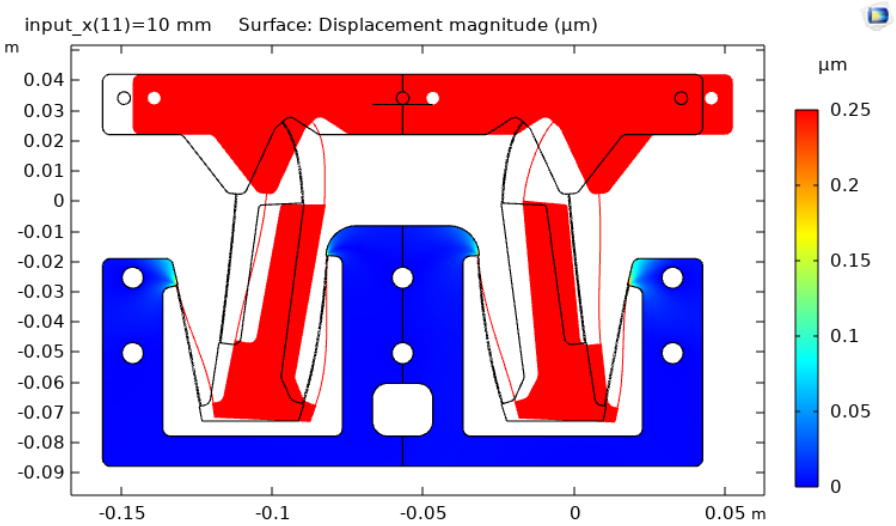

Figure H.5: Nonlinear FEA of the optimized linear motion guide ($0.4mm$ thick flexures) when taking the compliance of the base and moving bodies into account.

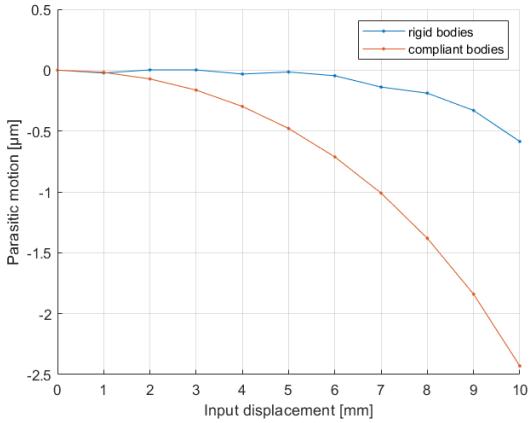

Figure H.6: Parasitic motion of the optimized linear guide with rigid bodies and non-rigid bodies. Instead of $0.8mm$ thick flexures the flexures are $0.4mm$ thick.